Enhancing Energy Efficiency and Privacy Protection of Smart Devices

Ge Peng
College of William and Mary - Arts & Sciences, gezikuaile@gmail.com

Enhancing Energy Efficiency and Privacy Protection of Smart Devices

Ge Peng

Hengyang, Hunan, China

Bachelor of Engineering, National University of Defense Technology, China, 2008

A Dissertation presented to the Graduate Faculty
of The College of William & Mary in Candidacy for the Degree of
Doctor of Philosophy

Department of Computer Science

College of William & Mary
May 2017

APPROVAL PAGE

This Dissertation is submitted in partial fulfillment of
the requirements for the degree of

Doctor of Philosophy

[illegible]

Ge Peng

Approved by the Committee, March 2017

[illegible]

Committee Chair
Associate Professor Gang Zhou, Computer Science
College of William & Mary

[illegible]

Professor Virginia Torczon, Computer Science
College of William & Mary

[illegible]

Professor Qun Li, Computer Science
College of William & Mary

[illegible]

Assistant Professor Xu Liu, Computer Science
College of William & Mary

[illegible]

Assistant Professor Shan Lin, Electrical and Computer Engineering
Stony Brook University

COMPLIANCE PAGE

Research approved by

The College of William & Mary Protection of Human Subjects Committee

Protocol number(s): PHSC-2014-11-25-9981-gzhou

Date(s) of approval: 12/03/2014

ABSTRACT

Smart devices are experiencing rapid development and great popularity. Various smart products available nowadays have largely enriched people's lives. While users are enjoying their smart devices, there are two major user concerns: energy efficiency and privacy protection. In this dissertation, we propose solutions to enhance energy efficiency and privacy protection on smart devices.

First, we study different ways to handle WiFi broadcast frames during smartphone suspend mode. We reveal the dilemma of existing methods: either receive all of them suffering high power consumption, or receive none of them sacrificing functionalities. To address the dilemma, we propose Software Broadcast Filter (SBF). SBF is smarter than the "receive-none" method as it only blocks useless broadcast frames and does not impair application functionalities. SBF is also more energy efficient than the "receive-all" method. Our trace driven evaluation shows that SBF saves up to 49.9% energy consumption compared to the "receive-all" method.

Second, we design a system, namely HIDE, to further reduce smartphone energy wasted on useless WiFi broadcast frames. With the HIDE system, smartphones in suspend mode do not receive useless broadcast frames or wake up to process useless broadcast frames. Our trace-driven simulation shows that the HIDE system saves 34%-75% energy for the Nexus One phone when 10% of the broadcast frames are useful to the smartphone. Our overhead analysis demonstrates that the HIDE system has negligible impact on network capacity and packet delay.

Third, to better protect user privacy, we propose a continuous and non-invasive authentication system for wearable glasses, namely GlassGuard. GlassGuard discriminates the owner and an imposter with biometric features from touch gestures and voice commands, which are all available during normal user interactions. With data collected from 32 users on Google Glass, we show that GlassGuard achieves a 99% detection rate and a 0.5% false alarm rate after 3.5 user events on average when all types of user events are available with equal probability. Under five typical usage scenarios, the system has a detection rate above 93% and a false alarm rate below 3% after less than 5 user events.

TABLE OF CONTENTS

ACKNOWLEDGMENTS

This dissertation is written with the support and help from many individuals. I would like to thank all of them.

First and foremost, I would like to express my deepest appreciation to my advisor, Dr. Gang Zhou. Without his guidance in my research, encouragement in my life, and confidence in my abilities, this dissertation would not have been possible.

I would also like to thank my dissertation committee, Dr. Virginia Torczon, Dr. Qun Li, Dr. Xu Liu, and Dr. Shan Lin, for serving on my Ph.D committee as well as their insightful comments.

My sincere thanks also go to all members of the LENS group past and present, Dr. Andy Pyles, Dr. Xin Qi, Dr. David T. Nguyen, Dr. Daniel Graham, Qing Yang, George Simmons, Kyle Wallace, Dr. Yantao Li, Dr. Shuangquan Wang, Amanda Watson, Hongyang Zhao, and Yongsen Ma, for the stimulating discussions, constructive suggestions, generous assistance, and effective teamwork.

Futhurmore, I would like to thank the faculty and staff at the Computer Science Department of the College of William & Mary. Special thanks to Vanessa Godwin, Jacqulyn Johnson, and Dale Hayes for their considerate and effective assistance.

Last but not the least, I would like to thank my family. Thanks to my parents, whose unwavering love and support has made me who I am today. Thanks to my husband, Daiping Liu, for lighting up my life with so much love and joy.

This dissertation was supported in part by the U.S. National Science Foundation under grants CNS-1250180 and CNS-1253506 (CAREER).

This dissertation is dedicated to my beloved parents and my lovely husband for their endless and selfless love and support.

LIST OF TABLES

LIST OF FIGURES

Enhancing Energy Efficiency and Privacy Protection of Smart Devices

Chapter 1

Introduction

Smartphone users have exploded in recent years. It is reported that worldwide smartphone sales to end users totaled nearly 1.5 billion units in 2016, five times as compared with 2010 [1]. The share of Americans that own smartphones reaches 77% in 2016, up from just 35% in 2011 [2]. With the wide spread of smartphones, other types of smart devices, such as tablets, smart watches, and smart wristbands, are also becoming more and more popular. Smart glasses, as a relatively new type of smart devices, are believed to become even more popular than smartphones in 10 years [3]. It is estimated that shipments of smart glasses will hit 1 billion around 2020, surpassing the expected shipments of mobile phones by 2025 [3]. These myriads of smart devices have largely enriched people's lives and people are now “addicted” to smart devices. According to a recent study, 89% of US and 77% of global consumers saying they can not live without their smartphone or always have it within arm's reach [4].

While users are enjoying their smart devices, there are two major user concerns. The first is energy efficiency. Users are spending more and more time on smartphones for games, music, Internet access, instant communications, and so on. Smartphone applications also tend to incorporate more complex functions, which require more computing capability and energy consumption. However, smartphone battery capacity has not kept up with the increase of user demands of smartphone usage and complexity of smartphone applications. Surveys [5, 6] show that improved battery life is the number one feature that users want from a new smartphone. The second user concern is privacy protection. On one hand, applications store various personal and sensitive data on the device, such as photos, emails, bank accounts, locations. On the other hand, people carry their smart devices around. The device can be easily misplaced, lost, or stolen. In the United States someone loses a cell phone every 3.5 seconds [7]. And in 96% of cases, a person who finds a lost smartphone tries to access sensitive data [8]. Moreover, research [9] has shown that privacy threats come from not only strangers but also insiders, e.g. friends and family, which imposes even bigger challenges for privacy protection on smart devices.

1.1 Problem Statements

In this dissertation, we propose solutions to enhance energy efficiency and privacy protection on smart devices. Specifically, we work on the following three problems.

(1) Handing WiFi Broadcast Traffic During Smartphone Suspend Mode. To enhance energy efficiency, one important and effective mechanism in smartphones is to enter low power suspend mode (i.e., the system-on-chip (SoC) of the device including CPU, ROM, and the micro-controller circuits for various components are suspended [10]) when the user becomes inactive. During user inactivity, a user is not actively interacting with the smartphone, but may be waiting for events from applications, such as application data received by WiFi. In addition to application data (unicast or broadcast), WiFi radio also receives background WiFi broadcast data, such as broadcast packets for printer discovery. To process these broadcast data, a smartphone needs to switch to high power active mode and stay there for a while. This definitely increases the power consumption and impairs smartphone energy efficiency, especially when useless broadcast traffic constitutes the majority of WiFi traffic. The question is how to handle broadcast traffic during smartphone suspend mode in an energy efficient way, without compromising normal function of applications in need of broadcast packets. To answer this question, we examine how current smartphones deal with broadcast traffic when they are in suspend mode and how these solutions impact smartphone energy consumption and functionality. Based on the findings, we propose Software Broadcast Filter to filter out useless broadcast frames in the WiFi driver and improve the energy efficiency during smartphone suspend mode.

(2) AP-assisted Broadcast Traffic Management to Save Smartphone Energy. WiFi energy consumption is critical to smartphone battery life. To save energy, one way is to reduce energy consumed by useless WiFi traffic, such as malicious traffic from attackers [11] and background broadcast traffic. In our first work, we study how to efficiently filter out useless WiFi broadcast traffic at client (smartphone) side after they are received by smartphones. However, in this way, smartphone energy is still wasted to receive and process these useless frames. Moreover, if a smartphone is in suspend mode, it still needs to wake up in order to do the processing. A smarter way is to filter out useless broadcast frames before they are received by smartphones. To achieve this, we propose a framework for cooperation between an AP and smartphone clients to deal with unwanted broadcast traffic. With the proposed system, presence of useless broadcast frames is hidden by the AP from smartphones. As a result, smartphones in suspend mode do not receive these useless broadcast frames as they never exist. Hence, smartphone energy for receiving and processing these unwanted traffic and for waking up from suspend mode is saved.

(3) Continuous and Non-invasive User Authentication on Wearable Glasses. As wearable glasses are becoming more and more popular, there is an urgent need to protect user privacy on these devices. An effective measure to protect user privacy is performing user authentication to prevent unauthorized access. A one-time authentication system, which only authenticates a user once when he/she tries to unlock the device, fails under various circumstances, for example when the owner is temporarily away from his/her device with the device unlocked and unattended, or when the password/PIN is acquired by an insider. Therefore, a continuous authentication system which continuously authenticates the user during the whole time of user operation is needed to better protect user privacy. To accomplish this, we propose a continuous and non-invasive authentication system for wearable glasses with the example of Google Glass which authenticates users with touch behavioral biometrics and voice features.

1.2 Contributions

This dissertation proposes three solutions towards enhancing energy efficiency or user privacy protection on smart devices. The overall contributions are as follows.

Handing WiFi Broadcast Traffic During Smartphone Suspend Mode. We reveal the dilemma of dealing with WiFi broadcast traffic on modern smartphones during suspend mode: receive all and suffer high power consumption, or receive none and sacrifice functionalities. We address the dilemma by designing a flexible packet filter that enables fine-grained policies to handle WiFi broadcast frames. Specifically, we make two contributions.

- Through measurements and analysis, we investigate how existing smartphones deal with broadcast traffic when in suspend mode. Four smartphones are used for the study: HTC Hero, Nexus One, Galaxy Nexus, and Galaxy S4. Through power consumption and functionality analysis, we reveal the problem of existing solutions, which we refer to as the dilemma of handling WiFi broadcast traffic during a smartphone's suspend mode.
- We propose Software Broadcast Filter (SBF) to address the dilemma, and compare it with solutions on modern smartphones. Through energy modeling and trace driven performance evaluation, we demonstrate the performance of the proposed method. Compared to the "receive-none" solution, SBF does not impair functionalities of smartphone applications. Compared to the "receive-all" solution, SBF reduces the power consumption by up to 49.9%.

AP-assisted Broadcast Traffic Management to Save Smartphone Energy. We propose a solution to filter out useless broadcast frames at APs before they are received by smartphones. Our main contributions are:

- We design a framework, namely HIDE, working between an AP and smartphone clients to reduce smartphone energy wasted on useless broadcast traffic. In our system, broadcast frames are managed at the AP. The AP hides presence of useless broadcast frames from each client. As a result, smartphones in suspend mode do not need to receive and wake up to process useless broadcast frames.

- We demonstrate the energy saving of our system with energy modeling and trace-driven simulation. With five broadcast traffic traces collected in five different real-world scenarios, we show that the HIDE system saves 34%-75% smartphone energy for Nexus One when 10% of the broadcast traffic are useful to the smartphone. Our overhead analysis demonstrates that our system has negligible impact on network capacity and packet round-trip time.

Continuous and Non-invasive User Authentication on Wearable Glasses. We design a continuous and non-invasive authentication system for wearable glasses with the example of Google Glass. The system authenticates users based on biometric features extracted from touch events and voice commands. Our main contributions are:

- We conduct a user study on Google Glass and collect user interaction data from 32 human subjects. The data we collect includes touch event data with corresponding sensor readings and voice commands. Six types of gestures are covered in the study: single tap, swipe forward, swipe backward, swipe down, two-finger swipe forward, and two-finger swipe backward.

- With the data collected, we define and extract 99 behavioral features for one-finger touch gestures, 156 features for two-finger touch gestures, and 19 voice features for user voice commands. We evaluate the discriminability of these features with one-class SVM model for user authentication purpose on Google Glass. Using the features selected by Sequential Forward Search, the average classification EERs

(Equal Error Rate) with only one touch event range from 9% to 18.5%, for different types of touch gestures. With one voice command, the EERs for different users are between 1% and 11.8%.

- We design a simple but effective online user authentication system for wearable glasses, named GlassGuard, which works in a continuous and non-invasive way. GlassGuard employs a mechanism adapted from Threshold Random Walking to make a decision from multiple user events only when it is confident. Our preliminary results indicate that it achieves a detection rate of of 99% and a false alarm rate of 0.5% after 3.5 user events on average when all types of user events are available with equal probability. Under 5 typical usage scenarios, the system has a detection rate above 93% and a false alarm rate below 3% after less than 5 user events.

1.3 Dissertation Organization

The rest of this dissertation is structured as follows. In Chapter 2, we discuss related work. In Chapter 3, we present our study of broadcast traffic management on smartphones during suspend mode. In Chapter 4, we propose our system with AP-assisted broadcast traffic management to save smartphone energy. In Chapter 5, we propose GlassGuard, a continuous and non-invasive authentication system for wearable glasses. Finally, we conclude the dissertation in Chapter 6.

Chapter 2

Related Work

This chapter reviews related work in energy efficiency on smartphones, traffic management for smartphones, and user authentication on smart devices respectively.

2.1 Energy Efficiency on Smartphones

A number of prior solutions have been proposed to reduce energy consumption on smartphones. We focus on those most closely related to our work.

Measuring WiFi Power Consumption. Balasubramanian et al. [12] measure energy consumption of different components of WiFi with downloading/uploading streams. Carroll et al. [13] measure WiFi power consumption under various scenarios, such as system suspend, system idle, emailing, SMS messaging and so on. Perrucci et al. [14] measure power consumption in different stages of WiFi when the phone is downloading data. Cuervo et al. [15] also measure WiFi power consumption with different amounts of downloading data. All these works focus on power consumed by application communication, while our work focuses on power consumption caused by background traffic.

Reducing WiFi Power Consumption. Catnap [16] takes advantage of the bandwidth gap between wireless and wired links. They batch the time that WiFi is idle listening for data from wired network and put WiFi into sleep mode during this time. Liu et al. [17] leverage traffic prediction to exploit idle intervals as short as several hundred microseconds. All these methods reduce the time a WiFi module stays at a high power active state. However, our method reduces the time an operating system spends in high power active state when the phone is not actively used. During this time, the WiFi driver is mostly in low power sleep state. So, these work are complementary to ours.

Pyles et al. [18] also check destination port number in WiFi frames to determine if there is a process listening on that port. They use this information to determine whether a frame is delay sensitive or not. However, transmission of broadcast frames are scheduled by AP for the whole local network. It can not be delayed for a specific client. Hence, their solution does not apply in our case.

Deng et al. [19] propose a solution to reduce energy consumed by 3G/LTE interface staying in active mode unnecessarily. Rozner et al. [20] try to mitigate power consumption increase when there is competitive background traffic. Bharadwaj et al. [21] study PSM (Power Save Mode) timeout in WiFi driver. These works control how wireless radio switches between active and sleep modes. We control how the system switches between suspend and active modes.

The authors in [10, 22] study energy bugs caused by wakelocks. The case they study is when a wakelock is activated but is unable to be released. In our work, the wakelock triggered by WiFi driver is due to normal behavior not a bug, as it can be released normally after the timer expires.

A similar work reducing system wakeup energy overhead caused by WiFi is done on PC [23]. They employ a peripheral low power processor to receive all broadcast/unicast frames with less energy cost when a PC is in suspend mode. In contrast, we determine whether to take actions for a broadcast frame or not, such as activating a wakelock, putting packet data into system network stack. As far as we know, we propose the first work that studies solutions for handling WiFi broadcast frames during a smartphone's suspend mode.

2.2 Traffic Management for Smartphones

Detecting/Filtering Unwanted Traffic. The authors in [24, 25] measure the impact of unwanted traffic on 3G networks. Raghavendra et al. [26] measure the impact of unwanted link layer WiFi frames due to client association/dissociation and probe activities. In this work, we focus on WiFi broadcast frames generated by upper-layer applications with UDP payload.

The authors in [27, 28] detect data traffic sent from DDoS attackers. Lu et al. [29] propose an authentication scheme to filter out false data from injected nodes in wireless sensor network. Gu et al. [30] consider null data frames from attackers as unwanted traffic and propose defense mechanisms against it. These works focus on detecting and filtering abnormal traffic from malicious nodes. However, in our work, we study WiFi broadcast frames that are normal traffic from benign nodes.

Singh et al. [31] detect and prevent smartphone traffic incurred by infrequently used applications. Their focus is more about outgoing traffic while our focus is about incoming traffic.

Smartphone Traffic Reduction. The authors in [32, 33, 34] propose to reduce data received by smartphones during video chatting or streaming. However, these methods target at unicast frames for a specific type of application. In this work, we consider broadcast frames that come from various applications.

Kim et al. [35] propose to let the server selectively send the data to a smartphone according to the smartphone's battery status. Smartphone advertising is also one source of unnecessary or unwanted traffic [36, 37]. Applications, such as Adblock [38], have been provided to block such kind of unwanted traffic. Again, all of these work study unicast traffic. We study broadcast traffic.

Qian et al. [39] propose to reduce general data traffic of smartphones by applying redundancy elimination at different protocol layers. Their work is orthogonal to ours.

2.3 User Authentication on Smart Devices

Continuous and Transparent Authentication. User authentication has been done via voice recognition [40] and face recognition [41]. However, voice commands are not always available. Asking users to speak from time to time is invasive. Google Glass only has a camera facing away from the wearers. As a result, methods based on face recognition does not work. Moreover, using a camera brings privacy concern.

Early research has studied continuous authentication on personal computers via mouse movements and keystroke dynamics [42, 43, 44]. These two biometrics are much different from touch gestures on wearable glasses.

The idea of using touch behavioral biometrics for user authentication has been validated for multi-touch devices [45, 46]. Since then, various touch behavioral base continuous authentication systems have been proposed. Some of them are based on keystrokes on smartphones [47, 48, 49]. These methods do not work with touch pads on wearable glasses since they do not support keystrokes. Others are based on touch gestures with features extracted from screen touch data [50, 51, 52] and/or features extracted from sensor data during a touch event [53, 54, 55]. However, due to differences in user interaction with wearable glasses and that with smartphones, these authentication systems cannot be directly applied to wearable glasses. The discriminability of those features needs to be evaluated on wearable glasses. Furthermore, users can control wearable glasses with voice commands and easily circumvent the touch-based authentication systems.

Gait information has also been studied [56, 57] for continuous authentication purpose. These works are complimentary to ours as we study the case when users are static.

Conti et al. [58] propose to authenticate a user based on how the user answers or places a phone call, e.g. the movement pattern during the process of bringing the phone to the ear after pressing the "start" button to initiate the call. This method, however, is specific to smartphones. It is not applicable on wearable glasses.

User Authentication on Wearable Devices. Physical characteristics of users are explored to do user authentication on wearable devices. Yang et al. [59] measure the difference in user responses to a vibration excitation. This method is intrusive. Cornelius et al. [60] design a new sensor that measures how tissue responds to an electrical current to verify identities of wearers. Similarly, Rasmussen et al. [61] propose to authenticate users based on the human body's response to an electric square pulse signal. These two methods require a specific hardware that is not available in today's smart glasses. Moreover, to apply them in the real world, user safety needs to be addressed.

Chan et al. [62] propose to use the glass camera to scan a QR code displayed on the user's smartphone for authentication. Li et al. [63] propose to authenticate users based on head movements in response to a music cue played on the Google Glass. Both of these options are intrusive.

A similar work to ours is presented by Chauhan et al. [64]. Our comparison in Subsection 5.4.3 shows that our system is more flexible and achieves better performance.

Other Sources for User Authentication. Das et al. [65] verify users with questions about the owner's day-to-day experience. This is invasive as users need to answer questions. Usage patterns of smartphone, such as SMS and voice call records, have also been used to do active authentication [66]. This method has long authentication delay as it needs to collect usage data during a long time interval to achieve high accuracy.

Shafagh et al. [67] use information of nearby devices to authenticate a user. Other novel features are also proposed, such as clothes [68] and shoes that a user wears [69]. These methods have potential to be applied in wearable glasses. However, they do not work well alone as a solution for continuous user authentication on wearable glasses because these features are not stable even for the owner. It requires re-training when a user visits a new place or gets new shoes or clothes. However, they can be combined with our system to provide more accurate predictions. Our work is complementary to theirs.

Chapter 3

All or None? The Dilemma of Handling WiFi Broadcast Traffic in Smartphone Suspend Mode

3.1 Introduction

Smartphones spend a large amount of time in a state where they are not actively used. This state is usually referred to as *suspend* or *sleep* mode. In this mode, the system-on-chip (SoC) of the device including CPU, ROM, and the micro-controller circuits for various components are suspended [10], so the phone consumes very little power. For example, power consumption of Nexus One is 11 mW in *suspend* mode while it is above 120 mW in *active* mode. By turning smartphones into suspend mode while they are not in use, considerable energy can be saved.

However, incoming WiFi traffic interrupts a smartphone's suspend mode and triggers the switch to the high power active mode. One example is application notification when the screen is off. Another example, which is often overlooked, is WiFi broadcast traffic. On some smartphones, such as Nexus One, the WiFi driver wakes up the whole system upon receiving a WiFi broadcast frame during suspend mode. Moreover, in order to allow enough time to process the frame and possible following transmission events, WiFi driver acquires a wakelock [70] of one second. The phone stays in active mode until the wakelock expires. As a result, battery drains fast even when a user is doing nothing on the smartphone. Many users have been complaining about this problem [71, 72, 73].

WLAN is not designed for smartphones at the beginning. Although WiFi broadcast frames are destined to the whole local area network, not all of them are useful to a smartphone, e.g., WiFi broadcast frames for printer service discovery. It is energy inefficient to wake up the whole system and stay awake just because of these useless background broadcast frames. Smartphones have very limited battery life. It is important to handle WiFi broadcast traffic in an energy efficient way. To improve energy efficiency, some smartphones, such as Galaxy Nexus and Galaxy S4, receive no broadcast frames except ARP and Multicast DNS frames when they are in suspend mode. With this policy, higher energy efficiency is achieved. However, this impairs the functionalities as applications can not receive any broadcast frame during suspend mode. Broadcast traffic is pervasive and important in modern networks. Many network protocols rely on broadcast to perform correctly or effectively, such as ARP, DHCP, and DNS. Some system services employ broadcast packets for resource discovery, such as NetBIOS Name Resolution. Applications also embrace broadcast packets to communicate with neighbors, such as LAN sync feature of Dropbox [74], neighbor discovery of Spotify [75], and crowdsourcing based content sharing applications [76, 77]. Failure to receive these broadcast frames results in malfunction of system services or user applications. Complaints regarding this issue [78, 79, 80, 81] have also been posted in many technical forums.

Whether to receive a broadcast frame or not? It is difficult to tell because WiFi driver has no information about what broadcast frames are needed by system services and user applications. This leads to the dilemma of dealing with WiFi broadcast traffic on modern smartphones during suspend mode: receive all and suffer high power consumption, or receive none and sacrifice functionalities. In this work, we address the dilemma by designing a flexible packet filter that enables fine-grained policies to handle WiFi broadcast frames. Specifically, we make two contributions.

- Through measurements and analysis, we investigate how existing smartphones deal with broadcast traffic when in suspend mode. Four smartphones are used for the study: HTC Hero, Nexus One, Galaxy Nexus, and Galaxy S4. Through power consumption and functionality analysis, we reveal the problem of existing solutions, which we refer to as the dilemma of handling WiFi broadcast traffic during a smartphone's suspend mode.

- We propose Software Broadcast Filter (SBF) to address the dilemma, and compare it with solutions on modern smartphones. Through energy modeling and trace driven performance evaluation, we demonstrate the performance of the proposed method. Compared to the "receive-none" solution, SBF does not impair functionalities of smartphone applications. Compared to the "receive-all" solution, SBF reduces the power consumption by up to 49.9%.

In literature, existing research mainly focuses on designing energy efficient broadcast/multicast protocols for wireless networks [82, 83] or reducing energy consumption of WiFi unicast traffic when a smartphone is in active mode [16, 84, 85]. However, we are different in that we study the impact of WiFi broadcast traffic when a smartphone is in suspend mode. This problem deserves attention because: (1) Broadcast traffic has a broad impact as it affects all nodes in a network. (2) Broadcast traffic is passive and typically arrives unexpectedly. To the best of our knowledge, we are the first to present measurements and analysis of different ways to deal with WiFi broadcast traffic during smartphone suspend mode.

3.2 Revealing The Dilemma With Experiments

To reveal the dilemma, we first introduce existing solutions on four modern smartphones. Then, we carry out experiments to show how they perform in terms of functionality and energy efficiency when WiFi broadcast traffic exists.

3.2.1 Understanding Existing Solutions on Modern Smartphones

To investigate how modern smartphones handle WiFi broadcast frames when in suspend mode, we analyze WiFi drivers of four commercial smartphones listed in Table 3.1. Note that some 802.11 control and management frames are also broadcast, such as beacon frames. However, we only focus on data frames as this is the part of traffic that we can leverage. Also, we focus on MAC layer broadcast since we study behaviors of WiFi driver. In IP layer, it can be either unicast address or broadcast/multicast address. In this work, by (UDP/ARP) broadcast frames/traffic we simply mean WiFi broadcast data frames/traffic (with UDP/ ARP data).

device	Android version	kernel version	WiFi driver
HTC Hero	2.3.7	2.6.29	wlan.ko
Nexus One	2.3.7	2.6.37	bcm4329.ko
Galaxy Nexus	4.2.1	3.0.31	bcmdhd.ko
Galaxy S4	4.2.2	3.4.0	bcmdhd.ko

Table 3.1: Devices used for analysis

HTC Hero. On this phone, the WiFi driver receives all broadcast frames and passes them to system network stack. When a broadcast frame arrives during suspend mode, the smartphone switches to active mode so as to wake up the CPU and other resources to process the frame. At the same time, the WiFi driver acquires a wakelock [70] of one second. This one-second wakelock prevents the system from going back to suspend mode until it expires. It allows enough time for the application to process the data. Also, subsequent frames can be processed immediately.

Nexus One. This phone is equipped with ARP offload [86], which enables a network adapter to respond to ARP requests without waking up the system. For other broadcast frames, it employs the same method as on HTC Hero: waking up (resuming), staying in active state for one second, and then going back to suspend mode. WiFi broadcast frames are usually small. It will not take too much energy for the radio to receive such frames. Figure 3.1 shows the power consumption when a Nexus One phone wakes up to receive a WiFi broadcast frame. Although the energy cost for the phone to resume and go back to suspend is not negligible, we find that the main part of energy is consumed during the one-second wakelock time triggered by the received broadcast frame.

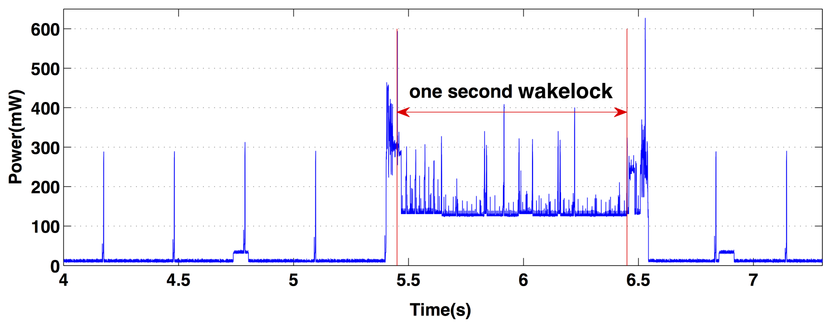

Figure 3.1: Power consumption when waking up to receive one WiFi broadcast frame (measured on Nexus One with Monsoon Power Monitor [87])

Galaxy Nexus and S4. The same as on Nexus One, these two phones are also equipped with ARP offload. In addition, they enable a firmware broadcast filter. This filter blocks all UDP broadcast frames with the only exception of Multicast DNS (MDNS) frames. As a result, no UDP broadcast frames other than MDNS frames are received by the system when the phone is in suspend mode.

3.2.2 Real World WiFi Broadcast Traffic Analysis

We collect traces to see how WiFi broadcast traffic looks like in real world. Traces are collected in five locations: a classroom building, an office in the Computer Science Department (CS_Dept), W&M college library (WML), an off-campus Starbucks store, and Williamsburg Regional Library (WRL). For each location, we capture all broadcast frames under an AP for 30∼60 mins during peek time.

We calculate percentages of UDP or ARP broadcast traffic as numbers of UDP or ARP broadcast frames divided by the total number of WiFi broadcast data frames. As shown in Figure 3.2(a), UDP and ARP broadcast frames account for more than 94% of WiFi broadcast traffic in all five scenarios.

We split each trace into 5-min slices and calculate the UDP broadcast traffic volume in

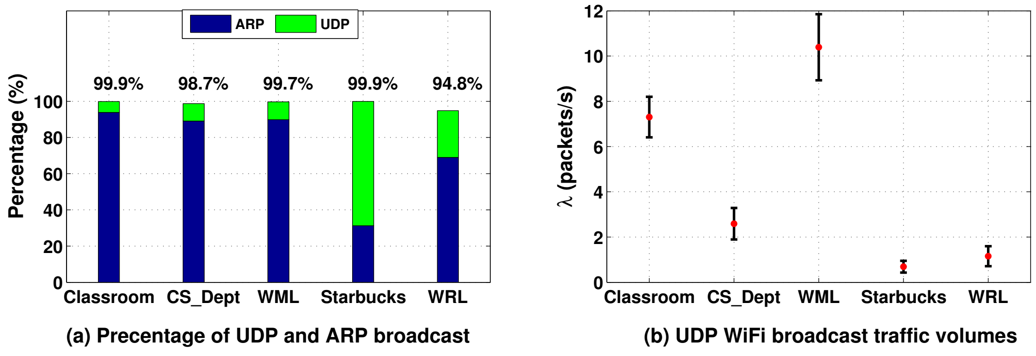

Figure 3.2: Statistics of five broadcast traffic traces

terms of frame arrival rate inside each slice. Figure 3.2(b) shows the mean and standard deviation of frame rates for each trace. The average UDP broadcast traffic volumes are all less than 11 frames/s. We also observe that traffic volumes differ largely among these locations. The lowest is 0.7 frame/s in the off-campus Starbucks store while the highest is 10.4 frames/s in the college library.

index	**UDP port**	**function**	**index**	**UDP port**	**function**
1	53	-unknown	17	6120	-unknown
2	67	DHCP bootps	18	6646	McAfee Shared Service Host, McAfee Integrated Security Platform
3	68	DHCP bootpc	19	8611	-unknown
4	137	Netbios-ns	20	8612	Canon BJNP Port 2, EMC2 (Legato) Networker or Sun Solcitice Backup, QuickTime Streaming Server
5	138	Netbios-dgm	21	9164	apani5, EMC2 (Legato) Networker or Sun Solcitice Backup, QuickTime Streaming Server
6	161	Simple Network Management Protocol	22	9200	-unknown
7	177	X Display Manager Control Protocol	23	9956	Alljoyn Name Service, QuickTime Streaming Server
8	631	Common Unix Printing System, Internet Printing Protocol (IPP)	24	10007	mvs-capacity
9	1004	Mac OS X RPC-based services. Used by NetInfo, for example.	25	10019	Stage Remote Service
10	1211	Groove dpp	26	17500	Dropbox
11	1900	ssdp, Microsoft SSDP Enables discovery of UPnP devices	27	23499	-unknown
12	2222	Ethernet-IP-1, trojan	28	27036	Steam In-Home Streaming Discovery Protocol
13	2223	Rockwell-csp2, Microsoft Office OS X antipiracy network monitor	29	43440	Cisco EnergyWise Discovery and Command Flooding
14	3289	enpc	30	57621	Spotify
15	3600	Trap-daemon(text relay-answer)	31	65080	-unknown
16	5353	mdns			

Table 3.2: UDP ports used by WiFi broadcast frames in traces

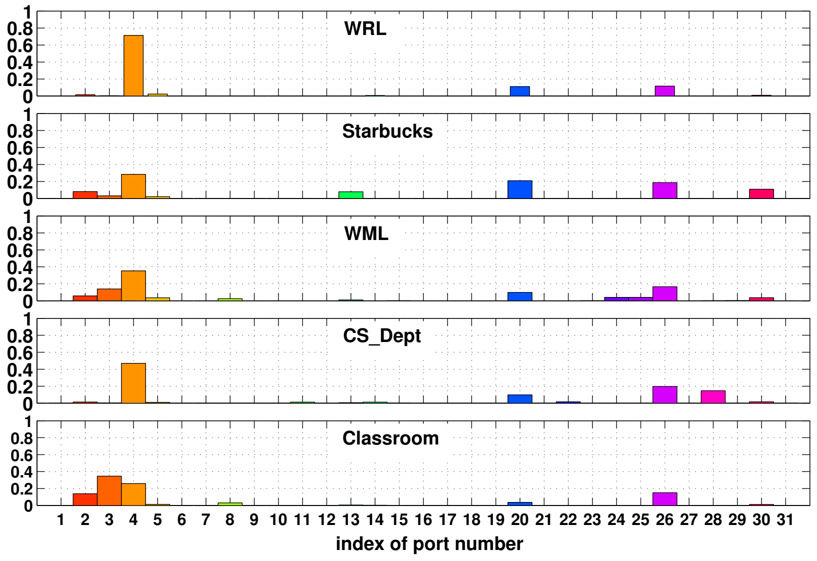

Figure 3.3: UDP ports distribution
(Indices are defined in Table 3.2)

From all five traces, we observe that 31 ports are used for UDP broadcast. We list them in Table 3.2 and show the distributions in Figure 3.3. Although there are 31 different UDP ports, the majority of broadcast frames lie in a small portion of them. While some of these broadcast frames are useless to a smartphone, such as Canon BJNP on Port 8612 (with index 20), some of them are useful and important to a smartphone. For example, users may keep smartphone screen off while waiting for connections from nearby devices. If the smartphone can not receive and respond to service discovery broadcast frames, such as UPnP and Steam, other devices nearby will not know its presence. Thus, the device can not be connected and the service can not be used. Another interesting finding during our experiments is that the LAN Sync feature of Dropbox is not included in its Android app. One reason would be that it can not work because some smartphones can not receive broadcast frames for neighbor discovery when in suspend mode. The "receive-none" solution sacrifices functionalities. What's worse, without system support to receive broadcast traffic during suspend mode, developers will be pushed to abuse wakelocks to prevent smartphones from suspending, so as to ensure reception of broadcast packets.

3.2.3 Power Impact Measurements

To have a better understanding of the impact of WiFi broadcast traffic on smartphone power consumption in suspend mode, we carry out experiments to show how the power consumption changes with different broadcast traffic volumes when smartphones are in suspend mode. As already shown in Figure 3.2(a), real word WiFi broadcast traffic mainly consists of UDP and ARP broadcast frames. Therefore, we measure the impact of UDP and ARP broadcast frames on power consumption of smartphone suspend mode respectively.

Setup. For the experiments, a private AP (a linux-based desktop, see Figure 3.4) is set up to control the background WiFi broadcast traffic volume. The traffic generator, which is a laptop, sends out UDP or ARP broadcast packets following a Poisson distribution [88]. Payloads of all broadcast packets are fixed to 50 bytes. We adjust the traffic volume by varying the value of arrival rate λ for the Poisson distribution. When $\lambda = 0$, there is no WiFi broadcast traffic. We suppress all outgoing application traffic in order to eliminate noise of transmission events. We keep WiFi connected and screen off, then measure power consumption of the whole phone with Monsoon power monitor [87], as shown in Figure 3.4. Each measurement lasts five minutes and each data point is the average value of five repeated measurements.

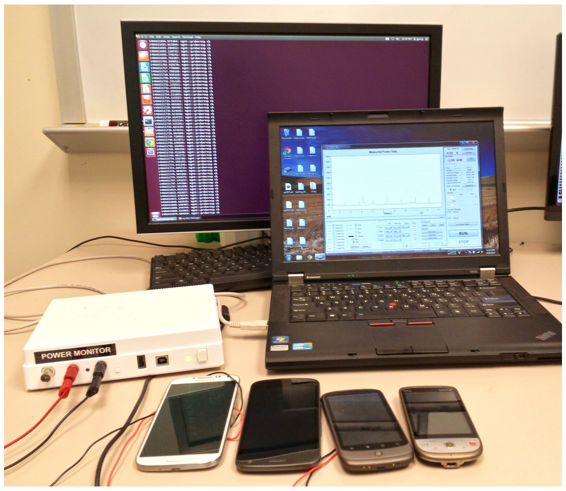

Figure 3.4: Experiment setup

Power Impact of UDP Broadcast. Since we only consider background WiFi broadcast traffic, we choose a UDP port number that is not listened to by the phone. We suppress all outgoing application traffic in order to get rid of the noise of transmission events. To measure the broadcast impact, we first measure the average power consumption of the whole phone with screen off and WiFi connected but no traffic (denoted as E_0). Then, we measure the average power consumption (denoted as E_1) of the whole phone with broadcast traffic added. The broadcast impact in terms of energy consumption is then calculated as $E_1 - E_0$. All power consumptions are measured with Monsoon power monitor.

Figure 3.5 shows the results of the aforementioned four phones. As we can see, power consumptions of Galaxy Nexus and Galaxy S4 do not increase too much because these two phones receive no UDP broadcast frames during suspend mode. In contrast, HTC Hero and Nexus One receive all UDP broadcast frames. Thus, power consumptions of these two phones increase dramatically as UDP broadcast sending rate increases. Power consumptions are less than 25mW for these two phones when there is no UDP broadcast traffic. They rise above 50mW when there is only one UDP broadcast packet per second. Similar trends are also observed for Galaxy Nexus and Galaxy S4 after disabling the firmware broadcast filter, which are indicated by the curves named "Galaxy Nexus disabled" and "Galaxy S4 disabled." Additionally, for all four phones, increase in power consumption slows down when the UDP broadcast sending rate exceeds 10 packets/s. This is because the smartphones already spend most of time in the high power active mode when there are 10 broadcast packets per second. Further increase of WiFi broadcast traffic volume does not obviously increase the portion of time in active mode.

Power Impact of ARP Broadcast. As our focus is energy consumed by useless broadcast frames, in all ARP broadcast packets, the IP address to be resolved does not belong to the smartphone. Thus, these ARP packets are all useless broadcast traffic to the smartphone. As shown in Figure 3.6, for HTC Hero, increase of power consumption

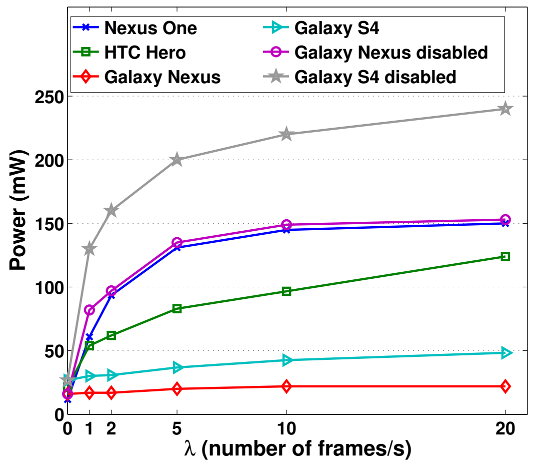

Figure 3.5: Power impact of UDP broadcast traffic

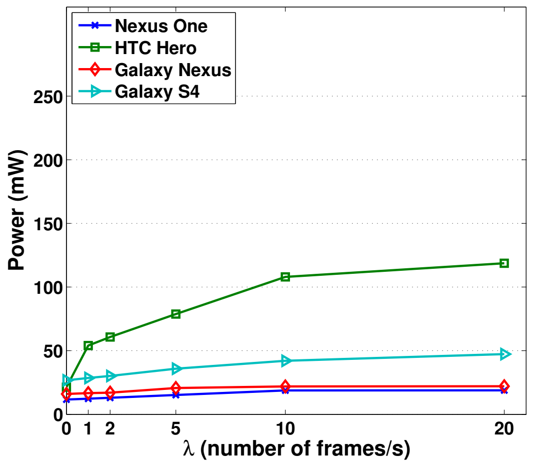

Figure 3.6: Power impact of ARP broadcast traffic

under ARP broadcast traffic is similar to that under UDP broadcast traffic. However, ARP broadcast traffic is observed to have little impact on the other three phones. For example, power consumption of Nexus One increases by less than 8mW when we increase the ARP broadcast traffic from 1 to 20 packets/s. From our analysis in the previous section, we learn that the reason is ARP offload. As observed, ARP offload is efficient enough to deal with ARP broadcast traffic. Therefore, in the rest of this work, we target at UDP broadcast traffic.

3.3 Software Broadcast Filter Design and Energy Saving Analysis

As we have demonstrated, current solutions of receiving all or no broadcast frames sacrifice either functionalities or battery life of a smartphone. To address the dilemma, we design a flexible and fine-grained Software Broadcast Filter (SBF). To demonstrate the energy efficiency of SBF, we first characterize the energy consumption when a smartphone system wakes up to receive a broadcast frame. Then, we calculate the energy saving of SBF by modeling the energy consumptions of both SBF and "receive-all" methods.

3.3.1 SBF Design

Figure 3.7 shows the work flow of SBF inside WiFi driver. Actions outside the shaded rectangle are logicals of the original WiFi driver. Actions inside the shaded rectangle are logicals of SBF. All actions are numbered in order along the work flow. For every UDP broadcast frame received by the WiFi radio, SBF extracts the UDP port number and checks with the system whether the UDP port is listened to or not (Linux kernel maintains a hash table for all UDP port numbers currently in use). If the UDP port is not listened to, this is a useless broadcast frame. SBF simply drops it without acquiring a wakelock; otherwise, SBF passes the frame and lets the WiFi driver continue with the processing.

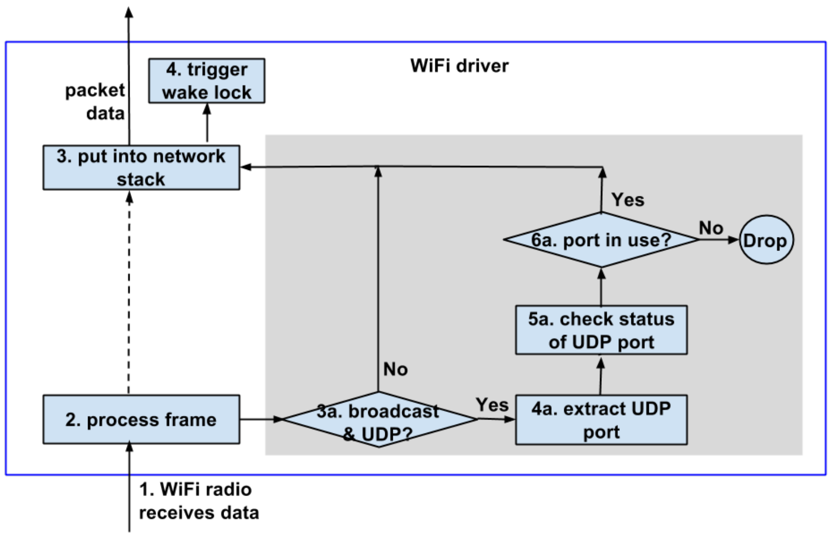

Figure 3.7: SBF work flow inside WiFi driver

Compared to the "receive-none" firmware broadcast filter, SBF is smarter in that it blocks all useless broadcast frames but lets the useful ones in. Thus, SBF does not impair functionalities. To analyze energy efficiency of SBF, we first build an energy model based on power profiles of Nexus One and Galaxy S4 phones. Then, we compare power consumption of SBF with that of the "receive-all" method based on trace driven simulation.

3.3.2 Energy Characterization

In Figure 1, we have already seen a typical process of receiving a WiFi broadcast frame during a smartphone's suspend mode: receiving broadcast frames, waking up from suspend, keeping awake for a while (one second if no traffic follows), and then going back to suspend. We zoom in the process and show a close look of the resume part and the suspend part in Figure 3.8.

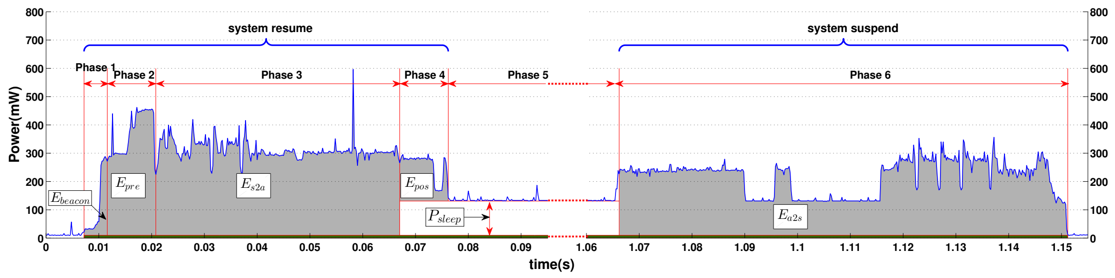

Figure 3.8: Power consumption during system resume and suspend (measured on Nexus One phone)

As marked in Figure 3.8, there are mainly six phases during the whole process. At first, the phone is in suspend mode with very low power consumption (~11mW). Then, the smartphone enters the following phases one by one.

- **Phase 1 - beacon.** This phase is the beginning of a Delivery Traffic Indication Message (DTIM) interval. During this phase, WiFi radio wakes up to receive the beacon frame carrying broadcast traffic information. If the beacon frame indicates that there is no frame buffered at the AP, the smartphone stays at suspend state. Otherwise, WiFi radio continues to receive data and enters Phase 2. Energy consumption during this phase is the energy consumed to receive the beacon frame E_{beacon}.

- **Phase 2 - pre-resume.** During this phase, WiFi radio receives the broadcast frame and sends an interrupt to the kernel. This triggers the system resume. Energy consumption during this phase is denoted as E_{pre}.

- **Phase 3 - resume.** The main task of this phase is system and device resume. At the end of this phase, WiFi driver processes the broadcast frame and starts the wakelock timer which expires in one second. Energy consumed during the whole phase is denoted as E_{s2a}.

- **Phase 4 - post-resume.** This is the post-resume phase. After this phase, if there are no more tasks to do and no more incoming WiFi data frames, the system becomes idle. However, as the wakelock timer is active, the system stays in active state until the timer expires. We calculate energy consumption of this phase E_{pos} as the extra power consumption when compared to power consumption during system idle.

- **Phase 5 - wake-lock.** During this phase, if there are more WiFi data frames coming in, WiFi driver can process them immediately as the system is in active state during the whole phase. At the same time, new incoming data frames will update the wakelock timer to one second. If there are no more data frames, the smartphone goes back to suspend state after the wakelock timer expires. The average power consumption of system idle during this phase is P_{sleep}. This is the phase that SBF tries to avoid or shorten. At the end of the post-resume phase or anytime during this phase, if SBF finds out that the broadcast data frame received is not listened to by any application and the "more data" bit in the frame header is not set (no more broadcast frames buffered at the AP), it goes directly to Phase 6.

- **Phase 6 - suspend.** This is the phase when the system transits from active state to suspend state. We denote the energy consumption as E_{a2s}.

During all phases, the small dark space right above the x-axis in Figure 3.8 is the average power consumption when the system is in suspend mode, denoted as $P_{suspend}$ ($\sim$11mW).

Energy consumption of handling WiFi broadcast frames during a smartphone's suspend mode can be divided into three aspects. (1) The first aspect E_1 is energy consumed by WiFi radio to receive WiFi frames, including idle listening, data transmission, and frame processing. (2) The second aspect E_2 is energy consumed by system state transfers, including transitions from suspend to active and transitions from active to suspend. (3) The third aspect E_3 is energy consumed in system idle state due to WiFi wakelock.

SBF is a software method. It does not stop WiFi radio from receiving any broadcast frame. So, SBF does not impact energy consumed by the first aspect. From Figure 3.1, we see this part of energy is not dominant when broadcast traffic is sparse. SBF increases energy consumption of the second aspect because SBF puts smartphone into suspend mode more aggressively than the "receive-all" solution. With SBF, the chance that a broadcast data frame comes in when the system is in suspend mode becomes higher. As a result, the frequency of system state transfer increases. This is the overhead of SBF. However, SBF reduces energy consumed in the third aspect because SBF reduces the time that the system spends at idle/active state after receiving a broadcast frame. During a smartphone's suspend mode, energy reduction of SBF in the third aspect is usually larger than the energy increase in the second aspect, which is why SBF saves energy. Later, in our evaluation results (Figure 3.9), we show how much energy is consumed in these three aspects respectively.

3.3.3 Energy Saving Modeling

Suppose that a smartphone receives n UDP broadcast frames during m beacon intervals. The i_{th} broadcast frame arrives at time t_i ($t_i > t_{i-1}$ for all $1 \leq i \leq n$) during beacon interval b_i ($1 \leq b_i \leq m$). The frame length is L_i and WiFi data rate is r_i. Beacon interval is τ_b and it is typically configured to be $102.4ms$ in real world WiFi networks. DTIM interval is set to 1, which means Delivery Traffic Indication Messages are sent with every beacon. WiFi wakelock timer length is τ_w, which is one second on the phones we used. In order to model energy saving of SBF, we need to calculate the following parameters for each frame F_i: system state when the broadcast frame arrives $s(i)$ (1 means suspend and 0 means active), start time of wakelock timer $tw(i)$, and wakelock effective time length $T_{wl}(i)$. Without loss of generality, and to simplify the model, we assume the first beacon interval starts at time 0 and the initial state of the smartphone system is suspend, which is

$$\begin{aligned} &s^a(1) = s^b(1) = 1 \\ &tw^a(1) = tw^b(1) = T_{beacon} + T_{pre} + T_{s2a} \end{aligned}$$

T_{beacon}, T_{pre}, and T_{s2a} are time lengths of the beacon phase, pre-resume phase, and resume phase, respectively. To differentiate variables under different methods, we use superscript 'a' for variables under the "receive-all" method and superscript 'b' for variables under SBF. Based on these two initial values, we can calculate the corresponding parameters for all following $n-1$ frames under the "receive-all" method and SBF, respectively.

Energy Consumption of "receive-all". If a frame i arrives after the suspend phase of frame $i-1$, then the system state upon frame arrival is suspend mode. Otherwise, the system is in active mode.

$$s^a(i) = \begin{cases} 0 & \text{, if } t_i \le tw^a(i-1) + \tau_w + T_{a2s} \\ 1 & \text{, otherwise} \end{cases} \tag{3.1}$$

If a frame arrives during the suspend phase of the previous frame, it interrupts the suspend process. We assume that suspend energy cost is evenly distributed across the suspend phase. Once a suspend process is interrupted, system transits back to active mode immediately without extra transition energy consumption. If $s^a(i) = 1$ for a frame i, then the system needs to transit from suspend mode to active mode to process the frame. So, $s^a(i)$ can also be used to indicate whether a broadcast frame triggers the system resume or not.

Wakelock timer for the $i_{th}(2 \leq i \leq n)$ broadcast frame starts at time

$$tw^a(i) = \begin{cases} t_i + L_i/r_i + T_{beacon} + T_{pre} + T_{s2a} & \text{,if } s^a(i) = 1 \\ max\{tw^a(i-1),\ t_i + L_i/r_i\} & \text{,if } s^a(i) = 0 \end{cases} \tag{3.2}$$

Wakelock effective time length for the $i_{th}(1 \leq i \leq n-1)$ broadcast frame is

$$T^a_{wl}(i) = min\{\tau_w, max\{0, t_{i+1} - tw^a(i)\}\} \tag{3.3}$$

With the above three variables, we calculate system state transfer energy consumption of "receive-all" method as

$$E^a_2 = (E_{pre} + E_{s2a} + E_{pos} + E_{a2s}) * \sum_{i=1}^{n} s^a(i) + E^a_{is} \tag{3.4}$$

where E^a_{is} is the energy consumed by interrupted suspends.

$$E^a_{is} = \frac{E_{a2s}}{T_{a2s}} * \sum_{i=2}^{n} T^a_{is}(i) \tag{3.5}$$

with

$$T^a_{is}(i) = \begin{cases} t_i - tw^a(i-1) - T^a_{wl}(i-1) & \text{, if } 0 < t_i - tw^a(i-1) - T^a_{wl}(i-1) < T_{a2s} \\ 0 & \text{, otherwise} \end{cases} \tag{3.6}$$

Then, the total energy consumed by the "receive-all" method is calculated as

$$E^a = E^a_1 + E^a_2 + E^a_3 \tag{3.7}$$

where E_2^a is already shown in Equation (3.4) and

$$E_1^a = P_{idle} * T_{idle} + P_r * \sum_{i=1}^{n} \frac{L_i}{r_i} + E_{fp} * N_b \tag{3.8}$$

$$E_3^a = P_{sleep} * \sum_{i=1}^{n} T_{wl}^a(i) \tag{3.9}$$

In Equation (3.8), P_{idle} is WiFi idle listening power consumption. P_r is the power consumption of WiFi when WiFi radio is receiving a frame. Since time to process a frame is very short, we assume that WiFi groups the processing of all data frames received during the same beacon interval. So, there is only a one-time frame processing energy cost during a beacon interval, denoted as E_{fp}. Also, we assume E_{fp} is constant across all beacon intervals. N_b is the number of beacon intervals with data frame(s). It is calculated as

$$N_b = \mid \phi \mid \quad \text{where} \quad \phi = \{i \mid \exists b_j = i \wedge 1 \leq i \leq m \wedge 1 \leq j \leq n\} \tag{3.10}$$

T_{idle} in Equation (3.8) is the total time that WiFi radio spends at idle listening between data transmission. Considering a beacon interval b_i, WiFi radio stays in idle listening between frame transmissions. If the "*more_data*" bit is set in the last frame of a beacon interval, WiFi radio also stays in idle listening after transmission of the last frame of this beacon interval and before start of the next beacon interval.

$$T_{idle} = \sum_{i \in \phi} [t_{x_i} + L_{x_i}/r_{x_i} - (b_i - 1) * \tau_b + d_{more}(x_i) * (b_i * \tau_b - t_{x_i} - L_{x_i}/r_{x_i})] - \sum_{i=1}^{n} L_i/r_i \tag{3.11}$$

with $x_i = max\{j \mid \ b_j = i \wedge 1 \leq j \leq n\}$

where $d_{more}(i)$ stands for the "more data" bit in the MAC layer header of the i_{th} frame.

Energy Consumption of SBF. When SBF operates in a WiFi driver, the system state upon frame arrival is

$$s^b(i) = \begin{cases} 0 & \text{, if } t_i < tw^b(i-1) + T^b_{wl}(i-1) + T_{a2s} \\ 1 & \text{, otherwise} \end{cases} \tag{3.12}$$

Also, we have wakelock start time

$$tw^b(i) = \begin{cases} t_i + L_i/r_i + T_{beacon} + T_{pre} + T_{s2a} & \text{,if } s^b(i) = 1 \\ max\{tw^b(i-1),\ t_i + L_i/r_i\} & \text{,if } s^b(i) = 0 \end{cases} \tag{3.13}$$

and wakelock effective time length

$$T^b_{wl}(i) = max\{0, d_{more}(i) * min(b_i * \tau_b, t_{i+1}) - tw^b(i)\} \tag{3.14}$$

where $d_{more}(i)$ stands for the "more data" bit in the MAC layer header of the i_{th} frame. If this bit is set, then SBF keeps the smartphone awake until the next broadcast frame or the next beacon interval, whichever comes first. Otherwise, SBF puts the smartphone into suspend state immediately.

Then, state transfer energy consumption by SBF is

$$E^b_2 = (E_{pre} + E_{s2a} + E_{pos} + E_{a2s}) * \sum_{i=1}^{n} s^b(i) + E^b_{is} \tag{3.15}$$

where E^b_{is} is energy consumed by interrupted suspends for SBF.

$$E^b_{is} = \frac{E_{a2s}}{T_{a2s}} * \sum_{i=2}^{n} T^b_{is}(i) \tag{3.16}$$

where

$$T^b_{is}(i) = \begin{cases} t_i - tw^b(i-1) - T^b_{wl}(i-1) & \text{, if } 0 < t_i - tw^b(i-1) - T^b_{wl}(i-1) < T_{a2s} \\ 0 & \text{, otherwise} \end{cases} \tag{3.17}$$

Similarly, the total energy consumption of SBF is

$$E^b = E_1^b + E_2^b + E_3^b \tag{3.18}$$

where E_2^b is already shown in Equation (3.15) and

$$E_1^b = E_1^a \tag{3.19}$$

$$E_3^b = P_{sleep} * \sum_{i=1}^{n} T_{wl}^b(i) \tag{3.20}$$

Energy Saving of SBF. With the total energy consumption of both SBF and "receive-all", we calculate energy saving percentage of SBF as

$$p = \frac{E^a - E^b}{E^a} \tag{3.21}$$

3.4 SBF Performance Evaluation

We evaluate performance of SBF in terms of energy efficiency and delay through trace driven simulation. The traces we used are the five traces we introduced in Section 3.2.2. With a Monsoon power meter, we measure and profile the power/energy consumption of two phones: Nexus One and Galaxy S4. The values are listed in Table 3.3. To demonstrate the energy efficiency of SBF, we compare energy consumption of SBF to the "receive-all" method and an oracle lower bound. To calculate this lower bound, we assume that SBF has the information of future frame arrival time. So, it can decide to keep the system active until the next broadcast frame when the wakelock energy consumption $E_3(i)$ is less than state transfer energy cost $E_2(i)$ for the current frame i (benefit is less than overhead). This also gives the upper bound of energy savings.

	E_{beacon}	E_{pre}	E_{s2a}	E_{pos}	E_{a2s}
NexusOne	0.41	2.72	13.88	1.11	17.66
S4	0.56	3.08	34.54	20.65	85.8
	E_{fp}	P_{idle}	P_{sleep}	$P_{suspend}$	P_r
NexusOne	1.022	370	125	11	530
S4	5.7	405	130	15	538
	T_{beacon}	T_{pre}	T_{s2a}	T_{pos}	T_{a2s}
NexusOne	0.0045	0.009	0.046	0.009	0.086
S4	0.0053	0.0114	0.044	0.039	0.165

Table 3.3: Energy profiles
energy in mJ, power in mW, time in *second*

3.4.1 Energy Saving

Energy savings of SBF are shown in Figure 3.9. In order to normalize energy consumptions across different traces, we translate energy consumption calculated with Equation (3.7) and (3.18) to average power consumption. Also, we divide the power consumption into three different aspects as presented in those two equations. For each trace, we plot three bars. The left bar is power consumption of the default "receive-all" method. In the middle is power consumption of SBF. The right bar is oracle lower-bound power consumption. The values above the bars are power saving percentages. The upper values are power savings of SBF and the lower values are power savings of the oracle method we defined.

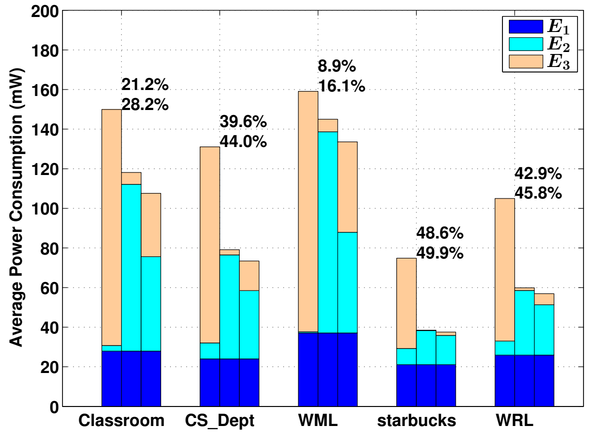

Figure 3.9: Power consumptions of different methods (Nexus One)
(left bar:"receive-all", middle bar: SBF, right bar: oracle.)

From Figure 3.9, we observe that SBF saves considerable power for all traces on Nexus One phone. The largest saving is 49.9% with the Starbucks trace while the smallest saving is 8.9% with the W&M college library trace. Another observation is that the power savings of SBF are very close to power savings of the oracle method. Referring to Figure 3.2, we notice that, in all five traces, SBF saves less energy when there are more broadcast traffic in the network.

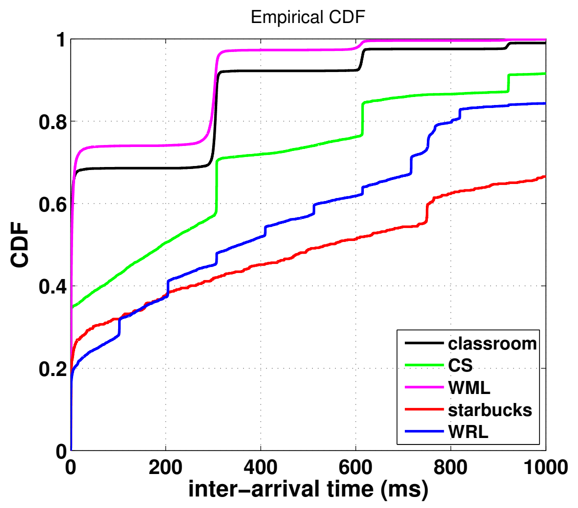

Figure 3.10: CDF of inter-arrival time of broadcast frames

In order to better understand energy saving differences across different traces, we show CDF of inter arrival time of broadcast frames in each trace in Figure 3.10. As can be observed from the figure, Starbucks trace and WRL trace have obviously longer frame inter arrival time than the other three traces. In this case, the "receive-all" method suffers because most of the smartphone's idle waiting turns out to be a waste as nothing happens. For the same case, SBF benefits the most as it reduces a lot of wakelock energy while only incurs a small amount of state transfer overhead. Figure 3.10 also shows that, for the college library (WML) and classroom traces, most of the inter-arrival times are less than 100ms: 69% and 74% respectively. This indicates that broadcast frames tend to arrive in batches. This is easy to understand as AP buffers these broadcast frames and sends them out together in the next DTIM interval.

We also evaluate performance of SBF with energy profile of Galaxy S4. For this phone, SBF only saves energy ($\sim$ 12.3%) under the Starbucks trace. This is because state transfer energy cost is quite high on S4 phone, as can be seen from Table 3.3. The overhead is too heavy to be counteracted by wakelock energy reduction of SBF when the broadcast traffic is not sparse. Even with the oracle solution, power saving is only 1.1% and 5.8% under the W&M college library trace and classroom trace respectively.

3.4.2 Delay Overhead

The delay overhead of SBF consists of two parts. (1) SBF takes the frame from WiFi driver, extracts the port number and looks it up in a hash table to decide whether to drop or pass the frame. So, the first part of delay is the *local processing delay.* (2) When a broadcast frame arrives during a smartphone's suspend mode, SBF needs to first wake up the system. So, the second part of delay is the *waking up latency*, which is around 60ms. Note that, this delay only impacts frames which trigger the system resume and it also incurs under the "receive-all" method. Besides, SBF works during a smartphone's suspend mode where user is not delay sensitive to the traffic. Therefore, this wake up latency is acceptable for suspend mode. So, our delay evaluation here will focus on the local processing delay, as it impacts every broadcast frame received by WiFi driver.

	mean (ms)	**stddev**
SBF	1.1464	0.0036
Receive-all	1.1343	0.0038

Table 3.4: Local processing delay of Software Broadcast Filter (λ=5)

To measure this local processing delay, we implement the work flow shown in Figure 3.7 in WiFi driver of Nexus One. During the experiments, we intentionally create 100 UDP sockets on the smartphone. Then, we send 1000 UDP broadcast packets through the local area network to the smartphone. We log the time (t_1) when a frame enters step 3a in Figure 3.7, and the time (t_2) when the frame is received by the application. Then, we calculate the mean and standard deviation of $t_2 - t_1$ from eight repeated runs. As indicated in Table 3.4, the local processing is very fast. With 100 UDP ports in use, the local processing delay only increases by 1.07%.

3.5 Conclusion and Future Work

This work studies different ways to handle WiFi broadcast traffic on modern smartphones during suspend mode. By examining WiFi drivers on four Android smartphones, we find that modern smartphones face the dilemma of handling broadcast frames during suspend mode: either receive all UDP broadcast frames suffering high power consumption or receive none UDP broadcast frame sacrificing functionalities. We analyze wireless traces under five different scenarios and show that the "receive-none" solution blocks both useless and useful broadcast frames. For the "receive-all" solution, we measure the impact of WiFi broadcast traffic on power consumption of smartphones in suspend mode. Results show that ARP broadcast traffic only slightly increases the power consumption due to ARP offload. However, power consumption increases dramatically as UDP traffic volume increases.

Based on these findings, we propose Software Broadcast Filter (SBF) for fine-grained UDP broadcast frame processing. Compared to "receive-none" approach, SBF does not impair functionalities of smartphone applications as it only blocks useless broadcast frames. Compared to "receive-all" approach, SBF saves up to 49.9% energy consumption. Meanwhile, SBF only increases the local processing delay by 1.07%.

Software broadcast filter is not perfect but opens the door for fine-grained WiFi broadcast filter research in smartphones. As future work, we plan to improve SBF in the following ways. First, we plan to adapt SBF to reduce state transfer overhead. For example, SBF can decide how long to keep awake according to the current broadcast traffic volume. Second, we will combine software broadcast filter and firmware broadcast filter, switching between them according to the current context. Finally, SBF works after a WiFi radio receives a frame and the system already switches to active mode. In future, we plan to leverage a low power radio, such as Bluetooth, to wake up the smartphone only when necessary.

Chapter 4

HIDE: AP-assisted Broadcast Traffic Management to Save Smartphone Energy

4.1 Introduction

WiFi is among the top biggest culprits for battery drain on smartphones, mainly due to two factors. First, WiFi consumes considerable amount of power on smartphones. For example, when WiFi is turned off, power consumption of Galaxy S4 is $\sim 130mW$ with system idle and screen off. When WiFi is receiving data, the power consumption adds up to $\sim 538mW$. Second, the amount of data traffic over WiFi is significant on smartphones. Global mobile data traffic grew 69 percent in 2014 and is expected to grow even faster [89]. Meanwhile, WiFi has been the major interface for data communication. A report shows that WiFi accounts for 73% of total traffic on Android smartphones [90]. With mobile data offloading [91, 89], more and more smartphone traffic will flow over WiFi.

Reducing WiFi energy consumption can effectively boost smartphone battery life. Generally, energy consumed by WiFi is spent for data downloading/uploading desired by users. In some cases, unwanted (or useless) traffic may become rampant and dominate WiFi energy consumption, such as malicious traffic from attackers (e.g., denial-of-service or energy attackers) [11, 28] and background broadcast data traffic that is useless to a smartphone [92] (e.g., WiFi broadcast frames for printer service discovery). Thus, to reduce WiFi energy consumption, we seek to cut down energy waste incurred by unwanted WiFi traffic.

Existing literature mainly focuses on how to receive desired traffic in a more energy efficient way, e.g., traffic scheduling or traffic shaping [93, 20, 94, 32]. With these methods, a client has no choice of what should be sent to it. In the previous chapter, we propose Software Broadcast Filter (SBF) to filter out useless broadcast frames in the WiFi driver after they are received by smartphones. In this way, useless broadcast data frames are still received by smartphones. Unnecessary energy has already been consumed to receive and process these useless data frames. What is worse, if a smartphone is in suspend mode (i.e., the system-on-chip (SoC) of the device including CPU, ROM, and the micro-controller circuits for various components are suspended [10]) when a useless frame arrives, the device still needs to switch to active mode in order to wake up the CPU and other resources to do the processing.

In this work, we improve smartphone energy efficiency by reducing energy wasted on useless WiFi broadcast traffic[1]. Specifically, we propose to filter out useless UDP-padded broadcast frames (MAC layer WiFi broadcast data frames with UDP payload) at APs before they are received by smartphones. Thus, no energy will be wasted on smartphones to receive or process these useless broadcast frames. We focus on broadcast traffic because broadcast traffic is normal traffic that naturally exists in almost every network. In contrast, malicious unicast traffic is abnormal traffic which only exists in the targeted network. It is trivial to extend our system to incorporate useless unicast traffic. Although it is also interesting to work on other types of WiFi broadcast frames, in this work, we focus on UDP-padded broadcast frames as they are the majority of WiFi broadcast data frames [92]. In the rest of this chapter, unless specifically stated, broadcast frame/traffic means UDP-padded broadcast frame/traffic. Also, we target at

[1]In this chapter, we use unwanted traffic and useless traffic interchangeably.

smartphones in suspend mode because power consumption is very low in this state. If a data frame arrives during a smartphone's suspend mode, the smartphone needs to switch to high power active mode and stays in that mode for a while. The energy impact of useless traffic on smartphones in suspend mode is much more serious than the impact on smartphones in active mode.

However, in order to filter out useless broadcast traffic at APs, two research questions need to be answered. The first question is *how to differentiate between useful and useless broadcast traffic.* APs have no idea about what broadcast frames are needed by clients. Moreover, the definition of "useful" and "useless" is different across clients. A broadcast frame which is useless to a client may be useful to another client. The second question is *how to manage useless broadcast traffic in an energy efficient way.* An AP cannot simply drop a useless broadcast frame for one client as it may be useful to other clients. Currently, the 802.11 network protocol assumes that broadcast frames are to be received by all clients. So, an AP uses only one bit in beacon frames to indicate any buffered broadcast frames to all clients. This cannot deliver client-specific notifications. Besides, communication between a client and AP has cost. It incurs energy overhead as well as brings extra traffic to the network which may decrease network throughput.

In this work, we answer the above two research questions. Our main idea is to enable cooperation between an AP and smartphone clients. Clients tell the AP what are needed. With the information from clients, the AP identifies useless broadcast frames for each client. Then, traffic notifications sent out within beacon frames are extended to offer one bit for each client. So, the AP can indicate to each client only useful broadcast frames. With our solution, no energy is wasted to receive useless broadcast frames. Moreover, if there are no useful frames, a client does not even need to wake up from suspend mode. Thus, our solution remarkably reduces the energy wasted on unwanted traffic. Our main contributions are:

- We design a framework, namely HIDE, working between an AP and smartphone clients to reduce smartphone energy wasted on useless broadcast traffic. In our system, broadcast frames are managed at the AP. The AP hides presence of useless broadcast frames from each client. As a result, smartphones in suspend mode do not need to receive and wake up to process useless broadcast frames.

- We demonstrate the energy saving of our system with energy modeling and trace-driven simulation. With five broadcast traffic traces collected in five different real-world scenarios, we show that the HIDE system saves 34%-75% smartphone energy when 10% of the broadcast traffic are useful to the smartphone. Our overhead analysis demonstrates that our system has negligible impact on network capacity and packet round-trip time.

4.2 Background

In 802.11 networks, an AP periodically sends out a beacon frame [95] (shown as in Figure 4.1). Every client under the AP must periodically wake up the WiFi radio and receive beacon frames.

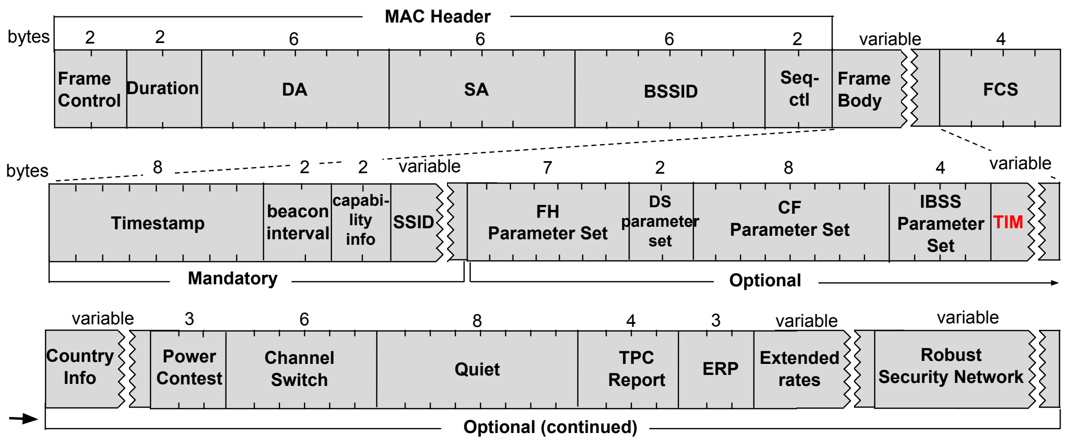

Figure 4.1: Structure of beacon frame

The AP buffers unicast frames for every client with WiFi radio in Power Saving (PS) mode. Notifications of unicast frames buffered at the AP are sent out in every beacon frames with a TIM (Traffic Indication Map) information element, shown in Figure 4.2. The notification data is encoded in the Partial Virtual Bitmap field, one bit for each

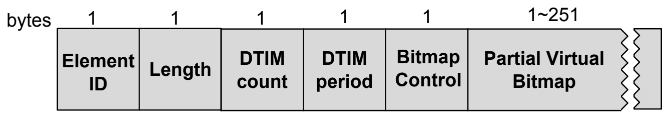

Figure 4.2: Traffic Indication Map information element

client. If there are unicast frames for it, the client must send a Power Save Poll (PS-Poll) control frame to retrieve each buffered frame from the AP.

The AP also buffers all broadcast/multicast frames as long as there is one client with WiFi radio in Power Saving Mode (PSM). Notifications of buffered broadcast/multicast frames are sent out with a special type of TIM called DTIM (Delivery Traffic Indication Map). This DTIM is generated within beacon frames at a frequency specified by the DTIM period (interval). In Figure 4.2, DTIM period is represented in unit of beacon intervals. Typical values are $1 \sim 3$. The DTIM count field indicates how many beacons must be transmitted before receiving the next DTIM. The DTIM count is zero when we reach a DTIM. The first bit of the Bitmap Control field is used to indicate whether broadcast/multicast frames are buffered at AP or not. If there are any broadcast/multicast frames buffered, i.e., the first bit of the Bitmap Control is set to one, every client must listen to the channel and receive the broadcast/multicast frames. After a DTIM, the AP sends the multicast/broadcast data on the channel following the normal channel access rules (CSMA/CA).

4.3 Proposed System

In this section, we present the proposed system. Our main idea is to use UDP ports to differentiate useless and useful UDP-padded broadcast frames. If the UDP port of a broadcast frame is opened (listened to by a process) on a client, then the AP considers this broadcast frame useful to the client; otherwise, the AP considers this broadcast frame useless to this client. Then in traffic indication, the AP hides the presence of useless broadcast frames from corresponding clients and only tells the presence of useful broadcast frames. We call the proposed system HIDE.

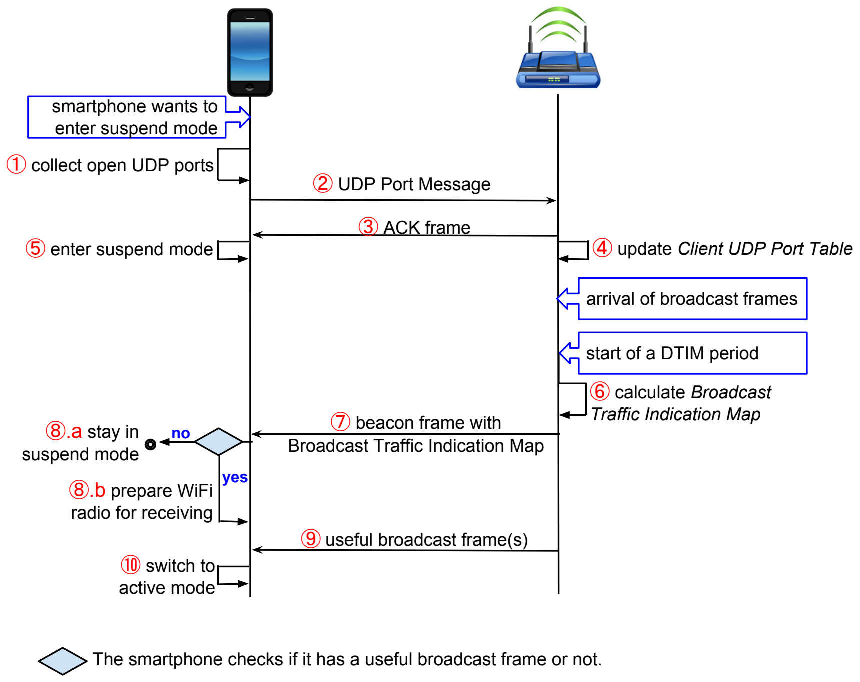
smartphone wants to enter suspend mode
① collect open UDP ports
② UDP Port Message
③ ACK frame
④ update *Client UDP Port Table*
⑤ enter suspend mode
arrival of broadcast frames
start of a DTIM period
⑥ calculate *Broadcast Traffic Indication Map*
⑦ beacon frame with Broadcast Traffic Indication Map
⑧.a stay in suspend mode
no
yes
⑧.b prepare WiFi radio for receiving
⑨ useful broadcast frame(s)
⑩ switch to active mode
The smartphone checks if it has a useful broadcast frame or not.

Figure 4.3: System Overview

4.3.1 System Overview

Figure 4.3 shows an overview of how the system works. Every time before a smartphone enters suspend mode, it collects all UDP ports currently opened and sends them to the AP in a *UDP Port Message*. Upon receiving a *UDP Port Message*, the AP responds with an ACK frame. At the same time, the AP stores all UDP ports received from clients in a hash table (*Client UDP Port Table*) and keeps the table updated with the latest data from clients. After receiving the ACK frame from the AP, the client now enters into suspend mode. During suspend mode, the smartphone screen is off. The CPU, ROM, and the micro-controller circuits for various components are suspended [10]. However, the WiFi chip is still able to receive beacon frames and check if there are any frames buffered at the AP. When a DTIM period starts, the AP calculates a flag for each client based on the *Client UDP Port Table*. This flag indicates whether there are useful broadcast frames buffered for the corresponding client or not. These flags are carried in the *Broadcast Traffic Indication Map* (BTIM) information element in a beacon frame. Every client checks its exclusive bit in the BTIM information element. If this bit is not set, then no useful broadcast frames are buffered at the AP. The client stays in suspend mode as long as there are no unicast frames buffered. If the corresponding bit is set, then the client has useful broadcast frames buffered at the AP. No matter there are unicast frames buffered or not, the client needs to prepare its WiFi radio for receiving data. And after data is received by the WiFi radio, the client needs to switch to active mode, i.e., waking up the CPU and other resources, to process the frames.

In the following subsections, we present more details of the proposed system about (1) how UDP port information is sent from clients to the AP with a UDP Port Message, (2) how the AP determines whether a client has useful broadcast frames, and (3) how broadcast traffic indication flags are delivered to clients in a beacon frame.

4.3.2 UDP Port Information Synchronization

In our HIDE system, an AP uses UDP ports to differentiate *useless* and *useful* broadcast frames. This policy requires that the AP has the information of all open UDP ports on each smartphone. As this information is only available on the client itself, a client needs to send the data to the AP. The structure of this frame is shown in Figure 4.4. It is called UDP Port Message.

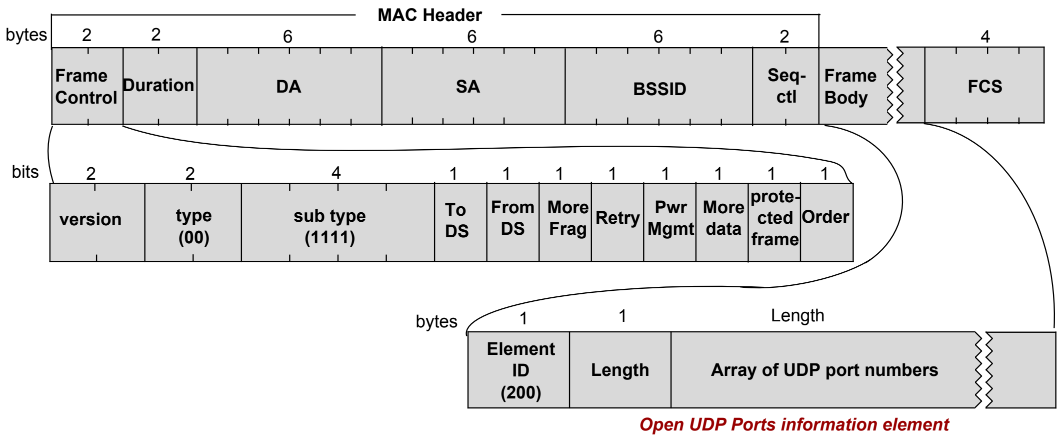

Figure 4.4: Frame structure of UDP port message

A UDP Port Message is a WiFi management frame (type=00, subtype=1111) sent from a client to an AP, reporting a set of UDP ports opened on the client. To reduce the size of the message, a client only reports UDP ports associated with the source address *INADDR_ANY*. To carry the UDP port information, we add a new information element, named *Open UDP Ports* information element (as in Figure 4.4) to the standard 802.11 protocol. We use 200, which is reserved and unused by 802.11 protocols, as the element ID for *Open UDP Ports* information element. This information element contains an array of UDP port numbers. Each UDP port number takes 2 bytes. Upon receiving a UDP Port Message, the AP responds with an ACK frame, so that the client knows the message is successfully delivered. If an ACK frame is not received by the client, the normal retransmission operation applies to the UDP Port Message.

Each time before a client enters suspend mode, it sends a UDP port message to the AP. If there is a change made to the set of open UDP ports on a client, such as adding a new open UDP port or deleting an existing open UDP port, the system should definitely have already resumed to active mode to process such an event. Next time when the system is about to enter suspend mode, a new UDP port message will be sent to the AP with the latest UDP port information. In this way, an AP can always get the updated open UDP ports from a client.

4.3.3 Traffic Differentiation at AP

A broadcast frame may be useful to one client while being useless to another client. So, in the HIDE system, the AP maintains a broadcast flag (one bit) for every associated client. If there is any useful broadcast frame buffered for a client, the corresponding broadcast flag is set to 1; otherwise, the broadcast flag is set to 0.

Open UDP ports of all clients are stored in a hash table (*Client UDP Port Table*). With this hash table, the AP then calculates the broadcast flag for each client. The procedure is described in Algorithm 1. Right before transmission of a beacon frame representing the start of a DTIM period, the AP resets all broadcast flags to 0. Then, for every broadcast frames currently buffered, the AP extracts the destination UDP port

Algorithm 1 Calculating broadcast flags

```
Require: broadcast frames currently buffered at the AP
         Client UDP Port Table
Ensure: broadcast flags for clients
 1: broadcast_flags[ ] ← {0}        // initialize the array of broadcast_flags to all 0
 2: for all broadcast frames currently buffered do
 3:     $O$ ← UDP port number from frame data
 4:     $C$ ← list of clients by Client_UDP_Port_Table lookup with key $O$
 5:     for $c_i$ in $C$ do
 6:         $k$ ← AID of $c_i$
 7:         $m \leftarrow \lceil k/8 \rceil - 1$        // octet number
 8:         $n \leftarrow k - 8 * m$        // bit number in the target octet
 9:         (the $n^{th}$ bit of broadcast_flags[m-1]) ← 1;
10:     end for
11: end for
```

number from the frame data. Then, the AP looks up the hash table using the UDP port number as the key and gets a list of clients C which have this UDP port opened. After that, the AP sets the broadcast flags for all clients in C to 1.

4.3.4 Broadcast Traffic Notification

The current traffic notification uses only one bit to notify all clients of the presence of any broadcast frames. To enable fine-grained notification of buffered UDP broadcast frames, we add an information element, shown in Figure 4.5, in the beacon frame.

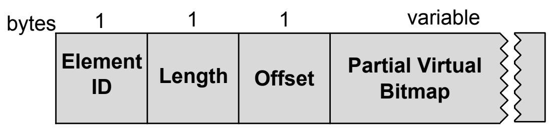

Figure 4.5: Broadcast Traffic Indication Map information element

We use 201 as the element ID for our *Broadcast Traffic Indication Map* (BTIM) information element. The *Length* field indicates the total length of the subsequent fields in bytes. The *Partial Virtual Bitmap* is constructed in a similar way as in TIM information element [96] in Figure 4.2. The Partial Virtual Bitmap consists of the broadcast flags introduced in the previous subsection. Each bit corresponds to an Association ID (AID) of a client. For example, the 1st bit is for the client with AID 1. If a bit is set to 1, then the corresponding client has useful broadcast frames; otherwise, the client does not have useful broadcast frames.

To shorten the length of this information element and reduce the protocol overhead, we do not put all flags for all clients in this bitmap. Instead, we compress the data and only put part of the flags in this field. An example is shown in Figure 4.6. Suppose the first N_1 (N_1 is an even number) bytes of the bitmap are all 0 and all bytes after the $(N_2)^{th}$ byte are also 0, then we can only put the $(N_1)^{th}$ to $(N_2)^{th}$ bytes in the Partial Virtual Bitmap. At the same time, we use the *Offset* field to indicate the start of the partial bitmap: $\mathit{Offset} = N_1$.

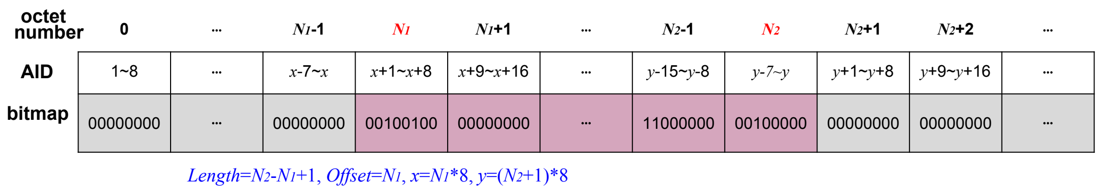

octet number	0	...	N_1-1	N_1	N_1+1	...	N_2-1	N_2	N_2+1	N_2+2	...
AID	1~8	...	x-7~x	x+1~x+8	x+9~x+16	...	y-15~y-8	y-7~y	y+1~y+8	y+9~y+16	...
bitmap	00000000	...	00000000	00100100	00000000	...	11000000	00100000	00000000	00000000	...

Length=N_2-N_1+1, *Offset*=N_1, x=N_1*8, y=(N_2+1)*8

Figure 4.6: An example of the Construction of Partial Virtual Bitmap

For clients who do not support this AP-assisted broadcast traffic management, they can still follow the standard 802.11 protocol: check the first bit of Bitmap Control field in the TIM information element (as introduced in the Background section) and discard our BTIM information element. So, our system works with co-existence of HIDE-enabled devices and legacy devices.

4.4 Energy Modeling

In this section, we present the energy modeling for the HIDE system. Table 4.1 lists all input variables used in the energy model.

Suppose an AP sends out n UDP broadcast frames at time t_1, t_2, ..., t_n, respectively. Also, suppose frame i is sent during beacon interval b_i with a length of L_i and a data rate of r_i. In the original system, a client receives and wakes up for every broadcast frame sent out by the AP. However, with the HIDE system, a client only receives and wakes up for broadcast frames that are useful to it. Let u_i denote whether a UDP broadcast frame i is useful to a client or not. If $u_i = 1$, then the i^{th} UDP broadcast frame is useful to the client; otherwise, the i^{th} UDP broadcast frame is useless to the client. Based on this, the UDP broadcast traffic from the AP, in the perspective of a HIDE-enabled client, is

$$\begin{aligned} n\prime &= \textstyle\sum_{i=1}^{n} u_i \\ t_i\prime &= \begin{cases} t_i & \text{, if } u_i = 1 \\ null & \text{, if } u_i = 0 \end{cases} \end{aligned} \tag{4.1}$$

With the filtered UDP broadcast traffic, the total energy consumed by the whole system for all the n UDP broadcast frames can be calculated as

$$E = E_b + E_f + E_{wl} + E_{st} + E_o \tag{4.2}$$

where E_b is the energy consumed to receive all beacon frames, E_f is the energy consumed to receive all broadcast data frames, E_{st} is the energy consumed by system state transfer, E_{wl} is the energy consumption during system idle periods due to WiFi wakelocks, and E_o is the energy overhead of the HIDE system.

1) System state. Energy consumed for a UDP broadcast frame depends on the system state when the frame arrives. Thus we derive the system state first. For each UDP broadcast frame received, a wakelock of duration τ is acquired in the WiFi driver. This wakelock keeps the whole device awake and allows time for applications to process and respond to this frame. Also, due to the wakelock, subsequent frames can be received immediately.

If a UDP broadcast frame arrives during the wakelock of the previous frame, it renews the wakelock time and resets the *time-to-expire* to τ. If a UDP broadcast frame arrives when the system is in suspend mode, the WiFi driver needs to first wake up the operating system. If a UDP broadcast frame arrives during system resume operation, activation of the WiFi wakelock will be delayed until the resume operation is finished.

Let $s(i)$ stands for the operating system state when frame i arrives. $s(i) = 0$ means

Var.	Explanation	Var.	Explanation
	WiFi Traffic Profile		
n	number of UDP broadcast frames sent by AP	l_i	length of UDP broadcast frame i
t_i	transmission start time of UDP broadcast frame i	r_i	data rate of UDP broadcast frame i
b_i	beacon interval index for UDP broadcast frame i	L_i	length of beacon frame i
L_{phy}	length of the PHY layer header i	T_b	beacon interval
L_{mac}	length of the MAC layer header i	u_i	=1 if UDP broadcast frame i is useful to the client
	Energy/Power Profile		
τ	WiFi wakelock duration	E_b^u	energy per byte for receiving beacon frames
T_{rm}	duration of system resume	E_{rm}	energy consumption of system resume operation
T_{sp}	duration of system suspend	E_{sp}	energy consumption of system suspend operation
P_r	WiFi power consumption when receiving data	P_{sa}	system power consumption with OS active and WiFi sleep
P_t	WiFi power consumption when sending data	P_{ss}	system power consumption during suspend mode
P_{idle}	WiFi power consumption during idle listening		
	HIDE system Profile		
f	frequency of sending UDP Port Message	r_i^m	data rate of the i^{th} UDP port message from the client
N_i	number of UDP ports in the i^{th} UDP port message	L_i^b	length of BTIM information element in beacon frame i

Table 4.1: Input variables of energy model

the system is in suspend mode. $s(i) = 1$ means the system is in active state, or is resuming or suspending. Assume the wakelock for frame i starts at time $t_r(i)$, then

$$t_r(i) = \begin{cases} t_i + l_i/r_i + T_{rm} & \text{, if } s(i) = 0 \\ \max\{t_i + l_i/r_i,\ t_r(i-1)\} & \text{, otherwise} \end{cases} \tag{4.3}$$

where T_{rm} is the duration of system resume operation. Immediately after a system resume operation is finished, the delayed wakelocks are activated one by one in a self-renewal way. Since all these happen in a very short time, we combine them into one single wakelock. Active duration of the wakelock for frame i is

$$t_{wl}(i) = \min\{t_r(i+1) - t_r(i),\ \tau\} \tag{4.4}$$

Then, we calculate the system state $s(i)$. Without loss of generosity, assume $s(1) = 0$.

For $2 \leq i \leq n$

$$s(i) = \begin{cases} 0 & \text{, if } t_i + l_i/r_i \geq t_r(i-1) + \tau + T_{sp} \\ 1 & \text{, otherwise} \end{cases} \tag{4.5}$$

where T_{sp} is the duration of system suspend operation.

2) Energy consumption of receiving beacon frames. The first item E_b in Eq. (4.2) is calculated as

$$E_b = E_b^u * \sum_{b_1 \leq i \leq b_n} L_i \tag{4.6}$$

where E_b^u is the energy consumption per byte of WiFi radio when receiving beacon frames and L_i is the length of the i^{th} beacon frame.

3) Energy consumption of receiving broadcast data frames. This second item in the right end of Eq. (4.2) E_f is calculated as

$$E_f = P_r * \sum_{i=1}^{n} tt(i) + P_{idle} * (\sum_{i=1}^{n} td(i) + \sum_{b_1 \leq i \leq b_n} tf(i)) \tag{4.7}$$

where P_r and P_{idle} are the power consumption of WiFi radio when receiving data and idle listening, respectively. $tt(i)$ is the transmission time of the i^{th} UDP broadcast frame, $td(i)$ is the length of time that the WiFi driver spends in idle listening state right after receiving the i^{th} UDP broadcast frame, and $tf(i)$ is the idle listening time between the i^{th} beacon frame and the first UDP broadcast frame in the i^{th} beacon interval. So,

$$tt(i) = \frac{l_i}{r_i} \tag{4.8}$$

$$tf(i) = \min_{j \in \{k | b_k = i\}} t_j - tb(i) \tag{4.9}$$

$$td(i) = \{\min\{t_{i+1}, tb(b_i + 1)\} - t_i - l_i/r_i\} * d_{more}(i) \tag{4.10}$$

where $d_{more}(i)$ is the 'more data' bit in the i^{th} UDP broadcast frame. If this bit is set, WiFi radio listens to the channel for future broadcast frames. $tb(i)$ is the start time of the i^{th} beacon interval and T_b is the beacon interval. Without loss of generosity, we assume $tb(1) = 0$. Then,

$$tb(i) = (i - 1) * T_b \tag{4.11}$$

4) Energy consumption of system idle due to WiFi wakelocks. E_{wl} in Eq. (4.2) is calculated as

$$E_{wl} = P_{sa} * \sum_{i=1}^{n} t_{wl}(i) \tag{4.12}$$

where P_{sa} is the power consumption when the system is active and idle. t_{wl} is the duration of wakelock for frame i being active which is presented in Eq. (4.4).

5) Energy consumption of state transfers. E_{st} in Eq. (4.2) is calculated as this.

$$E_{st} = (E_{rm} + E_{sp}) * \sum_{i=1}^{n} [1 - s(i)] + E_{sp} * \sum_{i=2}^{n} y(i) \tag{4.13}$$

where E_{rm} and E_{sp} are the energy consumption of system resume and suspend operations, respectively. It may happen that a WiFi driver tries to acquire a wakelock when the system suspend operation is in execution. In this case, the system aborts the suspend operation. Let $y(i)$ denote the time portion of system in suspend operation upon arrival of frame i $(2 \leq i \leq n)$, then

$$y(i) = \frac{\max\{0,\ t_r(i) - t_r(i-1) - t_{wl}(i-1)\} * s(i)}{T_{sp}} \tag{4.14}$$

6) Energy overhead. Energy overhead of our HIDE system contains two parts: energy consumed by transmission of UDP port messages E_o^1 and energy consumed by receiving extra bits in beacon frames E_o^2.

$$E_o = E_o^1 + E_o^2 \tag{4.15}$$

In the HIDE system, we add a Broadcast Traffic Indication Map information element in the beacon frame. So, the extra energy consumed to receive beacon frames in a HIDE system is

$$E_o^1 = E_b^u * \sum_{b_1 \leq i \leq b_n} L_i^b \tag{4.16}$$

where L_i^b is the total length of BTIM information element in beacon frame i.

In the HIDE system, a client sends out UDP Port Messages to synchronize open UDP ports with AP. This part of energy overhead, denoted as E_o^2, is calculated as

$$E_o^2 = M * P_t * \sum_i \frac{L_i^m}{r_i^m} \tag{4.17}$$

where M is the number of UDP Port Messages sent out by the client.

$$M = f * T_b * (b_n - b_i + 1) \tag{4.18}$$

In Eq. (4.17), P_t is the power consumption of WiFi radio when sending data. r_i^m is the data rate of the i^{th} UDP port message from a client and L_i^m is its length. From Figure 4.4, we see that it includes the PHY and MAC layer headers, 2 bytes of fixed fields plus a series of UDP port. Each UDP port takes 2 bytes. With N_i UDP ports in the message, we have

$$L_i^m = L_{phy} + L_{mac} + 2 + 2 * N_i \tag{4.19}$$

4.5 Network Capacity and Delay Analysis

The proposed system impacts network throughput and delay in two ways. First, in our system, AP is in charge of managing broadcast traffic. Frame processing at AP is slowed down. Consequently, packet delay is increased. Second, extra management frames (UDP Port Message) are introduced in the system. Protocol overhead is increased. Consequently, the network capacity, which is the maximum network throughput, is decreased. In this section, we quantify the impact of our system on network capacity and delay.

4.5.1 Network Capacity

Bianchi et al. [97] model the maximum network throughput that can be achieved in an 802.11 network with different numbers of nodes. We borrow their model to calculate the network capacity, denoted as S. Let Φ be the network throughput defined in [97], which is defined as the fraction of time the channel is used to successfully transmit payload bits. And let r be the average WiFi data rate (in bits/s) during transmission of payload bits. Then, the network capacity (in bits/s) of the original 802.11 network is

$$S_1 = \Phi * r \tag{4.20}$$

Assume that there are N clients in the network and the percent of clients with HIDE enabled is p. With our system, the total number of UDP Port Messages sent out per unit time by all clients is

$$n_u = N * p * f \tag{4.21}$$

where f is the frequency of sending UDP Port Messages from a client, the same as defined in Table 4.1. Meanwhile, in the original network, the number of data frames transmitted per unit time is

$$n = S_1/L \tag{4.22}$$

where L is the average length of payload bits in a data frame. Let L^m denote the average length of UDP Port Messages. Then, the network capacity with our HIDE system is

$$S_2 = (n - n_u * \lceil \frac{L^m}{L} \rceil) * L \tag{4.23}$$

Therefore, the percentage of decrease in network capacity is

$$c = 1 - S_2/S_1 \tag{4.24}$$

4.5.2 Network Delay

Delay overhead of the HIDE system is mainly due to maintenance of the Client UDP Port Table and table lookup for identifying useful broadcast frames. Here, we calculate the extra network delay incurred by the HIDE system through approximate estimation.

For each UDP port message received, an AP needs to refresh the table by deleting the old ports from the hash table and inserting the new ports to the table. Assume the original round-trip time of a packet is D. Let n_o be the average number of open UDP ports in a client. With N as the total number of clients in the network, p as the percent of clients with HIDE enabled, and f as the sending rate of UDP Port Messages from a HIDE-enabled client, frame processing time at the AP will be increased by

$$t_1 = f * D * N * p * n_o * (\tau_{del} + \tau_{ins}) \tag{4.25}$$

where τ_{del} and τ_{ins} are the durations of a delete operation and an insert operation, respectively.

At the start of each DTIM period, for each UDP broadcast frame currently buffered, an AP needs to look up the UDP port from the hash table. Frame processing time at the AP will be further increased by

$$t_2 = n_f * \tau_{lp} \tag{4.26}$$

where τ_{lp} is the duration of a table lookup operation and n_f is the average number of broadcast frames buffered at AP during each DTIM period.

Then, the percentage of increase in network delay is

$$d = (t_1 + t_2)/D \tag{4.27}$$

Here, the delay overhead calculated is actually the upper bound, because the processing time of UDP Port Messages at the AP may overlap with part of the packet round-trip time, such as the channel access time and packet forwarding time in the backbone network. Also, a packet exchange may start and end in the middle of one DTIM period. In this case, our system does not incur the delay overhead of t_2.

4.6 Evaluation

In this section, we demonstrate the performance of the proposed system, namely HIDE, by answering two questions: (1) how much energy can our HIDE system save in real-world scenarios? (2) how much does the system affect network throughput and delay?

4.6.1 Energy Efficiency

To show the energy efficiency of our system, we first present the solutions for comparison. Then, we show results of our trace-driven simulation.

4.6.1.1 Solutions for Comparison

To show the energy efficiency of the HIDE system, we compare its energy consumption to that of the "receive-all" method employed on modern smartphones and the lower bound energy consumption of the "client-side" solution [92].

"receive-all" solution. With the receive-all solution, the AP forwards all broadcast frames. The client receives all of these broadcast frames and activates a WiFi wakelock of one second [92] for each broadcast frame.

"client-side" solution. In the HIDE system, we differentiate useful and useless broadcast frames at the AP side by recognizing the UDP port in each broadcast frame. A "client-side" solution does a similar thing except that all these are done at the client. First, the WiFi radio at the client receives a UDP broadcast frame. Then the WiFi driver identifies it as a useless or useful frame with the UDP port in the frame. If this is a useful broadcast frame, then the WiFi driver passes it to the system network stack and acquires a wakelock of one second. If this is a useless broadcast frame, the WiFi driver drops it without acquiring a wakelock. As a result, the system goes back to suspend state immediately. A "client-side" solution reduces the time that the system spends in active state due to WiFi wakelocks triggered by useless broadcast frames. However, the overhead of this solution is more frequent state transfers. Without considering any specific strategy used in a "client-side" solution, we derive the lower bound energy consumption

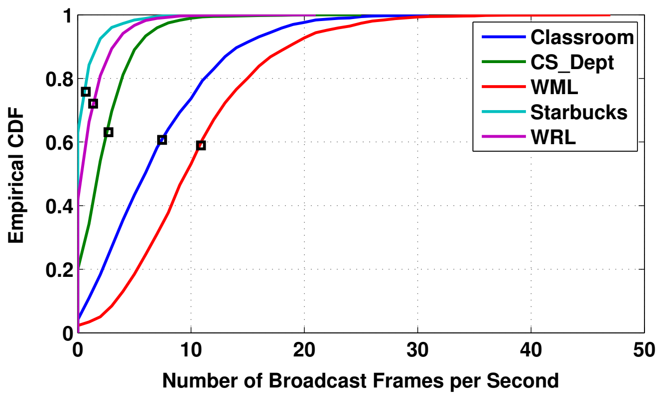

Figure 4.7: Broadcast traffic volumes in traces

for any "client-side" solution. This lower bound is calculated with the assumption that the WiFi driver knows the arrival times of future frames. If the energy consumption of keeping the system in active state until the arrival of the next broadcast frame is less than the energy overhead of state transfer, then the system stays awake even if this is a useless broadcast frame. Otherwise, the system goes back to suspend state immediately to maximize the energy saving.

4.6.1.2 Trace-driven Simulation

We collect broadcast traffic traces from five different real-world scenarios: a classroom building, a CS department, a college library (WML), an off-campus Starbucks store, and a city public library (WRL). Each trace contains 30∼60 minutes data during peek hours. The *cdf* plots of broadcast traffic volume in the traces, i.e., number of broadcast frames per second, are shown in Figure 4.7. The average value is indicated with a black square on each curve.

With these wireless traces and the energy model in Section 4.4, we calculate the energy consumption of different solutions through trace-driven simulation. The energy profile inputs for the model, which are introduced in Table 4.1, are measured with a Monsoon power monitor [87] from two phones: Nexus One and Galaxy S4. We list the values in Table 4.2. For the HIDE system setting, we assume that the UDP port message

	τ	T_{rm}	T_{sp}	E_{rm}	E_{sp}	E_b^u
Nexus One	1 s	46 ms	86 ms	18.26 mJ	17.66 mJ	1.25 mJ
S4	1 s	44 ms	165 ms	58.3 mJ	85.8 mJ	1.71 mJ
	P_r	P_t	P_{idle}	P_{ss}	P_{sa}	
Nexus One	530 mW	1200 mW	245 mW	11 mW	125 mW	
S4	538 mW	1500 mW	275 mW	15 mW	130 mW	

Table 4.2: Energy/Power consumption measured from phones

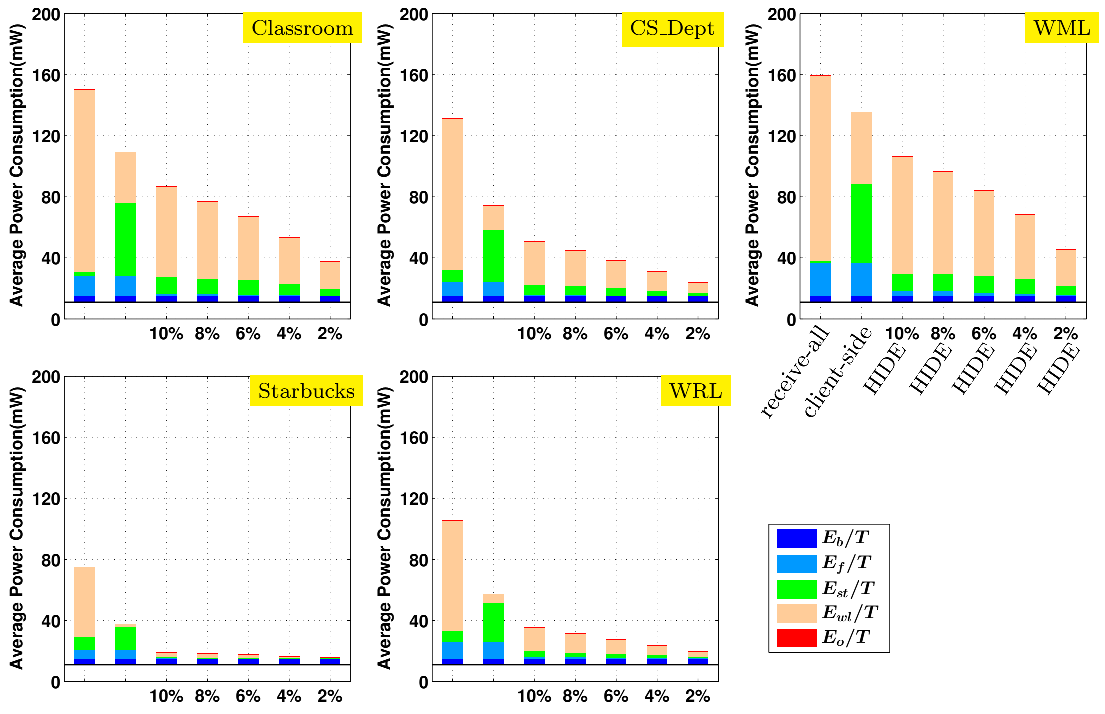

Figure 4.8: Energy consumption comparison (Nexus One).
(Numbers along x-axis are different percentages of useful broadcast frames.)

are sent out every 10 seconds from each HIDE-enabled client with the lowest data rate of 1 Mbits/s. And, the number of UDP ports included in a UDP Port Message is set to 100. This setting is able to represent smartphones in heavy usage. Thus, they are fair enough to show the overhead of our system when compared to others.

Figure 4.8 and Figure 4.9 show the average power consumption of handling broadcast traffic with different solutions on Nexus One and Galaxy S4, respectively. In each subfigure, the first bar is for the "receive-all" method and the second bar is for the "client-side" method. The last five bars are for the HIDE system with different percentages

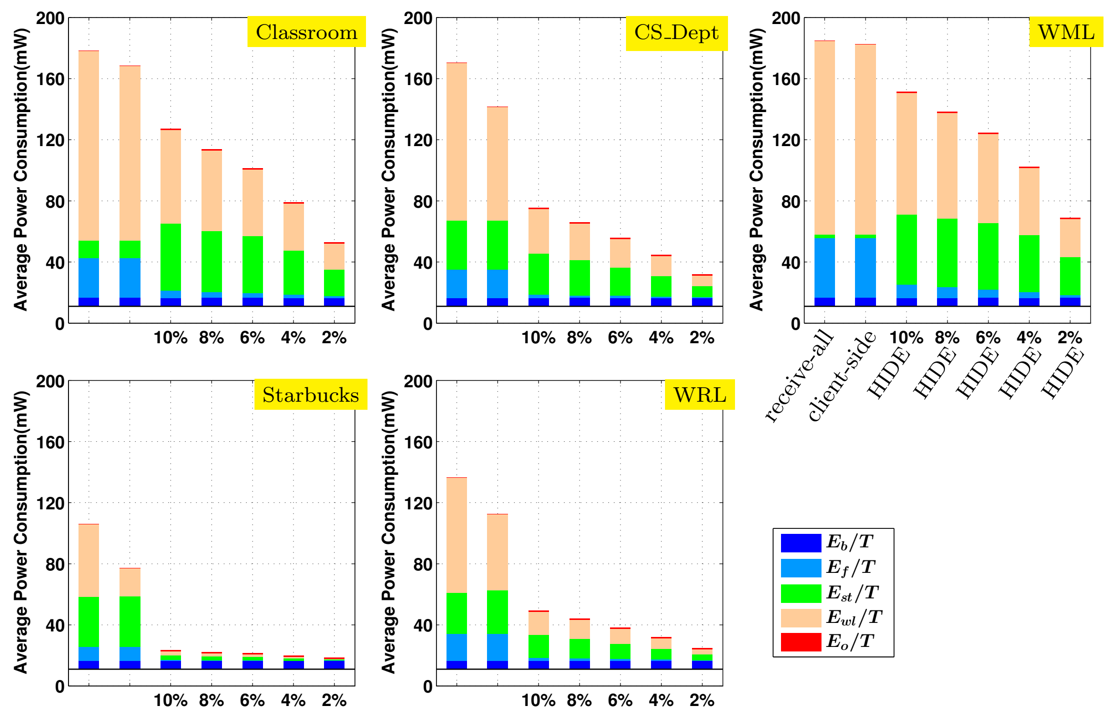

Figure 4.9: Energy consumption comparison (Galaxy S4).
(Numbers along x-axis are different percentages of useful broadcast frames.)

of useful broadcast frames. In order to remove the differences in duration between traces, we show the average power consumption instead of the total energy consumption. Five different colors stand for power consumed in five different aspects as introduced in Equation 4.2.

From Figure 4.8 and Figure 4.9, first, we see that our system saves significantly more energy than the "client-side" solution. With 10% of the broadcast frames being useful, we save 34%∼75% energy for Nexus One and 18%∼78% energy for Galaxy S4. We save even more energy when 2% of the broadcast frames are useful: 71%-82% for Nexus One and 62%-83% for Galaxy S4. On average, HIDE:10% (the HIDE system with 10% of the broadcast frames being useful to the client) saves 23% more energy for Nexus One and 35% more energy for Galaxy S4 than the "client-side" solution. HIDE:2% saves 62% more energy on average for Nexus One and 45% more energy for Galaxy S4 than the "client-side" solution.

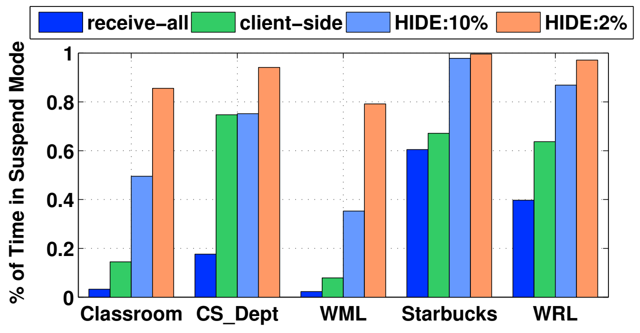

Figure 4.10: Fraction of time in suspend mode for Nexus One

Second, we observe that energy savings of the HIDE system are different across traces. This is mainly because different traces have different broadcast traffic volumes. Other factors, such as frame arrival pattern, frame length, and data rate, are also causing the energy saving differences between traces. The third observation is that the energy overhead of our system, which is shown in red color, is negligible. The overhead is minimal despite that the system setting used in the evaluation represents smartphones in heavy usage.

Third, we notice that state transfer overhead on Galaxy S4 is much higher than on Nexus One. As a result, the "client-side" solution does not save much energy when the broadcast traffic is heavy, as shown in Figure 4.9. For example, in the classroom and college library (WML) scenarios, the "client-side" solution barely saves energy. In contrast, our system still largely reduces the average power consumption.

In order to help understand the energy savings of our method, we show the fraction of time that the device stays in suspend mode in Figure 4.10. HIDE:10% (HIDE:2%) means the HIDE system is used and 10% (2%) of the broadcast frames are useful. Here, we only show the results for Nexus One. Similar results are obtained for Galaxy S4. Generally, the HIDE system spends much more time in suspend mode than both the "receive-all" method and the "client-side" solution. When the broadcast traffic is heavy, such as under the classroom scenario and under the WML scenario, the device spends less than 20% of the time in suspend mode when the "receive-all" or "client-side" solution is used. However, with our method, the device spends $\geq$80% of the time in suspend mode with

min contention window	32
max contention window	1024
slot time	20 us
SIFS	10 us
DIFS	50 us
propagation delay	1 us
channel data rate	11 Mbits/s
MAC Header	224 bits
PHY preamble +header	192 bits
average data payload size	1000 bits

Table 4.3: Network configuration for network capacity analysis

2% of useful broadcast frames. One exception is that, in the CS Department scenario, the fraction of time in suspend mode for HIDE:10% is only slightly larger than that of the "client-side" solution. Referring back to Figure 4.8, we know that the "client-side" solution saves much less energy because it wastes a lot more energy in switching between active mode and suspend mode.

4.6.2 Impact on Network Capacity and Delay

Impact on Network Capacity. Based on the analysis in Section 4.5.1, we calculate the percentage of decrease in network capacity with typical 802.11b network configurations as used in [98]. The parameters are listed in Table 4.3. In addition, the sending interval of UDP Port Messages from a client is set to 10 seconds. Each UDP Port Message contains 50 UDP ports.

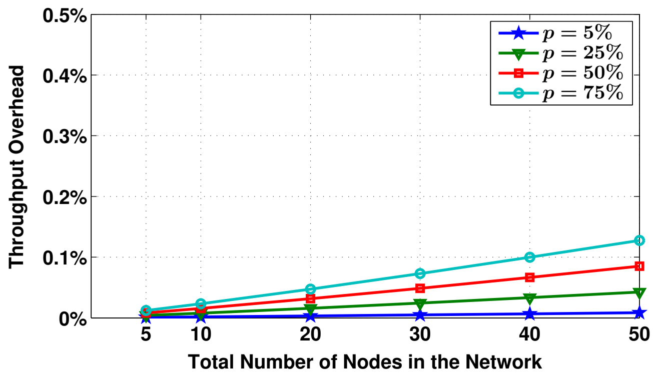

Figure 4.11: Percentage of decrease in network capacity

Figure 4.11 shows the results of the decrease in network capacity. We vary the total number of nodes in the network from 5 and 50. Also, we vary the percentage of nodes with HIDE enabled, denoted as p, from 5% to 75%. We made the following observations. First, the more the nodes in the network, the more the network capacity decreases. This is because the number of UDP Port Messages transmitted is linear to the number of nodes in the network. And, the original network capacity drops only slightly when the number of nodes in the network increases from 5 to 50. Second, the decrease of network capacity is negligible. With 50 nodes in the network and 75% of the nodes with HIDE enabled, the decrease of network capacity is only 0.13%.

Impact on Network Delay. To measure the network delay overhead of our system, we set the percent of clients with HIDE enabled p to 50%. In addition, we set the number of broadcast frames buffered at the AP during each DTIM period n_f to 10. Note that the n_f in the five traces we collected are all much smaller than 10. For the original network delay D, we measure the round-trip time (rtt) when connecting to a YouTube server under a deployed AP with *ping* command. In our experiments, the average rtt is $79.5ms$. We use this measured rtt as the original network delay D.

To get the time durations of hash table operations, including deleting τ_{del}, inserting τ_{ins}, and lookup τ_{lp}, we implement the Client UDP Port Table on an old smartphone. We use a smartphone instead of a computer because computers have much more powerful processing capability than wireless AP/routers. The processing time measured on a computer does not reflect actual processing time on wireless APs/routers. The smartphone we use has a 1 GHz ARM processor and 512 MB memory with Android system installed. This configuration is comparable to some wireless routers in the market [99, 100]. To measure the time of operations, we first initialize the hash table with $N * 50\% * 50$ randomly generated pairs of (UDP port, Association ID). The parameter is then calculated as the mean value from 10 repeated runs of 100 deleting, or inserting, or lookup operations.

First, we fix the average number of open UDP ports in a client n_o to 50 and vary the

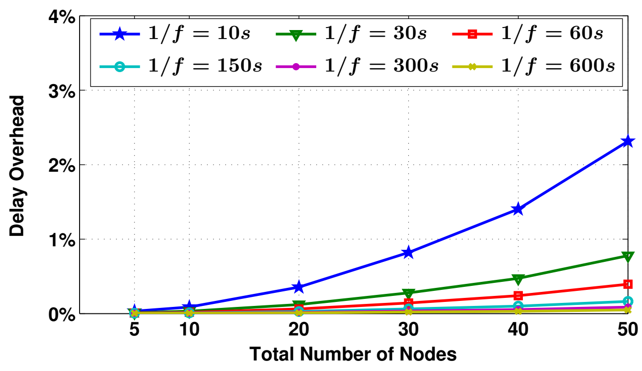

Figure 4.12: Percentage of increase in network delay with different percentages of HIDE-enabled clients

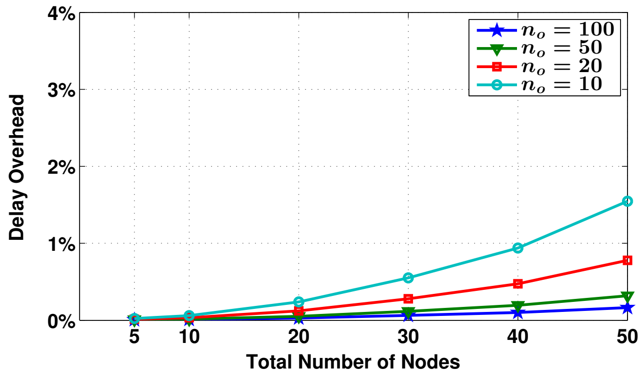

Figure 4.13: Percentage of increase in network delay with different numbers of open UDP ports on each client

average sending interval of UDP Port Messages. With this setup, the increase of packet delay with our HIDE system is shown in Figure 4.12. We observe that the more the nodes in the network, the more the packet delay increases. At the same time, the more frequently the UDP Port Messages are sent, the larger the increase is. The same as the impact on network capacity, the impact on packet delay is very small. When UDP Port Messages are sent every 10 minutes (600s), the increase of rtt is as small as 0.05%. Even when the UDP Port Messages are sent every 10 seconds, the increase is only 2.3%.

Second, we fix the sending interval of UDP Port Message to 30s and vary the average number of open UDP ports n_o in a client. The results for this configuration are shown in Figure 4.13. As expected, more open UDP ports means larger delay overhead. However, the overhead is less than 1.6% with 100 UDP ports in use on each HIDE-enabled client.

During our overhead analysis, we find that $t_1 \gg t_2$ in Equation (4.27). Meanwhile, according to Equation (4.25), t_1 is linear to the original network delay D. Our analysis results above actually have little dependence on the actual value of the original network delay, although we use a measured value of 79.5 ms.

4.7 Conclusion and Future Work

Energy is wasted on smartphones to receive broadcast frames that are useless to the smartphone and to switch from low power suspend mode to high power active mode to process these useless WiFi broadcast frames. In this work, we propose a framework, namely HIDE, to reduce energy wasted on smartphones due to useless broadcast frames, with assistance from the WiFi Access Point (AP). In the HIDE system, a client coordinates with the AP to identify useful broadcast frames. Then, traffic notifications sent out from AP only indicate useful broadcast frames that are currently buffered at the AP. The presence of useless broadcast frames is hidden by the AP from the client. As a result, a client in suspend mode does not need to receive the useless broadcast frames. Neither does it need to switch to active mode and process the useless frames.

With WiFi broadcast traces collected from five different real-world scenarios, we conduct trace-driven simulation with the energy model derived in this work. The results show that our system saves 34%-75% energy for the Nexus One phone and 18%-78% for the Galaxy S4 phone when 10% of the broadcast frames are useful to the smartphone. When 2% of the broadcast frames are useful to the smartphone, our system saves 71%-82% energy for Nexus One and 62%-83% for Galaxy S4. We also analyze the performance overhead of the proposed system. The impact of the HIDE system on network capacity is less than 0.2% and the impact on packet round-trip time is no more than 2.3%.

In future, we plan to evaluate the system with more broadcast traffic traces and for more smartphones. Combining the HIDE system with the "client-side" solution is also one direction to be explored.

Chapter 5

Continuous Authentication with Touch Behavioral Biometrics and Voice on Wearable Glasses

5.1 Introduction

Wearable glasses have attracted considerable attention over the years. More and more large companies are investing money on wearable glasses. Now, more than 20 wearable glasses are under production or development [101], including Google Glass, Microsoft HoloLens, Facebook Oculus Rift, Epson Moverio, Sony SmartEyeglass, Intel Radar Pace, and Osterhout Design Group (ODG) R-7. The hand-free nature and augmented reality capability of wearable glasses open up new opportunities for human-machine interactions. Wearable glasses are going to become an important part of our daily lives. A recent study by Juniper Research shows that more than 12 million consumer smart glasses will be shipped in 2020, increasing from less than one million in 2016 [102].

When using these wearable glasses, some personal information is stored on the devices for easy revisit, such as contacts information, location data, messages, emails, personal photos and videos, account information, and much more. When the owner takes off his/her smart glasses and puts them aside, for example, when the device is charging or when the owner needs to go to the restroom, an impostor will certainly have the chance to grab the device and access the owner's private information. In addition to privacy leakage of the owner, an imposter can also send e-mails/messages to any contact stored on the glasses in the guise of the owner, bringing privacy threats to the owner's friends, family, and colleagues.

To protect user privacy on wearable glasses, a continuous authentication system is more suitable than a one-time authentication system. A one-time user authentication system only authenticates a user when he/she tries to unlock the device, typically by asking the user to input a password or PIN, a graphical pattern, or a sequence of touch gestures (a user is authorized as long as the right gesture types are performed in the correct order). However, the owner may forget to lock the device right after using the device. There are mechanisms which automatically lock the device upon an event, such as screen timeout. Google Glass has on-head detection, which automatically locks the device when a user takes off the glass. However, on-head detection on Google Glass is not reliable. It does not work when the glass is not worn in the perfect position. It also does not work with Google Glass frames which are customized for users in need of vision correction. More importantly, even if the device is locked, a one-time authentication system can easily be broken into by peeking [103, 104, 105] or smudge attacks [106, 107]. Alternatively, wearable glasses can automatically pair with another trusted device, such as the owner's smartphone, to perform authentication. However, successful pairing only indicates that the owner is nearby. It does not necessarily mean that the current user is the owner. A one-time authentication solution does not work well. Therefore, a continuous authentication system which continuously authenticates the user during the whole time of user operation is needed to better protect user privacy.

Touch behavioral biometrics have been demonstrated to be effective in continuous user authentication on smartphones [45, 47, 53]. The hypothesis is that different users have different characteristics when interacting with smartphones and these behavioral biometrics are difficult to fake. We believe the same is also true on wearable glasses.

However, due to user interaction differences between wearable glasses and smartphones, systems proposed on smartphones cannot be applied directly on wearable glasses. First, users hold their smartphones with hand(s) but wear smart glasses on their head. Motion sensors, such as accelerometers and gyroscopes, respond to user touch events in a different pattern on wearable glasses. As a result, features working on smartphones may not work well on wearable glasses. Second, wearable glasses only have a touchpad with no virtual keyboard support. Keystroke biometric information [108] is not available on wearable glasses. Third, wearable glasses touchpad is much smaller than smartphone touch screen. Thus, the resolution of biometric information on wearable glasses, such as coordinates, is much lower than that on smartphones. Feature discriminability needs to be examined on wearable glasses. Finally, different touch gestures are used on wearable glasses. For example, there are no pinch gestures on Google Glass. To zoom in or out, a two-finger swipe forward or backward gesture is used. Thus, new features that are specific to wearable glasses need to be explored.

In this work, we study the performance of using touch gestures and voice commands for continuous user authentication on wearable glasses with the example of Google Glass. We consider both touch gestures and voice commands as they are two major channels for user interaction on wearable glasses. An authentication system based only on touch biometrics can be easily circumvented by using voice commands. Similarly, a system purely based on voice authentication does not always work, as voice commands are not available all the time. A user may be in a situation when speaking is not appropriate, e.g., at a meeting with quiet surroundings. Although touch behavioral based authentication [45, 47, 53] and voice based authentication [109, 40, 110] are two well-studied fields, our contributions lie in that we study them in a new platform and we integrate these two dimensions to accommodate various scenarios.

In our system, we use both touch behavioral features extracted from touchpad data as well as corresponding sensor data during touch gestures and voice features extracted from user-issued voice commands. These features can be easily extracted in the background when users normally interact with wearable glasses. It does not require extra efforts from users. Thus, our system works in a non-invasive way. Note that in this work, we focus on one specific model of wearable glasses: Google Glass. However, the method introduced and the authentication system framework proposed in this work also apply to other wearable glasses with a touch panel and built-in microphone and speakers, such as SiME Smart Glasses [111], Recon Jet [112], and Vuzix M300 [113].

We summarize our contributions as follows.

- We conduct a user study on Google Glass and collect user interaction data from 32 human subjects. The data we collect includes touch event data with corresponding sensor readings, and voice commands. Six types of gestures are covered in the study: single-tap, swipe forward, swipe backward, swipe down, two-finger swipe forward, and two-finger swipe backward.

- With the data collected, we define and extract 99 behavioral features for one-finger touch gestures, 156 features for two-finger touch gestures, and 19 voice features for user voice commands. We evaluate the discriminability of these features with one-class Support Vector Machine (SVM) model for user authentication purpose on Google Glass.

- We design a simple but effective online user authentication system for wearable glasses, namely GlassGuard, which works in a continuous and non-invasive manner. GlassGuard employs a mechanism adapted from Threshold Random Walking (TRW) to make a decision from multiple user events only when it is confident. Our preliminary results indicate that it achieves high accuracy with acceptable delay.

5.2 Features for Continuous User Authentication

In this section, we first introduce all the features that we are going to study. Then, we describe a user study that we have carried out to collect real user interaction data. With the data collected, we evaluate the performance of these features and conduct feature selection.

5.2.1 Key User Events

Common touch gestures on Google Glass are as follows: single-tap to select an item, swipe backward (forward) to move left (right) through items, swipe down to go back, and two-finger swipe forward (backward) to zoom in (out).

With a built-in microphone and speaker, Google Glass accepts voice commands as user inputs, such as “OK, Glass! Take a picture!” This offers a hand-free interaction which can be extremely useful for people with disabilities and for wearers with both hands busy.

When designing features, we focus on the above six types of touch gestures and all voice commands.

5.2.2 Proposed Features

We propose different feature sets for one-finger touch gestures, two-finger touch gestures, and voice commands. Our features for one-finger touch gestures are proposed based on several existing works on smartphones[45, 54, 50], as here we only want to obtain a list of potential features. Later, we conduct feature selection to find the best features that work on Google Glass.

Features for One-finger Touch Gestures. We divided our features for touch gestures into two categories: (1) touch-based features, which are features extracted from touchpad data; and (2) sensor-based features, which are features extracted from sensor readings during touch gestures.

Figure 5.1 gives an example of a one-finger touch gesture along the timeline. Table 5.1 lists all 18 touch-based features for a one-finger touch gesture. Note that each touch gesture generates multiple records in the raw touch data, as the touchpad is continuously sampling. The statistics below, such as minimum, maximum, and median, are calculated

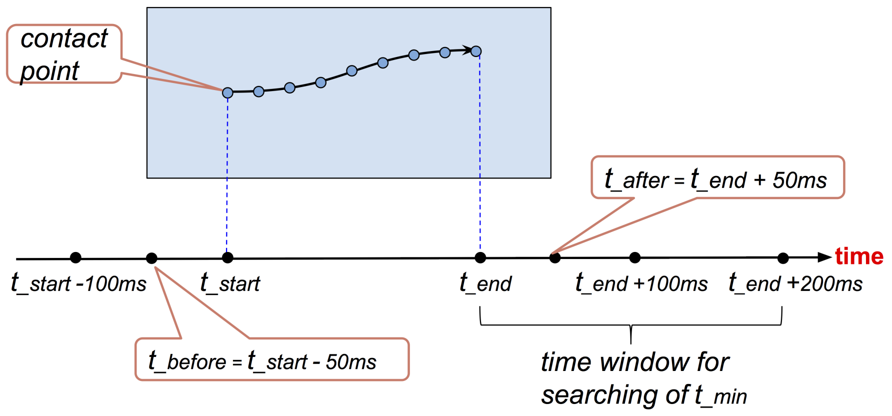

Figure 5.1: An example of a one-finger touch gesture

Aspect	**Feature**	**Explanation**
time	*duration*	time difference between the first and last records of a touch gesture
distance	*distance* *distance_x* *distance_y*	distance between contact points of the first and last records of a touch gesture, and its values along x-axis and y-axis
speed	*speed* *speed_x* *speed_y*	speed of finger movement on touchpad during a touch gesture, and its value along x-axis and y-axis
pressure	{*mean, max, min, median, stdev*}*_pressure*	mean, max, min, median, and standard deviation of pressure values during a touch gesture
	{*q1, q2, q3*}*_pressure*	the 25%, 50%, and 75% quartiles of pressure values during a touch event
	first_pressure *last_pressure*	pressure value of the first and last records respectively
	max_pressure_por	time portion to achieve the maximum value of pressure. $= (t_m - t_{start})/(t_{end} - t_{start})$ where t_m is the timestamp for the record with the maximum pressure value.

Table 5.1: Touch-based features

from multiple samples of one touch gesture starting at time t_{start} and ending at time t_{end}.

Let x, y, z be sensor readings (accelerometer, or gyroscope, or magnetometer) in each axis and $net = \sqrt{x^2 + y^2 + z^2}$. Table 5.2 lists all sensor-based features during a one-finger touch gesture.

Let ϕ_{max} be the maximum accelerometer readings during a touch event and t_{max} be the corresponding timestamp. Considering a 100ms time window before a touch gesture, let t_{before} be the center of the time window and ϕ_{before} be the average *net* value of accelerometer readings. Considering a 100ms time window after a touch gesture, let t_{after} be the center of the time window and ϕ_{after} be the average *net* value of accelerometer readings. Then, in Table 5.2, we list the sensor-based features. The following features in Table 5.2 are calculated as

$$acc\_after\_before\_net = \phi_{after} - \phi_{before} \tag{5.1}$$

$$acc\_mean\_before\_net = acc\_mean\_net - \phi_{before} \tag{5.2}$$

$$acc\_max\_before\_net = acc\_max\_net - \phi_{before} \tag{5.3}$$

$$acc\_ndt\_before\_after = \frac{t_{after} - t_{before}}{\phi_{after} - \phi_{before}} \tag{5.4}$$

$$acc\_ndt\_max\_after = \frac{t_{after} - t_{max}}{\phi_{after} - \phi_{max}} \tag{5.5}$$

$$acc\_time\_to\_restore = t_{min} - t_{end} \tag{5.6}$$

where t_{min} is the time instance within a $T_2 = 200$ms time window after a touch event when the sensor reading restores to the average value before this touch event.

$$t_{min} = \underset{t_j \in (t_{end}, t_{end}+T_2]}{\arg\min} \left| net_{t_j} - \phi_{before} \right| \tag{5.7}$$

In order to save space, we only list the 27 features based on accelerometer data. Features based on gyroscope and magnetometer are defined accordingly. In total, we have 81 sensor-based features. We do not include frequency domain features here as extracting frequency domain features is energy hungry and requires high computation capability. Later in Section 5.4, we show that our system achieves high accuracy with only these time domain features.

Aspect	**Feature**	**Explanation**
absolute value	*acc_mean_*{x, y, z, net}	**mean** values of sensor readings during a touch gesture
	*acc_median_*{x, y, z, net}	**median** values of sensor readings during a touch gesture
	*acc_std_*{x, y, z, net}	**standard deviations** of sensor readings during a touch gesture
change in value	*acc_after_before_*{x, y, z, net}	change of **average** sensor readings **after** a touch gesture compared to that **before** the touch gesture. See Eq. (5.1)
	*acc_mean_before_*{x, y, z, net}	the difference between the **average** sensor readings **during** a touch gesture and that **before** the touch gesture. See Eq. (5.2)
	*acc_max_before_*{x, y, z, net}	the difference between the **max** sensor readings **during** a touch gesture and the **average** sensor readings **before** the touch gesture. See Eq. (5.3)
time to change	*acc_ndt_before_after*	the normalized time duration for the **average** sensor readings to change from a state before a touch event ϕ_{before} to a state after the touch event ϕ_{after}. See Eq. (5.4)
	acc_ndt_max_after	the normalized time duration for sensor readings to change from the **max** value ϕ_{max} during a touch event to a state after the touch event ϕ_{after}. See Eq.(5.5)
	acc_time_to_restore	time duration after a touch event for sensor readings to **restore** to average value before the touch event. See Eq. (5.6)

Table 5.2: Sensor-based features

Features for Two-finger Touch Gestures. Two-finger touch gestures have two contact points on the touchpad. For each contact point, we define a set of touch-based features presented above for one-finger touch gestures. For example, duration for each contact point (denoted as $duration_1$, $duration_2$) and distance for each contact point (denoted as $distance_1$, $distance_2$). Moreover, the relative information between the two contact points may also be useful for user authentication. For two-finger touch gestures, we design the following 29 touch-based features additionally.

- *duration*: the duration of a touch gesture. It may be different from both $duration_1$ and $duration_2$ when the first and last records of a touch gesture belong to different fingers.
- mean, max, min, median, and standard deviation of distances (or distances along x axis, or distances along y axis) between two contact points.
- *q1_diff_dist*, *q2_diff_dist*, *q3_diff_dist*: The 25%, 50%, and 75% quartiles of distances between two contact points.
- *first_diff_dist*, *last_diff_dist*: the distance between the first (last) contact points of two fingers.
- The difference between the mean (or maximum, or minimum) pressure values for two fingers during a touch gesture.
- The maximum difference between pressure values of two fingers during a touch gesture.
- The minimum difference between pressure values of two fingers during a touch gesture.
- The difference between speeds (or speeds along the x axis, or speeds along the y axis) of two fingers.

Sensor-based features for two-finger touch gestures are the same as those for one-finger touch gestures. So, we have proposed 156 features in total for two-finger touch gestures, 81 from sensor data and 75 from touch data.

Features for Voice Commands. For voice features, we use Mel-Frequency Cepstral Coefficients (MFCC). MFCC is one of the most effective and widely used features in speech processing [114]. An audio file is recorded from each voice command. The audio file is then divided into frames with a sliding window of 25 ms and a step size of 10 ms. For each frame, we extract 20 coefficients. The first coefficient indicates the direct current of the voice signal. It does not convey any information about the spectral shape. So, we discard the first coefficient [110] and use the 2nd to the 20th coefficients to construct an MFCC vector. Before extracting MFCC vectors, we apply silence removal

[115] to the audio.

5.2.3 User Study

In order to evaluate the features listed above, we conduct a user study to collect real user data[1].

To obtain all the touch event data, we use the "getevent" tool [116]. With this tool, we are able to collect raw touch data (including coordinates of contact points, and pressure) at background without user perception.

To obtain sensor readings during a touch event, we write a Google Glass application that samples sensor data with system API. The application runs as a background service. It does not interrupt users' normal operations. The application logs down data from all three inertial sensors (accelerometer, magnetometer, and gyroscope) with a sampling rate of 200 Hz, 200 Hz, and 100 Hz, respectively.

Google Glass automatically records user commands and saves them locally. To analyze these voice commands, we pull these files out from Google Glass with *adb* [117] tool.

Using the tools introduced above, we conducted a user study and collected interaction data from 32 subjects. All of the participants are college students, comprising 13 females and 19 males. The data of each user is collected from multiple sessions in a two-hour time frame. In order to collect as many interested user events as possible, a user is asked to perform a specific task in each session. There are 7 tasks in the user study and each task is repeated multiple times: (1) swipe to view the application list one by one; (2) swipe to view the options in the settings menu one by one; (3) take pictures with touch gestures; (4) take pictures with voice commands; (5) Google search with voice commands; (6) delete pictures one by one; (7) use a customized application which asks the user to performance a series of randomly selected touch gestures. We carried out our user study on a Google Glass with system version XE 18.11. All data is collected in the

[1]This user study was approved by the Protection of Human Subject Committee at the College of William & Mary.

background while users are standing and interacting with Google Glass normally. Table 5.3 shows the amount of the data collected.

Touch data				
	Mean	Max	Min	Sum
# of single-tap	466.3	576	344	14281
# of swipe forward	629.0	1031	484	20127
# of swipe backward	599.7	862	433	19190
# of swipe down	483.0	615	354	15457
# of two-finger swipe forward	549.3	919	353	17576
# of two-finger swipe backward	534.3	722	341	17098
Sensor data				
Accelerometer (in MB)	45	66	35	1454
Gyroscope (in MB)	50	73	38	1599
Magnetometer (in MB)	23	33	18	733
Audio (voice commands)				
	Mean	Max	Min	Sum
# of audio	39.06	52	17	1250
Length of audios (in seconds)	2.28	15	0.95	2855.6

Table 5.3: Amount of the data collected

5.2.4 Feature Selection

We have proposed a set of features for each touch gesture. However, not all of them perform well in user authentication. We conduct feature selection to remove poor features and select features with high discriminability. By doing this, we also reduce the number of features needed, cutting down the computation cost of the online authentication system. The algorithm we use is Sequential Forward Search [118], and the classification Equal Error Rate (EER) is used as the criterion function.

Users have different characteristics when interacting with Google Glass. Some features work for all users as everyone is different in those aspects. Some features only work for a specific user because the owner has his (her) own peculiarity discriminating himself (herself) from others. So, we conduct user-specific feature selection: repeat the feature selection process 32 times, each time for a different user. Figure 5.2 shows the performance ranking of these features when only 5 features are used in the model for

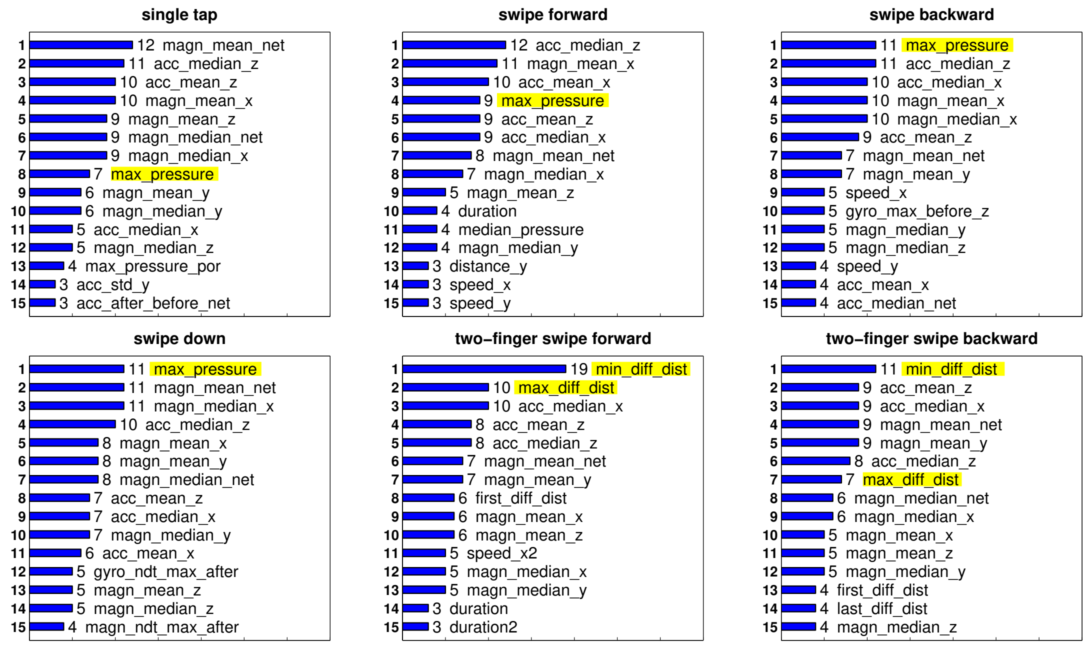

Figure 5.2: Top 15 features among all users when five best features are selected for each user.
(The number on the left side of a bar indicates the rank of the feature. The number on the right side of a bar shows the number of users for whom this feature has been selected, followed by the name of the feature.)

each user. The number on the left side of a bar indicates the rank of a feature. The number on the right side of a bar shows the number of models which have used this feature, followed by the name of the feature. We have the following observations from the figures. First, *max_pressure* performs well for all one-finger touch gestures. Second, the minimum distance between two fingers, *min_diff_dist*, is the best feature for two-finger touch gestures. The maximum distance between two fingers, *max_diff_dist*, is also among the tops. Third, accelerometer features and magnetometer features generally rank higher than gyroscope features. This also indicates that the device rotation is not as obvious as acceleration during touch events.

Comparing our features to those used on smartphones [45, 47, 53, 50], we have the following findings. (1) The touch size (area covered by fingertips) is an effective feature on smartphones. However, this information is not available on Google Glass. (2) The speed features of swipe gestures perform well on Google Glass, same as on smartphones.

An exception on Google Glass is the swipe down gesture. This is because the vertical length of the touchpad here is much smaller than that on smartphones. (3) Two-finger swipe gestures are new gestures on Google Glass. Although there are also two-finger gestures (e.g. pinch) on smartphones, they have totally different definitions. Thus, different features are used. For example, the distance between two fingers are not useful for pinch gestures on smartphones. However, they perform pretty well for two-finger swipe gestures on Google Glass.

5.3 The GlassGuard System

In this section, we present the framework of our online authentication system, which we call GlassGuard. Figure 5.4 shows the architecture of the GlassGuard authentication system. There are five modules in the system. The Feature Extraction module calculates a set of features determined by offline training. In the following part of this section, we introduce each of the other four modules.

5.3.1 Event Monitor

The Event Monitor continuously monitors all user events when the screen is on, including touch events and voice commands. If it is a touch event, the Event Monitor forwards the touch data and the corresponding sensor data for feature extraction. If it is a voice command, the Event Monitor forwards the audio file for feature extraction.

The Event Monitor also communicates with the Power Control module. On one hand, it reports occurrences of user events to the Power Control module. On the other hand, it gets instructions from the Power Control module about whether it should forward data for feature extraction or not. The details are explained in the Power Control subsection.

5.3.2 Classifiers

After features are extracted, they are passed to one of the classifiers. To achieve high accuracy, we train one classifier for each gesture type and for voice command, respec-

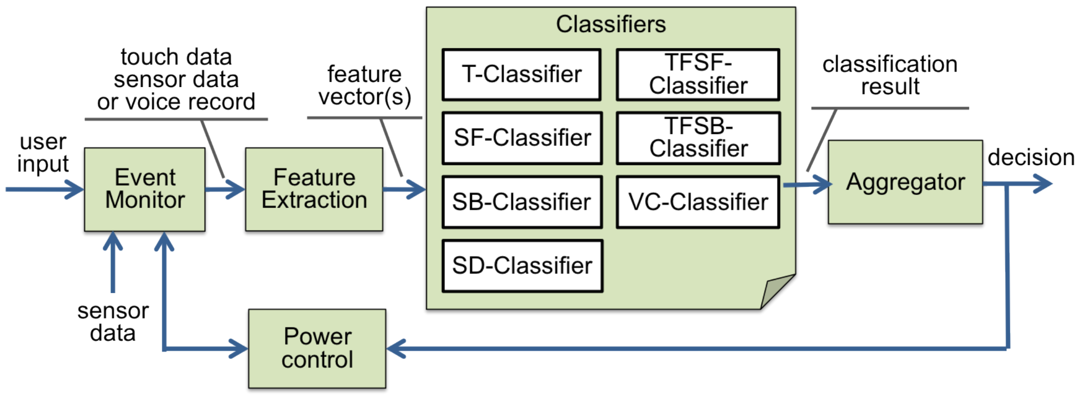

Figure 5.4: System architecture of GlassGuard

tively. There are seven classifiers in the system: T-Classifier for single-tap gestures, SF-Classifier for Swipe Forward gestures, SB-Classifier for Swipe Backward gestures, SD-Classifier for Swipe Down gestures, TFSF-Classifier for Two-Finger Swipe Forward gestures, TFSB-Classifier for Two-Finger Swipe Forward gestures, and VC-Classifier for Voice Commands.

To do user authentication, a classifier only needs to tell whether or not an observation belongs to the owner. In our system, an observation can be either a voice command or a touch event belonging to any of the aforementioned gesture types. In reality, a Google Glass only has observations from its owner, rather than impostors, for training. Thus, we use one-class SVM (Support Vector Machine) [119] as the model to do classification. We select SVM because it provides high accuracy and it is effective in high-dimensional spaces and flexible in modeling diverse sources of data [120, 121]. SVM has been demonstrated to perform well in detecting user patterns in various applications, such as mouse movement pattern [42], voice pattern [122], motion pattern [123], and user-generated network traffic pattern [124], and so on.

Touch Gesture Classifiers. We train the classifiers via ten-fold cross validation following the training routine suggested in the LIBSVM website [125]. To train a classifier for gesture type i, we divide all feature vectors of gesture type i into *positive* samples and *negative* samples. Positive samples are feature vectors from the user currently treated as the owner. Negative samples are feature vectors from all other users. We randomly divide all positive samples into k (k=10) equal size subsets, and do the same for negative samples. Then, we train a one-class SVM model with $k-1$ positive subsets, leaving one subset of positive samples for testing. Then, we test the same model with one subset of negative samples. We repeat the training and testing steps until each subset of positive samples and each subset of negative samples are used exactly once for testing. With all the decision values calculated from the SVM models, we plot the Receiver Operating Characteristic (ROC) curve, which is insensitive to class skew [126]. The mis-prediction ratio of all positive samples is False Reject Rate (FRR) and the mis-prediction ratio of all negative samples is False Accept Rate (FAR).

VC-Classifier. Classification of voice features (MFCC vectors) is done in the same way as classification for touch gestures. However, the FAR and FRR are calculated in a different way. To get the EER for the voice command classifier, we treat all MFCC vectors extracted from the same audio file as a whole. If the percentage of misclassified MFCC vectors in an audio file is greater than a threshold p, then we think this audio file is misclassified and treat this as one error. The FAR and FRR are calculated as percentage of misclassified audio files in owner's data and in other users' data, respectively. We do this because it is normal to treat one user voice command as one user event. A threshold p is used because the classification results of MFCC vectors are noisy as the audio contains background sound and notification sound of the glass system. The value of p can be experimentally decided.

5.3.3 Aggregator

GlassGuard has seven classifiers. All classifiers make predictions independently. For each user event, we obtain one classification result. Once a classification result is generated, it is passed to the Aggregator module. To improve the accuracy of the authentication system, the Aggregator combines multiple classification results, which may come from different classifiers, and makes one final decision: whether or not the current wearer is the owner. In order to do that, we need to solve two problems: (1) how to combine multiple classification results and (2) when to make decisions.

In the GlassGuard system, the Aggregator employs a mechanism adapted from Threshold Random Walking (TRW) to make decisions when and only when it is confident. TRW is an online detection algorithm that has been successfully used to detect port scanning [127], botnets [128], and spam [129]. With TRW, predictions are made based on the likelihood ratio, which is the conditional probability of a series of classification results given the FAR and FRR of the classifier. When the likelihood ratio falls below a lower threshold, the system identifies the current user as an impostor. When the likelihood ratio reaches an upper threshold, the system identifies the current user as the owner. If the likelihood ratio is between the two thresholds, the system postpones making a prediction. In this project, we choose TRW because it is simple but performs fast and accurately. However, TRW was originally designed to combine multiple results from a single classifier. In our system, we have multiple classifiers with different FARs and FRRs. We need to adapt TRW to accommodate multiple classifiers. Figure 5.5 shows the processing flow.

Assume that there are M classifiers ($M = 7$ in our GlassGuard system). For classifier c_k ($1 \leq k \leq M$), we have the estimated FAR_{c_k} and FRR_{c_k}. Suppose that at some point in time, we have gathered n classification results from the M classifiers, denoted as $Y = \{Y_i^{c_k} | 1 \leq i \leq n, 1 \leq k \leq M\}$, $Y_i^{c_k}$ is the i_{th} classification result and it is from classifier c_k. $Y_i^{c_k} = 1$ means classifier c_k predicts the event is from the owner. We call it a *positive* classification result. $Y_i^{c_k} = 0$ means classifier c_k predicts the event is not from the owner, which we call a *negative* classification result.

Let H_1 be the hypothesis that the current user is the owner and H_0 be the hypothesis that the current user is an impostor. Then the Aggregator calculates the following conditional probabilities

$$\begin{array}{ll} P(Y_i^{c_k} = 0|H_1) = FRR_{c_k}, & P(Y_i^{c_k} = 1|H_1) = 1 - FRR_{c_k} \\ P(Y_i^{c_k} = 1|H_0) = FAR_{c_k}, & P(Y_i^{c_k} = 0|H_0) = 1 - FAR_{c_k} \end{array}$$

With n classification results and the above conditional probabilities for each classifier,

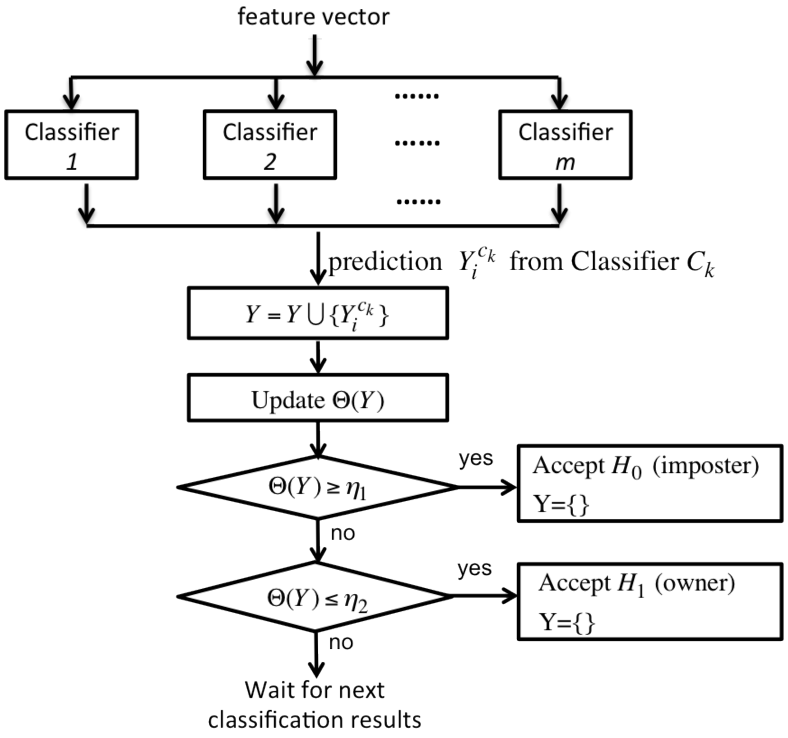
feature vector
Classifier 1
Classifier 2
......
Classifier m
prediction $Y_i^{c_k}$ from Classifier C_k
$Y = Y \bigcup \{Y_i^{c_k}\}$
Update $\Theta(Y)$
$\Theta(Y) \geq \eta_1$
yes
Accept H_0 (imposter) Y={}
no
$\Theta(Y) \leq \eta_2$
yes
Accept H_1 (owner) Y={}
no
Wait for next classification results

Figure 5.5: Processing flow of the Aggregator module

the Aggregator calculates the likelihood ratio

$$\Theta(Y) = \prod_{i=1}^{n} \frac{P(Y_i^{c_k}|H_0)}{P(Y_i^{c_k}|H_1)} \tag{5.8}$$

In practice, both FAR and FRR are smaller than 50%. We have

$$\frac{P(Y_i^{c_k} = 0|H_0)}{P(Y_i^{c_k} = 0|H_1)} = \frac{1 - FAR_{c_k}}{FRR_{c_k}} > 1$$

Similarly,

$$\frac{P(Y_i^{c_k} = 1|H_0)}{P(Y_i^{c_k} = 1|H_1)} = \frac{FAR_{c_k}}{1 - FRR_{c_k}} < 1$$

which means, a negative classification result increases the value of $\Theta(Y)$ while a positive classification result decreases the value of $\Theta(Y)$.

When $\Theta(Y) \geq \eta_1$, the system takes hypothesis H_0 (is an impostor) to be true. When $\Theta(Y) \leq \eta_2$, the system takes hypothesis H_1 (is the owner) to be true. A basic principle of choosing values for η_1 and η_2 is [127]

$$\eta_1 = \frac{\beta}{\alpha} \qquad \eta_2 = \frac{1-\beta}{1-\alpha} \tag{5.9}$$

where α and β are two user-selected values. α is the expected false alarm rate (H_0 selected when H_1 is true) and β is the expected detection rate (H_0 selected when H_0 is true) of the whole system. The typical values are $\alpha = 1\%$ and $\beta = 99\%$.

5.3.4 Power Control

As with smartphones, energy consumption is an important user concern on Google Glass. In addition, if the power consumption of the system is too high, the temperature on the surface of Google Glass can easily get very high [130]. This may make users uncomfortable as well as slow down the system. So, while we aim to achieve high accuracy for the protection of the device owner's privacy, we also want to reduce the power consumption. In the GlassGuard system, the Power Control module is designed to improve the energy efficiency of the whole system. The basic idea is to pause feature extraction and classification whenever the privacy risk becomes low and restart those processes whenever the privacy risk reverts back to high.

When to pause? In the GlassGuard system, the Power Control module gets all decisions made by the Aggregator module and communicates with the Event Monitor module. If a negative decision (the current user is an impostor) is made by the Aggregator, then the glass system needs to do something to restrict access to the device, for example, lock the device and send an alert to the owner. The specific strategy to take when an impostor is detected is beyond the scope of this work. Whenever a positive decision (the current user is the owner) is made by the Aggregator, the Power Control module instructs the Event Monitor module to temporarily pause forwarding data for feature extraction. As a result, data will not be processed by the Feature Extraction module or the Classifiers. To save more energy, when feature extraction is paused, the Event Monitor module also stops sampling sensor data.

When to restart? After sending a pause instruction to the Event Monitor module, the Power Control module starts a timer T for checking restarting conditions. T is set to a short interval, for example, 15 seconds. The Event Monitor module monitors all user events all the time and keeps updating the Power Control module with user activities. If there is no report of user events from the Event Monitor before timer T expires, it is possible that the user has been changed since the previous authentication decision. The Power Control module restarts feature extraction by instructing the Event Monitor module to continue forwarding data. As a result, feature extraction is enabled. The system extracts features and does all the following processing beginning from the next user event. If the Power Control module receives a report of user events from the Event Monitor module before timer T expires, it considers that the current user has not been changed since the previous positive decision from the Aggregator. The Power Control module does not restart feature extraction. At the same time, the timer T is reset. The basic assumption for this is that it is unlikely for the user to be changed in 15 seconds. And even if this happens, the owner should be able to instantly notice this as the owner was using the glass 15 seconds ago. In real world, there are cases when the owner wants to share something on the glass screen with his/her friends. The owner takes off the glass and passes it to his/her friends. In this case, the user is changed within a short time, perhaps less than 15 seconds. However, the owner knows this and the owner actually wants it to happen. Hence it does not lie in the scope of our privacy protection.

5.4 Evaluation

In this section, we evaluate the performance of the GlassGuard authentication system through offline analysis by answering two questions. (1) How well do the classifiers perform? We address this by showing the EER for each classifier in the system. (2) How well does the whole system work? Here, we show the accuracy of all decisions made by the system and the average delay to make a decision. To evaluate the accuracy, we show the detection rate and false alarm rate when only one single type of user event

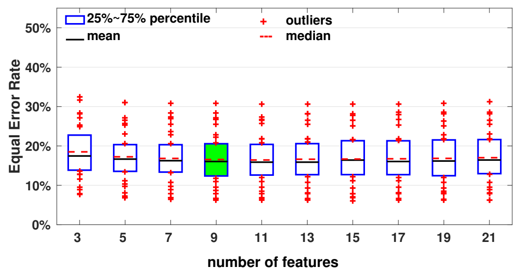

(a) single-tap gesture

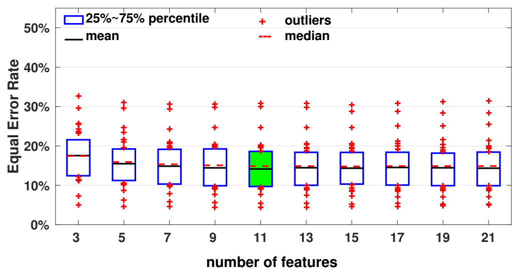

(b) one-finger swipe forward

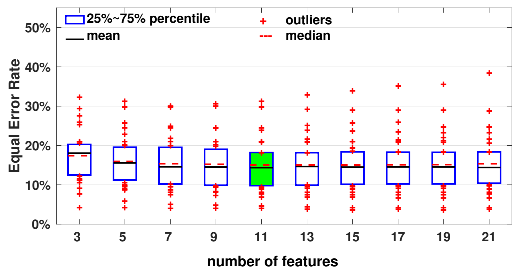

(c) one-finger swipe backward

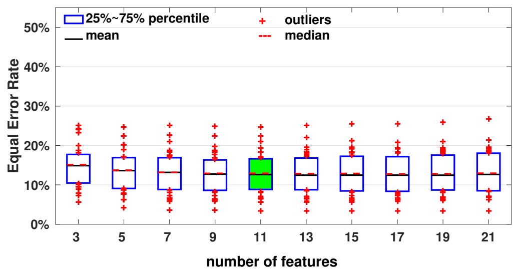

(d) one-finger swipe down

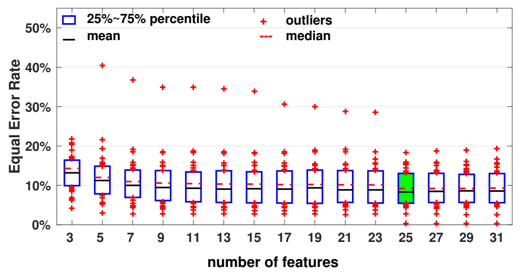

(e) two-finger swipe forward

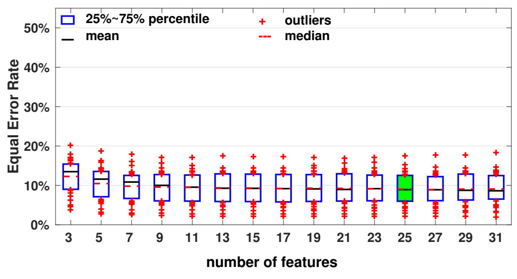

(f) two-finger swipe backward

Figure 5.6: Equal Error Rate with different numbers of features

is available, as well as when different types of events are mixed together with equal probability. To evaluate the delay, we show the number of user events needed for the system to make a decision. We also show the accuracy and decision delay under five typical usage scenarios and compare our system with state of the art.

5.4.1 Performance of Classification

We use EER as the performance metric for classification. EER is the error rate when FAR is equal to FRR. It can be obtained by intersecting the Receiver Operating Characteristic (ROC) curve with a diagonal of a unit square [131].

Classification of touch gestures. Figure 5.6 depicts the EERs of the six classifiers for touch gestures. For each classifier, we vary the number of features used and plot the EERs for all 32 users. From all six classifiers, we see that the average EERs decrease at the beginning as the number of features increases. However, as we continue to add more features, the improvement of EER is subtle. In some cases, using more features even results in a higher EER. For example, for the swipe backward classifier, the lowest average EER (15.02%) is achieved with 11 features. When 21 features are used, the average EER rises to 15.35%.

When choosing the best number of features to use in the system, we need to consider both the average EER and the maximum EER. We should also balance between accuracy and computation cost. Take the classifier for single-tap gestures as an example. The average EERs with 9 and 11 features are 16.56% and 16.43%, respectively. By adding two more features, the average EER only increases by 0.07%. Taking all these factors into consideration, the best configuration is: 9 features for the single-tap classifier, 11 features for one-finger swipe classifiers, and 25 features for two-finger swipe classifiers. We mark them in Figure 5.6 with green shade. Later, we use this configuration to evaluate the performance of our GlassGuard system.

Classification of voice commands. The authentication system makes one decision for each audio file, which is recorded from each voice command. With a sliding window, multiple MFCC vectors are extracted from an audio file. And from each MFCC vector, we get a SVM score. If the scores of 80% of the frames in an audio file favor the owner, then the audio file is marked as "true" (from the owner). Otherwise, the audio clip is marked as "false" (from an impostor). Figure 5.7 shows the EERs of the voice classifier for different users. Although one user has an EER of as high as ∼12%, for most users, the EER is below 5%. The red line shows the average EER, which is 4.88%. These EERs are much lower than those of classifiers for touch gestures.

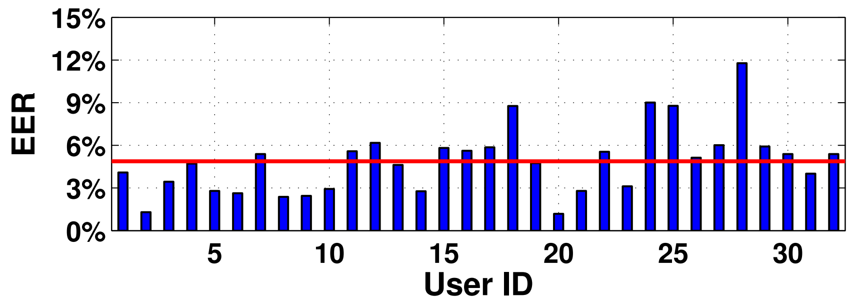

Figure 5.7: Classification EERs for voice commands

5.4.2 Performance of GlassGuard

To evaluate the performance of the GlassGuard system, we first test the system with only one single type of user event. Then, we mix all types of user events together and test it again. We do grid search [132] to find the best parameters for SVM classifiers. For parameters of the Aggregator, we choose 99% as the expected detection rate and 1% as the expected false alarm rate. As a result, η_1 and η_2 are 99 and 0.0101 respectively, calculated from Equation (5.9).

To do the first test where we only have one single type of user event, we extract all user events of the target type from all users. These events are then used as a user event sequence to feed into our GlassGuard system and test the system performance. Classifications are done in the same way as described in Section 5.3.2. The Aggregator gathers classification results and makes a decision only when it is confident. Every decision is made with events from the same user. If a decision is wrong, we count it as one error. The detection rate of the system is calculated as the ratio of correct decisions with the owner's data. The false alarm rate is calculated as the error rate with impostors' data. To carry the second test, we mix different types of user events together as user input sequences. In addition, we make sure that each event type has the same probability to be chosen for the next user event.

Accuracy. Figure 5.8 shows the detection rates when different users are taken as the owner. The corresponding false alarm rates are shown in Figure 5.9. The box shows the 25% and 75% percentiles. The solid line inside the box is the mean value, and the dashed

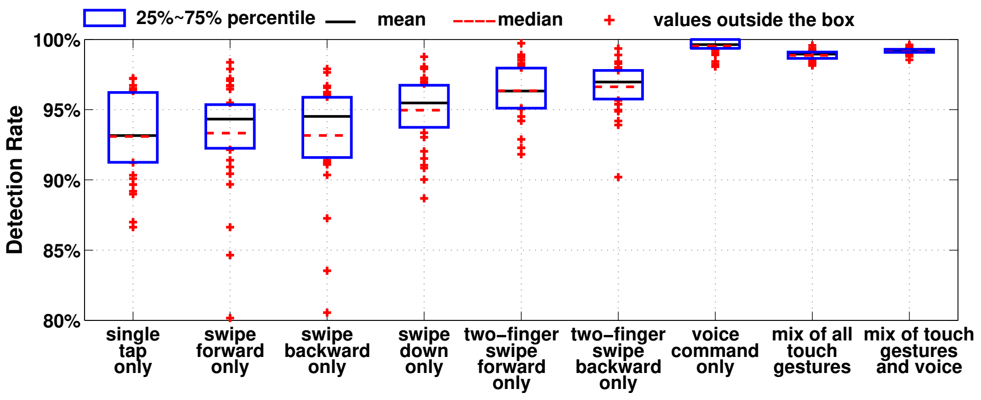

Figure 5.8: Detection rate of GlassGuard system

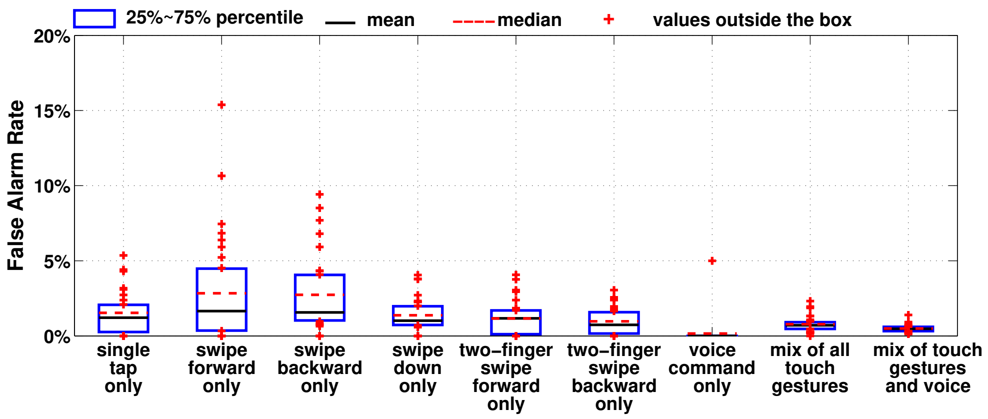

Figure 5.9: False alarm rate of GlassGuard system

line is the median. First, let us look at the cases when only one single type of user event is available. We see that two-finger touch gestures perform better than one-finger touch gestures. With two-finger touch gestures, all detection rates are above 90% and all false alarm rates are below 5%. With one-finger touch gestures only, both the detection rates and false alarm rates are not as good as those of two-finger touch gestures. A possible reason for this is that two-finger touch gestures have features describing the relative information between two fingers, which are not available in one-finger touch gestures. We also see that in the cases when only a single type of one-finger touch gesture is available, some users have much lower accuracy than others. For example, when only swipe forward gestures are used, user 19 has the lowest detection rate of 81%, and user 5 has the highest false alarm rate of 15%. The deep reason for the lower accuracy of

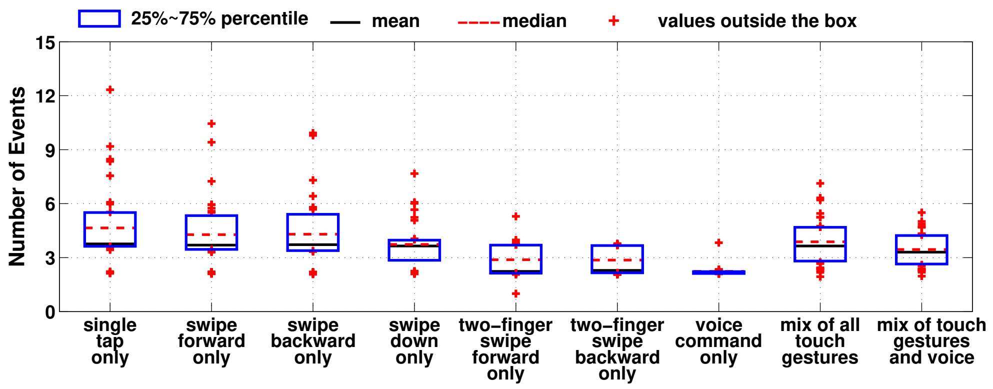

Figure 5.10: Number of events needed to make a decision

these users needs to be further explored. However, generally, the system works very well. For most of the users, the system achieves a detection rate of more than 90% and a false alarm rate below 10% in all cases. When only voice commands are used, the accuracy is much better than those with any single type of touch gesture. The system has zero false alarm rate with only one exception. In this case, even the lowest detection rate is above 98%. With the low EERs already shown in Figure 5.7, it is not surprising to see this.

In Figures 5.8 and 5.9, we also show the system accuracy when all types of touch gestures are used, and when voice commands are mixed together with touch gestures. The accuracy with all touch gestures is better than any of those individual cases. This is easy to understand as two users may have a similarity in one type of touch gesture but they are different in another one. The mean detection rate in this case is 98.7%, and the mean false alarm rate is 0.8%. With voice commands added, the accuracy is further improved. The mean detection rate increases to 99.2%, and the mean false alarm rate drops to 0.5%. Although they are not as good as those with only voice commands only, they are quite close.

Delay. Figure 5.10 shows the number of events needed by the system to make a decision when different users are taken as the owner. Similar to the trends of accuracy, when only one type of two-finger touch gesture is used, the average number of touch events needed to make a decision is noticeably less than that when only one type of one-finger touch gesture is used. The case with voice commands only requires the smallest number of events to make a decision, which is below 4 for all users with a mean of 2.24. The number of events needed for the case with all touch gestures mixed is in between that of the case with only one type of one-finger touch gesture and that of the case with only one type of two-finger touch gesture. When touch gestures are mixed together with voice commands, the system needs 3.5 user events on average to make a decision.

Accuracy and delay in typical usage scenarios. We have demonstrated the performance of our system when only one type of user event is available. We also show the performance when all types of user events are mixed together with equal probability. However, in reality, the distribution of these event types largely depends on what a user wants to do, how the data is organized on the Google Glass, and also a user's own preference (touch gesture or voice command).

Here we take five typical usage scenarios and show the accuracy and decision delay under each of the scenarios. (1) Skim through the timeline. A user can access pictures, videos, emails, and application notifications in timeline. Under this scenario, the user swipes forward to see the items in the timeline one by one. The user event sequence consists of only swipe forward gestures. (2) Delete a picture in the timeline. A user does the followings: swipe forward to enter the timeline, continue swipe forward (assume once) to find the group of pictures, single-tap to select the pictures, tap to show the options, swipe forward twice to reach the "Delete" option, and then tap to delete. (3) Take a picture and share it using voice commands. A user event sequence for this is as follows: "OK Glass!", "Take a picture", "OK, glass!", "Share it with...", and swipe down to go back. (4) Take a picture and share it using touch gestures: tap to go to applications, swipe forward (assume twice) to find the picture application, tap to select the application, tap to get the options, tap to select the "Share" option, tap to select a contact, and swipe down to go back. (5) Google search. A user event sequence for this is: tap to go to applications, swipe forward (assume once) to find the Google Search application, tap to select the application, (speak the keyword), tap to show the options when the content is ready, tap to view the website, two-finger swipe forward to zoom in, and swipe down to return.

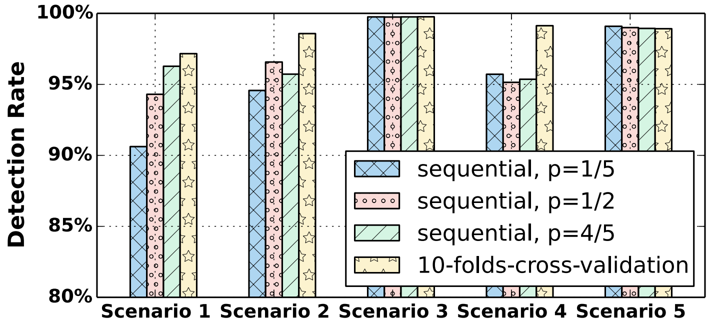

(a) detection rate

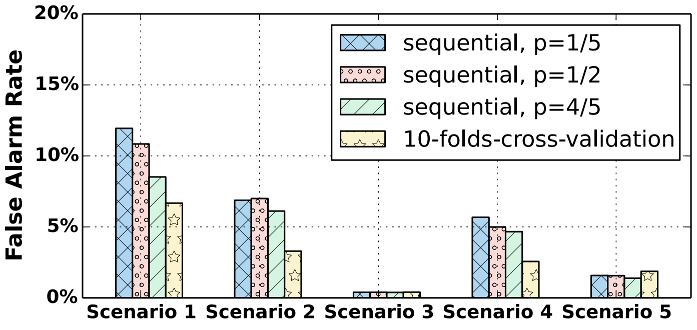

(b) false alarm rate

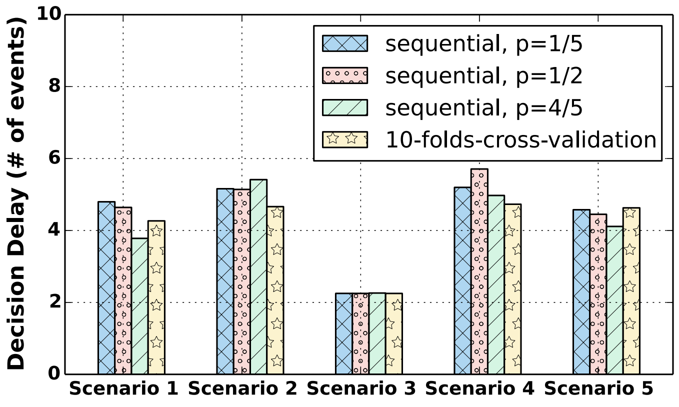

(c) decision delay

Figure 5.11: Performance with different training sizes and validation methods under five real usage scenarios

Our aforementioned performance analysis is based on the 10-fold cross validation where training samples are randomly selected. In another word, the training phase happens in parallel with the testing phase. To better indicate the system performance during real deployment, we perform sequential validation where the training phase and testing phase happen in sequence. All N samples are ordered in time sequence. We select the first $p * N$ (p=1/5, 1/2, or 4/5) samples for training and the remaining $(1 - p) * N$ samples for testing (except for voice commands of which we have less than 40 samples per user).

We present the average performance in Figure 5.11. Form the figure, we have three main observations. First, Scenario 1 has the lowest detection rate as it only contains swipe forward gestures. Scenario 3 mainly consists of voice commands, so it performs the best. Second, in general, larger training size results in better performance. However, the performance gap is small. When $p = 1/5$, we still have detection rate above 90% and false alarm rate below 12%. Third, different validation methods have very similar performance under Scenario 3 because the training for voice commands remain the same.

5.4.3 Performance Comparison

As far as we know, the work presented by Chauhan et al. [64] is the only study covering touch behavior based user authentication on wearable glasses. In their work, the authors also study the performance of touch behavioral biometrics for user authentication on Google Glass. Specifically, they consider four types of touch events: single-tap (T), swipe forward (F), swipe backward (B), and swipe down (D). And they consider seven gesture combinations: T, F, B, D, T+F, T+F+B, T+F+B+D. Different classification models are trained for different gesture combinations. All classification models make predictions independently. To obtain n samples of a gesture combination, each gesture type should appear at least n times. For example, under the Google search scenario (Scenario 5) introduced in the previous subsection, the user event sequence is: TFTVTT$\underline{\text{F}}$D (where V denotes voice command and $\underline{\text{F}}$ denotes two-finger swipe forward gesture). Their system can get one prediction from the T model with four samples, one prediction from the F model with one sample, and one prediction from the T+F model with one sample. The T+F+B model and the T+F+B+D model, which are able to provide higher accuracy,

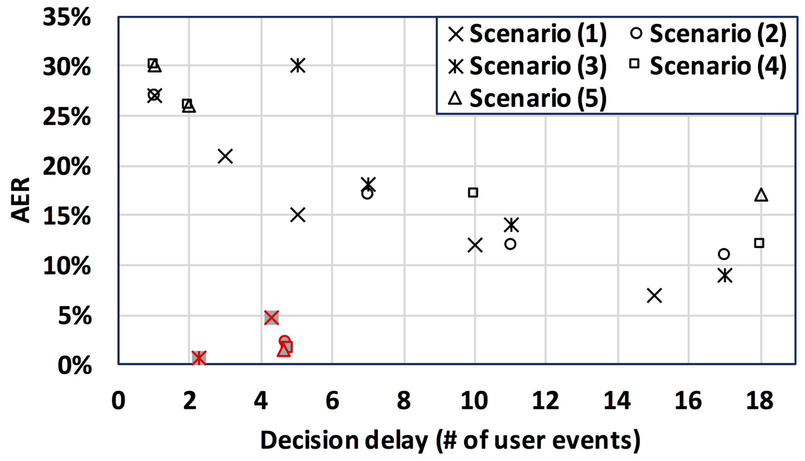

Figure 5.12: Comparison of GlassGuard with the reference

(Black markers are for the work presented by Chauhan et al. [64] and red markers with shade are for GlassGuard.)

do not work under this scenario as the swipe backward gesture is not available. Also, the three predictions may be different which makes their system ambiguous. In contrast, our system can freely combine all events within any user sequence and make one final and better decision.

We compare the performance of GlassGuard with the work of Chauhan et al. by showing in Figure 5.12 the average error rate (AER), which is defined by Chauhan et al. as 1/2*(1 - detection rate + false alarm rate), and decision delay under the five typical usage scenarios introduced in the previous subsection. In the figure, markers in black are for the method described by Chauhan et al., and markers in red are for GlassGuard. Different shapes stand for results under different usage scenarios. For the performance of Chauhan et al.'s work, the lowest AER of all available models is presented. From Figure 5.12, we see that error rates of Chauhan et al.'s work are above 15% with decision delay of 5 user events. With the same decision delay, our system has much lower error rates. Thus, compared to the work of Chauhan et al., our system achieves better performance.

Also, we notice that, with a certain number of test samples, the highest accuracy of their method is achieved with the model for the T+F+B+D combination. When one of the gesture types is not available, this model is not usable. We have used more samples for training than Chauhan et al. but the difference is not as large as it appears. In their work, 75 samples for the combination of T+F+B+D add up to 300 user events. Besides, even if their accuracy can be improved by increasing the training size, their decision delay does not change because they still need to wait for a fixed number of test samples. And our comparison shows that our system has much shorter decision delay.

5.5 Conclusion and Future Work

In this work, we study a set of touch behavioral features and voice features for user authentication on wearable glasses. With data collected from a user study consisting of 32 participants with Google Glass, the discriminability of these features are then evaluated with SVM models and Sequential Forward Search. With 9 features for single-tap gestures, 11 features for swipe forward/backward/down gestures, and 25 features for two-finger swipe forward/backward gestures, we show that the average EERs of classification based on single type of touch gesture are between 9% and 16.6%. With MFCC vectors extracted from audios, the EER of classification on voice commands is 4.88% on average.

We propose a continuous and non-invasive user authentication system for wearable glasses, named GlassGuard. GlassGuard continuously monitors user touch gestures and voice commands. It employs a mechanism adapted from Threshold Random Walking to make a decision from multiple user events only when it is confident. Our evaluation results based on data collected with Google Glass show that, when decisions are made purely on a single type of user event, the average detection rate is above 93% with a false alarm rate below 3% after less than 5 user events. When all types of user events are mixed with equal probability, our GlassGuard system achieves a detection rate of 99% and a false alarm rate of 0.5% after 3.46 user events. We also demonstrate the performance of GlassGuard with 5 typical usage scenarios, under which the detection rates are above 93.3% and the false alarm rates are below 2.84% after 4.66 events.

In the future, we plan to deploy the proposed system on Google Glass and measure the power consumption. Once the system is deployed on real devices, we would like to measure the performance under routine daily use by different people other than the five typical usage scenarios evaluated in this work. Also, we plan to validate the applicability of the authentication system over longer term.

Chapter 6

Conclusion

In this dissertation, we propose solutions to enhance energy efficiency and privacy protection on smart devices.

First, to the best of our knowledge, we are the first to present measurements and analysis of different ways to deal with WiFi broadcast traffic during smartphone suspend mode. Through power consumption and functionality analysis, we reveal the dilemma of dealing with WiFi broadcast traffic on modern smartphones during suspend mode: receive all and suffer high power consumption, or receive none and sacrifice functionalities. We address the dilemma by proposing Software Broadcast Filter (SBF). SBF passes useful broadcast frames for normal application functions. SBF blocks useless broadcast frames without triggering unnecessary wakelock time. Compared to the "receive-none" solution, SBF does not impair functionalities of smartphone applications. Compared to the "receive-all" solution, SBF reduces the power consumption by up to 49.9% for the Nexus One phone.

Second, we propose HIDE, an AP-assisted broadcast traffic management scheme, to further reduce smartphone energy wasted on useless broadcast frames. In the HIDE system, a client coordinates with the AP to enable traffic differentiation between useful and useless broadcast frames at the AP. Then, the AP hides the presence of useless broadcast frames from smartphones. As a result, a smartphone in suspend mode does not receive useless broadcast frames. Neither does it switch to active mode and process useless broadcast frames. With WiFi broadcast traces collected from five different real-world scenarios, we conduct trace-driven simulation with an energy model derived. The results show that our system saves 34%-75% energy for the Nexus One phone and 18%-78% for the Galaxy S4 phone when 10% of the broadcast frames are useful to the smartphone. When 2% of the broadcast frames are useful to the smartphone, our system saves 71%-82% energy for Nexus One and 62%-83% for Galaxy S4. We also analyze the performance overhead of the proposed system. The impact of the HIDE system on network capacity is less than 0.2% and the impact on packet round-trip time is no more than 2.3%.

Third, we propose GlassGuard for continuous and non-invasive user authentication on wearable glasses with the example of Google Glass. GlassGuard system collects data and extracts features from six types of touch gestures (single tap, swipe forward, swipe backward, swipe down, two-finger swipe forward, and two-finger swipe backward) as well as voice commands. A one-class SVM is trained for each user event type. By aggregating multiple classification results, which may come from different classifiers, with adapted Random Threshold Walking, GlassGuard makes a decision from multiple user events only when it is confident. Our evaluation results show that, when decisions are made purely on a single type of user events, the average detection rate is above 93% with false alarm rate below 3% after less than 5 user events. When all types of user events are mixed with equal probability, our GlassGuard system achieves a detection rate of 99% and a false alarm rate of 0.5% after 3.46 user events. We also demonstrate the performance of GlassGuard with five typical usage scenarios, under which the detection rates are all above 93.3% and the false alarm rates are below 2.84% after no more than 4.66 events.

As future work, we would like to study the energy efficiency during user privacy protection. We will explore how to make the current continuous authentication systems more energy efficient.

Bibliography

[1] Market Share: Final PCs, Ultramobiles and Mobile Phones, All Countries, 4Q16. http://www.gartner.com/newsroom/id/3609817, February, 2017.

[2] Mobile Fact Sheet. http://www.pewinternet.org/fact-sheet/mobile/, January, 2017.

[3] Smart Glasses Market Report 2015. http://www.augmentedreality.org/#!smartglassesreport/c88h, January, 2015.

[4] How Consumers Are Engaging With Mobile Video Around the World. http://advertising.aol.com/mobile-video-global, 2017.

[5] What do consumers want? Better batteries, not wearables. http://fortune.com/2015/01/07/what-do-consumers-want-better-batteries-not-wearables/, January, 2015.

[6] Few smartphone users interested in phones without headphone jacks. https://today.yougov.com/news/2016/09/22/smartphone-longer-battery-life-headphone-jack/, September, 2016.

[7] Lookout Projects Lost and Stolen Phones. http://www.businesswire.com/news/home/20120322005325/en/Lookout-Projects-Lost-Stolen-Phones-Cost-U.S., 2012.

[8] Symantec Smartphone Honey Stick Project. `http://www.symantec.com/about/news/resources/presskits/detail.jsp?pkid=symantec-smartphone-honey-stick-project`, 2012.

[9] Ildar Muslukhov, Yazan Boshmaf, Cynthia Kuo, Jonathan Lester, and Konstantin Beznosov. Know your enemy: the risk of unauthorized access in smartphones by insiders. In *Proceedings of the 15th international conference on Human-computer interaction with mobile devices and services*, pages 271–280. ACM, 2013.

[10] Abhilash Jindal, Abhinav Pathak, Y Charlie Hu, and Samuel Midkiff. Hypnos: understanding and treating sleep conflicts in smartphones. In *ACM Eurosys*, 2013.

[11] Radmilo Racic, Denys Ma, and Hao Chen. Exploiting mms vulnerabilities to stealthily exhaust mobile phone's battery. In *Securecomm and Workshops, 2006*, pages 1–10. IEEE, 2006.

[12] Niranjan Balasubramanian, Aruna Balasubramanian, and Arun Venkataramani. Energy consumption in mobile phones: a measurement study and implications for network applications. In *ACM IMC*, 2009.

[13] Aaron Carroll and Gernot Heiser. An analysis of power consumption in a smartphone. In *Proceedings of the 2010 USENIX conference on USENIX annual technical conference*, pages 21–21, 2010.

[14] Gian Paolo Perrucci, Frank HP Fitzek, and Jörg Widmer. Survey on energy consumption entities on the smartphone platform. In *Vehicular Technology Conference (VTC Spring), 2011 IEEE 73rd*, pages 1–6, 2011.

[15] Eduardo Cuervo, Aruna Balasubramanian, Daeki Cho, Alec Wolman, Stefan Saroiu, Ranveer Chandra, and Paramvir Bahl. MAUI: Making Smartphones Last Longer with Code Offload. In *ACM MobiSys*, 2010.

[16] Fahad R Dogar, Peter Steenkiste, and Konstantina Papagiannaki. Catnap: ex-

ploiting high bandwidth wireless interfaces to save energy for mobile devices. In *ACM Mobisys*, 2010.

[17] J. Liu and L. Zhong. Micro power management of active 802.11 interfaces. In *ACM Mobisys*, 2008.

[18] Andrew J Pyles, Xin Qi, Gang Zhou, Matthew Keally, and Xue Liu. SAPSM: Smart adaptive 802.11 psm for smartphones. In *Proceedings of the 2012 ACM Conference on Ubiquitous Computing*, pages 11–20. ACM, 2012.

[19] Shuo Deng and Hari Balakrishnan. Traffic-aware techniques to reduce 3G/LTE wireless energy consumption. In *ACM CoNEXT*, 2012.

[20] E. Rozner, V. Navda, R. Ramjee, and S. Rayanchu. NAPman: network-assisted power management for wifi devices. In *ACM Mobisys*, 2010.

[21] Arun Ramanatha Bharadwaj. *Managing wifi energy in smartphones by throttling network packets.* PhD thesis, Applied Sciences: School of Computing Science, Simon Fraser University, 2014.

[22] Abhinav Pathak, Abhilash Jindal, Y Charlie Hu, and Samuel P Midkiff. What is keeping my phone awake?: characterizing and detecting no-sleep energy bugs in smartphone apps. In *ACM Mobisys*, 2012.

[23] Yuvraj Agarwal, Steve Hodges, Ranveer Chandra, James Scott, Paramvir Bahl, and Rajesh Gupta. Somniloquy: Augmenting Network Interfaces to Reduce PC Energy Usage. In *NSDI*, 2009.

[24] Fabio Ricciato, Eduard Hasenleithner, Philipp Svoboda, and Wolfgang Fleischer. On the impact of unwanted traffic onto a 3g network. In *Security, Privacy and Trust in Pervasive and Ubiquitous Computing, 2006. SecPerU 2006. Second International Workshop on*, pages 8–pp. IEEE, 2006.

[25] Ismo Puustinen and Jukka K Nurminen. The effect of unwanted internet traffic on cellular phone energy consumption. In *New Technologies, Mobility and Security (NTMS), 2011 4th IFIP International Conference on*, pages 1–5. IEEE, 2011.

[26] Ramya Raghavendra, Elizabeth M Belding, Konstantina Papagiannaki, and Kevin C Almeroth. Unwanted link layer traffic in large IEEE 802.11 wireless networks. *Mobile Computing, IEEE Transactions on*, 9(9):1212–1225, 2010.

[27] Yu Chen and Kai Hwang. Collaborative detection and filtering of shrew DDoS attacks using spectral analysis. *Journal of Parallel and Distributed Computing*, 66(9):1137–1151, 2006.

[28] Thomas Martin, Michael Hsiao, Dong Ha, and Jayan Krishnaswami. Denial-of-service attacks on battery-powered mobile computers. In *Proceedings of the Second IEEE International Conference on Pervasive Computing and Communications (PerCom'04)*, PERCOM '04, pages 309–. IEEE Computer Society, 2004.

[29] Rongxing Lu, Xiaodong Lin, Haojin Zhu, Xiaohui Liang, and Xuemin Shen. BECAN: a bandwidth-efficient cooperative authentication scheme for filtering injected false data in wireless sensor networks. *Parallel and Distributed Systems, IEEE Transactions on*, 23(1):32–43, 2012.

[30] Wenjun Gu, Zhimin Yang, Dong Xuan, Weijia Jia, and Can Que. Null data frame: A double-edged sword in IEEE 802.11 WLANs. *Parallel and Distributed Systems, IEEE Transactions on*, 21(7):897–910, 2010.

[31] Indrajeet Singh, Srikanth V Krishnamurthy, Harsha V Madhyastha, and Iulian Neamtiu. Zapdroid: Managing infrequently used applications on smartphones. *IEEE Transactions on Mobile Computing*, 2016.

[32] Xin Qi, Qing Yang, David T Nguyen, Gang Zhou, and Ge Peng. Lbvc: towards low-bandwidth video chat on smartphones. In *Proceedings of the 6th ACM Multimedia Systems Conference*, pages 1–12. ACM, 2015.

[33] Lorenzo Keller, Anh Le, Blerim Cici, Hulya Seferoglu, Christina Fragouli, and Athina Markopoulou. MicroCast: cooperative video streaming on smartphones. In *Proceedings of the 10th international conference on Mobile systems, applications, and services*, pages 57–70. ACM, 2012.

[34] Mohammad Ashraful Hoque, Matti Siekkinen, and Jukka K Nurminen. Using crowd-sourced viewing statistics to save energy in wireless video streaming. In *Proceedings of the 19th annual international conference on Mobile computing & networking*, pages 377–388. ACM, 2013.

[35] Min Woo Kim, Dong Geun Yun, Jong Min Lee, and Seong Gon Choi. Battery life time extension method using selective data reception on smartphone. In *Information Networking (ICOIN), 2012 International Conference on*, pages 468–471. IEEE, 2012.

[36] Abdurhman Albasir, Kshirasagar Naik, Bernard Plourde, and Nishith Goel. Experimental study of energy and bandwidth costs of web advertisements on smartphones. In *Mobile Computing, Applications and Services (MobiCASE), 2014 6th International Conference on*, pages 90–97. IEEE, 2014.

[37] Jiaping Gui, Stuart Mcilroy, Meiyappan Nagappan, and William G.J. Halfond. Truth in Advertising: The Hidden Cost of Mobile Ads for Software Developers. In *Software Engineering (ICSE), 2015 IEEE/ACM 37th IEEE International Conference on*, volume 1, pages 100–110, May 2015.

[38] Adblock Plus for Android. `https://adblockplus.org/android-about`. Accessed February 2017.

[39] Feng Qian, Junxian Huang, Jeffrey Erman, Z Morley Mao, Subhabrata Sen, and Oliver Spatscheck. How to reduce smartphone traffic volume by 30%? In *Passive and Active Measurement*, pages 42–52. Springer, 2013.

[40] Hong Lu, AJ Bernheim Brush, Bodhi Priyantha, Amy K Karlson, and Jie Liu. Speakersense: energy efficient unobtrusive speaker identification on mobile phones. In *Pervasive Computing*, pages 188–205. Springer, 2011.

[41] Shaxun Chen, Amit Pande, and Prasant Mohapatra. Sensor-assisted facial recognition: an enhanced biometric authentication system for smartphones. In *Proceedings of the 12th annual international conference on Mobile systems, applications, and services*, pages 109–122. ACM, 2014.

[42] Nan Zheng, Aaron Paloski, and Haining Wang. An efficient user verification system via mouse movements. In *Proceedings of the 18th ACM conference on Computer and communications security*, pages 139–150. ACM, 2011.

[43] Rick Joyce and Gopal Gupta. Identity authentication based on keystroke latencies. *Communications of the ACM*, 33(2):168–176, 1990.

[44] Chao Shen, Zhongmin Cai, and Xiaohong Guan. Continuous authentication for mouse dynamics: A pattern-growth approach. In *Dependable Systems and Networks (DSN), 2012 42nd Annual IEEE/IFIP International Conference on*, pages 1–12. IEEE, 2012.

[45] Michael Frank, Ralf Biedert, En-Di Ma, Ivan Martinovic, and Dong Song. Touchalytics: On the applicability of touchscreen input as a behavioral biometric for continuous authentication. *Information Forensics and Security, IEEE Transactions on*, 8(1):136–148, 2013.

[46] Napa Sae-Bae, Kowsar Ahmed, Katherine Isbister, and Nasir Memon. Biometric-rich gestures: a novel approach to authentication on multi-touch devices. In *Proceedings of the SIGCHI Conference on Human Factors in Computing Systems*, pages 977–986. ACM, 2012.

[47] Nan Zheng, Kun Bai, Hai Huang, and Haining Wang. You are how you touch: User

verification on smartphones via tapping behaviors. In *Network Protocols (ICNP), 2014 IEEE 22nd International Conference on*, pages 221–232. IEEE, 2014.

[48] Cristiano Giuffrida, Kamil Majdanik, Mauro Conti, and Herbert Bos. I sensed it was you: authenticating mobile users with sensor-enhanced keystroke dynamics. In *Detection of Intrusions and Malware, and Vulnerability Assessment*, pages 92–111. Springer, 2014.

[49] Benjamin Draffin, Jiang Zhu, and Joy Zhang. Keysens: Passive user authentication through micro-behavior modeling of soft keyboard interaction. In *Mobile Computing, Applications, and Services*, pages 184–201. Springer, 2013.

[50] Hui Xu, Yangfan Zhou, and Michael R Lyu. Towards continuous and passive authentication via touch biometrics: An experimental study on smartphones. In *Symposium On Usable Privacy and Security, SOUPS*, volume 14, pages 187–198, 2014.

[51] Tao Feng, Jun Yang, Zhixian Yan, Emmanuel Munguia Tapia, and Weidong Shi. Tips: Context-aware implicit user identification using touch screen in uncontrolled environments. In *Proceedings of the 15th Workshop on Mobile Computing Systems and Applications*, page 9. ACM, 2014.

[52] Lingjun Li, Xinxin Zhao, and Guoliang Xue. Unobservable re-authentication for smartphones. In *NDSS*, 2013.

[53] Cheng Bo, Lan Zhang, Xiang-Yang Li, Qiuyuan Huang, and Yu Wang. Silentsense: silent user identification via touch and movement behavioral biometrics. In *Proceedings of the 19th annual international conference on Mobile computing & networking*, pages 187–190. ACM, 2013.

[54] Zdenka Sitova, Jaroslav Sedenka, Qing Yang, Ge Peng, Gang Zhou, Paolo Gasti, and Kiran Balagani. HMOG: New Behavioral Biometric Features for Continuous

Authentication of Smartphone Users. *IEEE Transactions on Information Forensics and Security*, 11(5):877–892, May 2016.

[55] Jiang Zhu, Pang Wu, Xiao Wang, and Joy Zhang. Sensec: Mobile security through passive sensing. In *Computing, Networking and Communications (ICNC), 2013 International Conference on*, pages 1128–1133. IEEE, 2013.

[56] Jani Mäntyjärvi, Mikko Lindholm, Elena Vildjiounaite, Satu-Marja Mäkelä, and HA Ailisto. Identifying users of portable devices from gait pattern with accelerometers. In *Acoustics, Speech, and Signal Processing, 2005. Proceedings.(ICASSP'05). IEEE International Conference on*, volume 2, pages ii–973. IEEE, 2005.

[57] Claudia Nickel, Tobias Wirtl, and Christoph Busch. Authentication of smartphone users based on the way they walk using k-nn algorithm. In *Intelligent Information Hiding and Multimedia Signal Processing (IIH-MSP), 2012 Eighth International Conference on*, pages 16–20. IEEE, 2012.

[58] Mauro Conti, Irina Zachia-Zlatea, and Bruno Crispo. Mind how you answer me!: transparently authenticating the user of a smartphone when answering or placing a call. In *Proceedings of the 6th ACM Symposium on Information, Computer and Communications Security*, pages 249–259. ACM, 2011.

[59] Lin Yang, Wei Wang, and Qian Zhang. VibID: User Identification through Bio-Vibrometry. In *2016 15th ACM/IEEE International Conference on Information Processing in Sensor Networks (IPSN)*, pages 1–12. IEEE, 2016.

[60] Cory Cornelius, Ronald Peterson, Joseph Skinner, Ryan Halter, and David Kotz. A wearable system that knows who wears it. In *Proceedings of the 12th annual international conference on Mobile systems, applications, and services*, pages 55–67. ACM, 2014.

[61] Kasper B Rasmussen, Marc Roeschlin, Ivan Martinovic, and Gene Tsudik. Au-

thentication using pulse-response biometrics. In *Proceedings of the Network and Distributed Systems Security Symposium (NDSS)*, 2014.

[62] Pan Chan, Tzipora Halevi, and Nasir D. Memon. Glass OTP: Secure and Convenient User Authentication on Google Glass. In *Financial Cryptography Workshops*, volume 8976, pages 298–308. Springer, 2015.

[63] Sugang Li, Ashwin Ashok, Yanyong Zhang, Chenren Xu, Janne Lindqvist, and Macro Gruteser. Whose move is it anyway? authenticating smart wearable devices using unique head movement patterns. In *PerCom*, 2016.

[64] Jagmohan Chauhan, Hassan Jameel Asghar, Mohamed Ali Kaafar, and Anirban Mahanti. Gesture-based continuous authentication for wearable devices: the google glass case. *arXiv preprint arXiv:1412.2855*, 2014.

[65] Sauvik Das, Eiji Hayashi, and Jason I Hong. Exploring capturable everyday memory for autobiographical authentication. In *Proceedings of the 2013 ACM international joint conference on Pervasive and ubiquitous computing*, pages 211–220. ACM, 2013.

[66] Paul Giura, Ilona Murynets, Roger Piqueras Jover, and Yevgeniy Vahlis. Is it really you?: user identification via adaptive behavior fingerprinting. In *Proceedings of the 4th ACM conference on Data and application security and privacy*, pages 333–344. ACM, 2014.

[67] Hossein Shafagh and Anwar Hithnawi. Poster: come closer: proximity-based authentication for the internet of things. In *Proceedings of the 20th annual international conference on Mobile computing and networking*, pages 421–424. ACM, 2014.

[68] Stephan Richter, Christian Holz, and Patrick Baudisch. Bootstrapper: recognizing tabletop users by their shoes. In *Proceedings of the SIGCHI Conference on Human Factors in Computing Systems*, pages 1249–1252. ACM, 2012.

[69] He Wang, Xuan Bao, Romit Roy Choudhury, and Srihari Nelakuditi. Insight: recognizing humans without face recognition. In *Proceedings of the 14th Workshop on Mobile Computing Systems and Applications*, page 7. ACM, 2013.

[70] Android Power Management. `http://elinux.org/Android_Power_Management`, November 2013.

[71] Android battery drain. `http://forums.sonos.com/showthread.php?t=37497`, December 2013.

[72] How to find the root cause of your Android battery problems. `http://www.reddit.com/r/Android/comments/19kq0a/how_to_find_the_root_cause_of_your_android`, March 2013.

[73] Dropbox on your home PC may be contributing to poor battery life on your phone! `http://forum.xda-developers.com/showthread.php?t=2094997`, January 2013.

[74] Dropbox LAN sync. `https://www.dropbox.com/help/137/en`. Accessed February 2017.

[75] M. Goldmann and G. Kreitz. Measurements on the Spotify peer-assisted music-on-demand streaming system. In *Peer-to-Peer Computing (P2P), 2011 IEEE International Conference on*, pages 206–211, 2011.

[76] Jin Teng, Boying Zhang, Xinfeng Li, Xiaole Bai, and Dong Xuan. E-shadow: Lubricating social interaction using mobile phones. In *ICDCS*, June 2011.

[77] Ngoc Do, ChengHsin Hsu, and Nalini Venkatasubramanian. CrowdMAC: A Crowdsourcing System for Mobile Access. In *Proceedings of the 13th International Middleware Conference*, Middleware, pages 1–20, 2012.

[78] Why are UDP packets dropped while sleeping? `https://groups.google.com/forum/#!topic/android-platform/DxlkphoLsd4`, July 2012.

[79] Udp broadcast packets not received in sleep mode. `http://stackoverflow.com/questions/9363389/udp-broadcast-packets-not-received-in-sleep-mode`, February 2012.

[80] Reception of UDP packets in sleep mode. `https://groups.google.com/forum/#!topic/android-platform/OpbSdp9FTmA`, June 2011.

[81] Wifi network connectivity issues and a possible fix. `http://forum.xda-developers.com/nexus-4/general/wifi-network-connectivity-issues-fix-t2072930`, December 2012.

[82] Ranveer Chandra, Sandeep Karanth, Thomas Moscibroda, Vishnu Navda, Jitendra Padhye, Ramachandran Ramjee, and Lenin Ravindranath. Dircast: A practical and efficient Wi-Fi multicast system. In *IEEE ICNP*, 2009.

[83] Shuai Wang, Song Min Kim, Yunhuai Liu, Guang Tan, and Tian He. Corlayer: A transparent link correlation layer for energy efficient broadcast. In *ACM MobiCom*, 2013.

[84] Enhua Tan, Lei Guo, Songqing Chen, and Xiaodong Zhang. Psm-throttling: Minimizing energy consumption for bulk data communications in wlans. In *Network Protocols, 2007. ICNP 2007. IEEE International Conference on*, pages 123–132. IEEE, 2007.

[85] Ronny Krashinsky and Hari Balakrishnan. Minimizing Energy for Wireless Web Access Using Bounded Slowdown. In *ACM MOBICOM*, 2002.

[86] ARP offload. `http://alliedtelesis.com/manuals/at2911GP/ah1072914.html`. Accessed July 2014.

[87] Monsoon solutions. `http://www.msoon.com/LabEquipment/PowerMonitor/`, 2014.

[88] Traffic generation model. `http://en.wikipedia.org/wiki/Traffic_generation_model`. Accessed February 2017.

[89] Cisco Visual Networking Index: Global Mobile Data Traffic Forecast Update 2014-2019 White Paper. `http://www.cisco.com/c/en/us/solutions/collateral/service-provider/visual-networking-index-vni/white_paper_c11-520862.html`, 2015. Accessed February 2015.

[90] Understanding today's smartphone user. `http://www.informatandm.com/wp-content/uploads/2013/06/Mobidia-ITM-June-2013.pdf`. Accessed July 2014.

[91] Mobile data offloading. `https://en.wikipedia.org/wiki/Mobile_data_offloading`. Accessed July 2014.

[92] Ge Peng, Gang Zhou, David T Nguyen, and Xin Qi. All or None? The Dilemma of Handling WiFi Broadcast Traffic in Smartphone Suspend Mode. In *IEEE INFOCOM*, 2015.

[93] Andrew J Pyles, Zhen Ren, Gang Zhou, and Xue Liu. Sifi: exploiting voip silence for wifi energy savings insmart phones. In *UbiComp, Proceedings of the 13th international conference on Ubiquitous Computing*, pages 325–334. ACM, 2011.

[94] J. Manweiler and R. Roy Choudhury. Avoiding the rush hours: Wifi energy management via traffic isolation. In *Proceedings of the 9th international conference on Mobile systems, applications, and services*, pages 253–266. ACM, 2011.

[95] Matthew Gast. *802.11 wireless networks: the definitive guide.* O'Reilly Media, Inc, 2005.

[96] Pejman Roshan and Jonathan Leary. *802.11 Wireless LAN fundamentals.* Cisco press, 2004.

[97] Giuseppe Bianchi. Performance analysis of the IEEE 802.11 distributed coordina-

tion function. *Selected Areas in Communications, IEEE Journal on*, 18(3):535–547, 2000.

[98] Haitao Wu, Yong Peng, Keping Long, Shiduan Cheng, and Jian Ma. Performance of reliable transport protocol over IEEE 802.11 wireless LAN: analysis and enhancement. In *INFOCOM 2002. Twenty-First Annual Joint Conference of the IEEE Computer and Communications Societies. Proceedings. IEEE*, volume 2, pages 599–607. IEEE, 2002.

[99] Linksys WRT1200AC. `https://wikidevi.com/wiki/Linksys_WRT1200AC`. Accessed August 2015.

[100] Netgear R7000. `https://wikidevi.com/wiki/Netgear_R7000`. Accessed August 2015.

[101] Smartglasses. `https://en.wikipedia.org/wiki/Smartglasses`. Accessed February 2017.

[102] Consumer & Enterprise Smart Glasses: Opportunities & Forecasts 2015-2020. `http://www.juniperresearch.com/researchstore/devices-wearables/smart-glasses/consumer-enterprise-smart-glasses`. Accessed February 2016.

[103] Diksha Shukla, Rajesh Kumar, Abdul Serwadda, and Vir V Phoha. Beware, your hands reveal your secrets! In *Proceedings of the 2014 ACM SIGSAC Conference on Computer and Communications Security*, pages 904–917. ACM, 2014.

[104] Nur Haryani Zakaria, David Griffiths, Sacha Brostoff, and Jeff Yan. Shoulder surfing defence for recall-based graphical passwords. In *Proceedings of the Seventh Symposium on Usable Privacy and Security*, page 6. ACM, 2011.

[105] Susan Wiedenbeck, Jim Waters, Leonardo Sobrado, and Jean-Camille Birget. Design and evaluation of a shoulder-surfing resistant graphical password scheme. In

Proceedings of the working conference on Advanced visual interfaces, pages 177–184. ACM, 2006.

[106] Adam J Aviv, Katherine Gibson, Evan Mossop, Matt Blaze, and Jonathan M Smith. Smudge attacks on smartphone touch screens. *WOOT*, 10:1–7, 2010.

[107] Stefan Schneegass, Frank Steimle, Andreas Bulling, Florian Alt, and Albrecht Schmidt. Smudgesafe: Geometric image transformations for smudge-resistant user authentication. In *Proceedings of the 2014 ACM International Joint Conference on Pervasive and Ubiquitous Computing*, pages 775–786. ACM, 2014.

[108] Benjamin Draffin, Jiang Zhu, and Joy Zhang. Keysens: passive user authentication through micro-behavior modeling of soft keyboard interaction. In *Mobile Computing, Applications, and Services*, pages 184–201. Springer, 2014.

[109] Douglas A Reynolds. Speaker identification and verification using gaussian mixture speaker models. *Speech communication*, 17(1):91–108, 1995.

[110] Chenren Xu, Sugang Li, Gang Liu, Yanyong Zhang, Emiliano Miluzzo, Yih-Farn Chen, Jun Li, and Bernhard Firner. Crowd++: unsupervised speaker count with smartphones. In *Proceedings of the 2013 ACM international joint conference on Pervasive and ubiquitous computing*, pages 43–52. ACM, 2013.

[111] SiME Smart Glasses. `http://www.chipsip.com/archive/SiME%20Smart%20Glasses_2015Jan(1).pdf`. Accessed August 2016.

[112] Recon Jet. `http://www.reconinstruments.com/products/jet/tech-specs/`. Accessed August 2016.

[113] Vuzix M300 Smart Glasses. `https://www.vuzix.com/Products/m300-smart-glasses`. Accessed August 2016.

[114] Douglas A Reynolds. Experimental evaluation of features for robust speaker identification. *Speech and Audio Processing, IEEE Transactions on*, 2(4):639–643, 1994.

[115] Silence removal in speech signals. `http://www.mathworks.com/matlabcentral/fileexchange/28826-silence-removal-in-speech-signals`. Accessed February 2017.

[116] Getevent. `https://source.android.com/devices/input/getevent.html`. Accessed February 2017.

[117] Android Debug Bridge. `http://developer.android.com/tools/help/adb.html`. Accessed February 2017.

[118] Isabelle Guyon and André Elisseeff. An introduction to variable and feature selection. *The Journal of Machine Learning Research*, 3:1157–1182, 2003.

[119] Corinna Cortes and Vladimir Vapnik. Support-vector networks. *Machine learning*, 20(3):273–297, 1995.

[120] Asa Ben-Hur and Jason Weston. A user's guide to support vector machines. *Data mining techniques for the life sciences*, pages 223–239, 2010.

[121] Bernhard Schölkopf, Koji Tsuda, and Jean-Philippe Vert. *Kernel methods in computational biology*. MIT Press, 2004.

[122] William M Campbell, Joseph P Campbell, Douglas A Reynolds, Elliot Singer, and Pedro A Torres-Carrasquillo. Support vector machines for speaker and language recognition. *Computer Speech & Language*, 20(2):210–229, 2006.

[123] Rezaul Begg and Joarder Kamruzzaman. A machine learning approach for automated recognition of movement patterns using basic, kinetic and kinematic gait data. *Journal of biomechanics*, 38(3):401–408, 2005.

[124] Alice Este, Francesco Gringoli, and Luca Salgarelli. Support vector machines for TCP traffic classification. *Computer Networks*, 53(14):2476–2490, 2009.

[125] Chih-Chung Chang and Chih-Jen Lin. LIBSVM Tools. `http://www.csie.ntu.edu.tw/~cjlin/libsvmtools/`. Accessed February 2017.

[126] Tom Fawcett. Roc graphs: Notes and practical considerations for researchers. *Machine learning*, 31:1–38, 2004.

[127] Jaeyeon Jung, Vern Paxson, Arthur W Berger, and Hari Balakrishnan. Fast portscan detection using sequential hypothesis testing. In *Proceedings of IEEE Symposium on Security and Privacy*, pages 211–225. IEEE, 2004.

[128] G Gu, J Zhang, and W Lee. Botsniffer: Detecting botnet command and control channels in network traffic. In *Proceedings of the 15th Annual Network and Distributed System Security Symposium, NDSS*, 2008.

[129] Mengjun Xie, Heng Yin, and Haining Wang. An effective defense against email spam laundering. In *Proceedings of the 13th ACM conference on Computer and communications security*, pages 179–190. ACM, 2006.

[130] Robert LiKamWa, Zhen Wang, Aaron Carroll, Felix Xiaozhu Lin, and Lin Zhong. Draining our glass: An energy and heat characterization of google glass. In *Proceedings of 5th Asia-Pacific Workshop on Systems*, APSys '14, pages 10:1–10:7, New York, NY, USA, 2014. ACM.

[131] Plotting AP and ROC curves. `http://www.vlfeat.org/overview/plots-rank.html`. Accessed August 2016.

[132] Chih-Wei Hsu, Chih-Chung Chang, Chih-Jen Lin, et al. A practical guide to support vector classification. Technical report, 2003.